First-principles Studies of Impurity Defects Formation and their Implications on Electronic and Magnetic Properties in a Two-dimensional Solid:
The case of Silicene

DOCTOR PAUL AGGRIPA MABOE

First-principles Studies of Impurity Defects Formation and their Implications on Electronic and Magnetic Properties in a Two-dimensional Solid:
The case of Silicene

by

DOCTOR PAUL AGGRIPA MABOE

submitted in accordance with the requirements
for the degree of

DOCTOR OF PHILOSOPHY

in the subject

PHYSICS

at the

UNIVERSITY OF SOUTH AFRICA

SUPERVISOR: DR. A.T. RAJI
CO-SUPERVISOR: DR. E.M. BENECHA

July 2024

Declaration

Name: Doctor Paul Agrippa Maboe
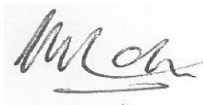
Student number: 8298831

Degree: Doctor of Philosophy

First-principles Studies of Impurity Defects Formation and their Implications on Electronic and Magnetic Properties in a Two-dimensional solid: The case of Silicene

I declare that the above thesis is my own work and that all the sources that I have used or quoted have been indicated and acknowledged by means of complete references.

I further declare that I submitted the thesis to originality checking software and that it falls within the accepted requirements for originality.

I further declare that I have not previously submitted this work, or part of it, for examination at UNISA for another qualification or at any other higher education institution.

31 July 2024

_____   _____

SIGNATURE   DATE

(D.P.A. MABOE)

Dedication

This is dedicated to my late father, Tsebane Solomon Maboe; and my late mother, Gezephi Sylvia Maboe.

Acknowledgement

I would like to express my sincere gratitude to the following individuals:

- Dr. A.T. Raji, my supervisor, for his expert knowledge, unwavering support, and inspiration. His belief in me has kept my spirits and motivation high during this research work.
- Dr. E.M. Benecha, my co-supervisor, for his excellent guidance, continuous assistance, and encouragement. This research work would not have been feasible without his initialisation.
- Dr. M.M. Tibane, Head of Physics Department of the University of South Africa, for exposing me to the field of two-dimensional materials.

I would also like to extend my sincere gratitude to:

- Sefako Makgatho Health Sciences University, for providing financial support.
- Members of the Physics Department of the University of South Africa, for their moral support.
- Members of the Research and Academic Computing (High Performance Computing) of the University of South Africa, for granting permission to use their facilities.
- Members of Centre for High Performance Computing of National Integrated Cyberinfrastructure System, for also granting permission to use their facilities.
- My wife, Puleng; my children, Kabelo and Keketso; the entire tribe of grandchildren; and my brothers, for their patience, understanding, and encouragement during this research journey.

Abstract

We report on first-principles density functional theory (DFT) calculations of interactions between extrinsic defects and intrinsic structural defects in silicene. Specifically, we investigate the stability, structural, magnetic and electronic properties of a monolayer silicene containing vanadium (V), hydrogen (H) and oxygen (O) atoms. Vanadium is a magnetic transition-metal and its incorporation in silicene lattice introduces magnetization. Thus, we have considered various configurations of vanadium either as interstitial or substitutional atoms, and their interactions with silicene vacancies. Hydrogen and oxygen are ubiquitous elements which are inadvertently introduced during material synthesis. Therefore, for practical purposes, it is important to investigate how their presence impact on the host material which in this case, are silicene or silicene containing vanadium impurities.

We show that a monovacancy introduces a magnetic moment of 2.02 μ_B in an otherwise non-magnetic monolayer silicene. Nonetheless, the vacancy possesses a significant formation energy of 3.52 eV, which suggest that it may only be produced through external perturbation such as electron irradiation. Also, we show that a divacancy is more stable than a single vacancy, but unlike a single vacancy, it has a zero magnetic moment. Also, divacancies at different separation in silicene lattice have a similar formation energy irrespective of their separation. Furthermore, when a silicene atom is substituted by a vanadium atom, the latter makes the monolayer silicene metallic while introducing a magnetic moment of 2.61 μ_B. The presence of a vacancy at a different atomic separation from vanadium shows that the nearest-neighbour vanadium-vacancy defect complex, that is, vanadium in a divacancy has the highest stability, however, all the substitutional vanadium-vacancy configurations are stable and both types of defects can co-exist in a monolayer silicene.

Regarding small vanadium clusters consisting of a pair of vanadium at varying separations, we found that the relative stability of the V-V pair is sublattice dependent, which oscillates between ferromagnetic (FM) and antiferromagnetic (AFM) configuration as the substitutional lattice sites of the V-V pair varies. When the V-V dimer are on a similar sublattice type, they prefer to couple together antiferromagnetically. However, when they are on a different sublattice type, the V-V dimer prefer to be in ferromagnetic configuration.

Comparison between the binding energy of substitutional V-vacancy pair and V-V pair shows that vanadium clustering is more probable without the vacancy than with vacancy. Consideration of interstitial hole V-V pair, that is, V-V pair at the centre of silicene hexagons affirms that indeed, small V-V pair are stable without vacancies. The presence of V atoms, however, induces finite magnetic moment in monolayer silicene, while annihilating the Dirac point and opening a narrow band gap of under 0.1 eV in the monolayer silicene electronic band structures.

We found that the V atom attracts the O and H either in atomic or molecular form, and when adsorbed they impact on the magnetization of V-doped monolayer silicene by reducing or annihilating its magnetic moment. Furthermore, a V-doped silicene having adsorbed atomic H and O behaves like a ferromagnetic semiconductor. On the other hand, molecular H_2 and O_2 adsorbed on a V-doped silicene do not result in a ferromagnetic semiconductor, although the resulting structures are metallic with a finite magnetization. We also found that the impact of H and O on the electronic and magnetic properties of V-doped silicene depends on their respective lattice locations, that is, whether these adsorbates are on the V atom or on the silicene atom near to the V dopant.

Contents

List of Figures

List of Tables

CHAPTER 1

Introduction

1.1 Background to the research

Scientific research on two-dimensional (2D) materials blossomed in 2004 when an atom-thick two-dimensional honeycomb material was exfoliated from graphite by Novoselov *et al.* [1]. This material referred to as graphene, showed exotic physical and chemical properties such as long electron mean-free paths, great mechanical strength, ballistic transport, superior thermal conductivity, ultrahigh electron mobility, room-temperature quantum Hall Effect and remarkable flexibility, with potential applications in nanoscale electronics, spintronics, sensing, photonics, energy storage and biotechnology [2], to mention but a few. Graphene's high mechanical and chemical stability, exceptional ballistic conductance [3], has led researchers to seek other two-dimensional materials that possess similar properties. Silicon, belonging to the same group with carbon is worth to be investigated. In recent times, 2D layer of silicon atoms, that is silicene, started to attract intensive research studies [4]. This is partly motivated by the role of bulk silicon crystal as a workhorse of semiconductor technology. Researchers then opined that a 2D layer of silicon atoms, that is silicene, will represent a new material capable of further revolutionizing electronics technology. Hence the ongoing interest in the material.

In this thesis, our focus is silicene, a single atom-thick two-dimensional honeycomb material. Silicene forms hexagonal lattice structures similar to graphene, however, while silicene exhibit a buckled shape, graphene exhibits a flat shape [5]. These two materials are also known to possess similar electronic properties, such as linear electronic dispersion around the Dirac points, charge carriers that behaves like massless electrons, and quantum spin Hall effect. Silicene has an unstable mixture of sp^2 and sp^3 hybridization, and it is this unstable dual hybridization that leads silicene not to be easily exfoliated from silicon bulk crystal [5]. Also, comparable to graphene, silicene possess a stronger spin-orbit coupling, and a tuneable electronic structure. These characteristics makes silicene an important two-dimensional material with potential applications in nanotechnology. Indeed, there are ongoing efforts devoted to investigations of silicene for quantum anomalous Hall effect,

valleytronics, spintronics, superconductivity, field and tunneling-field effect transistor, thermoelectricity, chemical sensing, hydrogen storage, and electrode material for lithium battery [6].

One of the ways to tune or modify the intrinsic properties of a material is through the incorporation of a defect into its structure. Defects have impact on the physical properties and applications of materials, and this may include properties such as mechanical, electrical, optical and magnetic properties. A material system may possess intrinsic or extrinsic defects, or both. Extrinsic defects may include an externally introduced impurity atoms, while intrinsic defects may include point defects or their clusters. Defects may also be classified into various categories that depends on dimensionality [7,8]. Points defects are categorized as zero-dimensional (0-D) defects. This category encompasses vacancies, substitutional impurities, adatoms, and Stone-Wales (SW) defects. One-dimensional (1-D) defects include line defect, grain boundaries, and edges [7,8]. The two-dimensional (2-D) defects include free surfaces, inter-crystalline boundaries and internal defects. Three-dimensional (3-D) defects include defects such as precipitates, dispersants, 3-D defect clusters and voids [7]. The aforementioned defects may be found in three-dimensional crystalline solids as well as two-dimensional materials, including silicene. The aforementioned defects may be found in three-dimensional crystalline solids as well as two-dimensional materials, including silicene.

In this work, we focus on point defects, including vacancies, substitutional impurities, and adatoms, as well as the clusters formed by the agglomeration of these defects. Figure 1.1 illustrates examples of these defects. With respect to a 2D material in particular, a vacancy represents an empty space created by a missing atom of the material. This type of point defect is mostly observed at high temperatures where atoms often and unpredictably shift their locations, creating vacant lattice sites in the process [7]. There are various methods responsible for creating vacancies, such as ion irradiation and so on. A substitutional impurity may be described as a foreign atom that has replaced one or more host atoms, while an adatom may be described as a foreign atom that is placed on the surface of the host such as silicene sheet. An adatom may become physisorbed when the bond between the adatom and the surface of the host is weak, or it may become chemisorbed when a strong bond exists between the adatom and the surface of the host such as silicene sheet [8,9]. In silicene, sigma (σ) bonds are the strong covalent bonds that form between sp^2 orbitals in-plane, while

pi (π) bonds are the weak covalent bonds that form between p_z orbitals out-of-plane. This means, sigma bonds occur when two atomic orbitals connect in an end-to-end manner, while pi bonds arise when two atomic orbitals overlap in a sideways orientation.
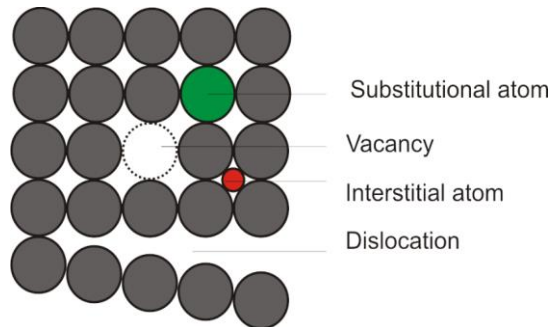
Figure 1.1: Schematic illustration of various defect types, that is, substitutional atom (green sphere), a vacancy (white sphere), interstitial atom (red sphere) as well as dislocation (white line), as explained in the main text. Grey spheres are atoms of the host material.

Point defects have the ability to alter the functionality of any material, including with silicene. Thus, the defects when present in silicene may alter its structural, electrical, and magnetic properties. The effects of defects on 2-D silicene is the main focus of this work. In particular, this thesis focuses on the effects of single and double vacancies, interactions of single vacancies in silicene, substitutional vanadium atom in silicene, interaction of vanadium atom with vacancies, as well as small vanadium clusters in silicene. We also considered the interactions of the aforementioned defects with oxygen and hydrogen when they all co-exist in silicene. We characterize monolayer silicene containing these defects for their electronic and magnetic properties.

The study employs density functional theory (DFT) approach to obtain the electronic structure and magnetic properties of silicene [10]. DFT calculates the ground-state properties of material systems based on its ground state electron density. This theory asserts that the total energy of a material system can be determined from its electron density. This assertion, received its practical meaning from Kohn and Sham [11], who considered a single-particle wavefunction that has a ground-state density as the many-body material system, and that the total energy of such a system may be given by the addition of the kinetic energy of non-interacting electrons, the classical Coulomb repulsion between the electrons, the potential energy of the electrons in the field of nuclei, and the exchange and correlation

energy [10]. However, the successes and failures of density functional theory are discussed in sub-section 3.14 of Chapter 3.

1.2 Knowledge gap and motivation of the research

As stated in Section 1.1, introducing defects in a solid material is one way of altering its intrinsic properties. To this end, defects can be intentionally introduced into a material, or inadvertently introduced in a material during synthesis. The latter is particularly the case for environmental gases such as hydrogen and oxygen atoms.

Silicene is a non-magnetic material in its pristine form. However, introducing a paramagnetic atom in its lattice may alter its electronic and magnetic properties. Also, intrinsic point defects, in particular, vacancies are routinely formed in a material. Therefore, a comprehensive study of a dopant (that is, an externally introduced atom) in a material should include intrinsic point defects. Furthermore, environmental gases such as H and O are ubiquitous and may contribute to changing the properties of a material when present. Therefore, in this work, we study the vanadium (V) atom inclusion in a monolayer (that is, single layer) silicene, and the interactions of the V dopant with vacancies, O and H atoms. In order to achieve this, we considered single and double vacancies, substitutional V dopant, and small V clusters in a monolayer silicene. We considered defect complexes formed by these defects and their interactions with the O and H atoms. Vanadium has been chosen in this work since it has a finite magnetic moment, and thus it is expected to induce magnetization in the silicene lattice. It should be emphasized that, in principle, other transition metals (TMs) with magnetic moments, such as nickel, iron and other $3d$ and $4d$ transition metals, exist However, V has been chosen as a representative paramagnetic metal to facilitate the study of metal dopant-induced magnetization in silicene. Furthermore, we note that there are previous studies on transition metal inclusion in silicene [12], however, the interactions of these metal dopants with intrinsic defects and the role of O and H have not been explored. Hence, the motivation for this study.

1.3 Aim and objectives

The primary goal of this research work is to study the possibility of monolayer vanadium-embedded silicene as a potential material for spintronic device applications. In order to achieve this, we investigate, using computational approach, the energetics, structural,

electronic, and magnetic properties of silicene containing vanadium and intrinsic defects, including hydrogen and oxygen external impurity atoms. We have employed DFT calculations as our computational approach. The objectives of this research are broadly divided into two parts:

1. To investigate the stability, structural, magnetic, and electronic properties of a monolayer silicene containing:

   (a) vacancy and vacancy complexes.

   (b) vanadium and vanadium clusters.

   (c) vacancy-vanadium defect complexes.

2. To determine the effects of atomic and molecular oxygen and hydrogen, that is, O, O_2, H, and H_2 on the properties of silicene atoms containing the defects stated in 1(a-c). As indicated in section 1.2, these gases have been chosen since they are ubiquitous environmental gases present in experimental synthesis processes.

1.4. Outline of the thesis

The thesis outline is as follows: Chapter 2 deals with the physics of two-dimensional silicene material. In this Chapter, basic structural and electronic properties of silicene and graphene are discussed. Also, recent theoretical and experimental developments in silicene research are reviewed.

The theoretical method of DFT and its implementation are discussed in Chapter 3, in particular, the nitty-gritties of DFT and its numerical implementation in the Quantum Espresso (QE) code. This Chapter includes the discussions of the computational methods used for obtaining various defects parameters.

In Chapter 4, calculated properties of pristine silicene are presented, including the optimization of the input parameters.

Chapter 5 presents vacancies formation and interaction in silicene. The effects of vanadium dopant, vacancy-vanadium defect complexes, and the small vanadium clusters in silicene are discussed in Chapter 6.

Chapter 7 discusses the effects of adsorption of atomic and molecular hydrogen and oxygen in vanadium-doped silicene.

Chapter 8 presents conclusions and recommendations for further research.

CHAPTER 2

Physics of 2-D silicene

2.1 Structure and comparison with graphene

Silicene is a one-atom thick allotrope of silicon, while graphene is a one-atom thick allotrope of carbon. Silicon and carbon belong to the same elemental group in the periodic table, that is group IV, which suggests that these two-dimensional materials may have similar electronic properties, however, with some differences mostly due to their nature of bonding. Structurally, both graphene and silicene have a hexagonal honeycomb lattice, as shown in figures 2.1(a) and 2.1(c), respectively. However, while graphene has a flat arrangement of carbon atoms, silicene has a buckled arrangement of silicon atoms with a relative displacement of h between the upper and lower sublattice. In some notation, the lower atoms (relative to the atoms at h) are called 'valley' atoms. The unit cell of each honeycomb structure (that is, silicene and graphene) contains two atoms as a basis set, one from each sublattice.
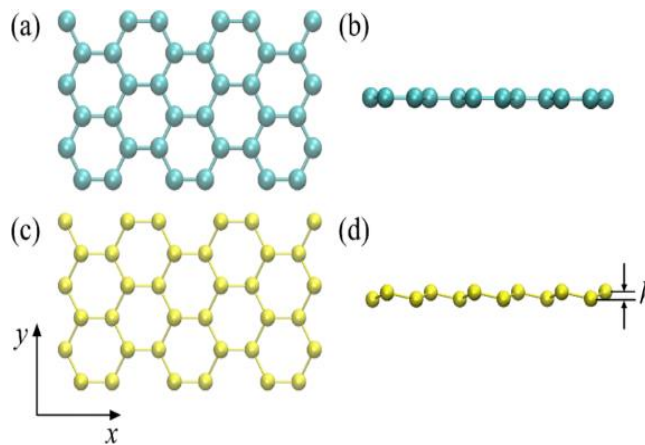
Figure 2.1: (a) Top view, (b) Side view of graphene, (c) Top view, and (d) Side view of silicene. The blue and yellow spheres represent the graphene and silicene atoms, respectively [13].

Table 2.1 shows the comparison of the lattice constant, bond length, bond angle, and buckling length of silicene and graphene.

Table 2.1: Structural parameters of silicene and graphene: Lattice constant, bond length, bond angle, and buckling length. All values were taken from Ref. [4].

System	Lattice constant (Å)	Bond length (Å)	Bond Angle (°)	Buckling length (Å)
Silicene	3.88	2.27	116.90	0.41
Graphene	2.46	1.42	120.00	0.00

From table 2.1, the lattice constant of silicene is larger than that of graphene by 1.42 Å. The bond length of silicene is also larger than that of graphene by 0.85 Å. The larger bond length in silicene is caused by the existence of sp^3 nature of bonding between silicene atoms, which results in the buckling of the material system [4]. The buckling character is stabilized by the overlapping of orbitals. Table 2.1 also shows that the bond angle between the nearest neighbour silicene atoms is 116.90°, while the bond angle in graphene is 120° [4]. These bond angles are indication of a sp^2 hybridization in the case of graphene and a mixture of sp^2 and sp^3 hybridization which supports the buckling nature of silicene. Finally, the 'valley' sublattice atom in silicene is displaced by about 0.41 Å from the top atom [14]. Graphene shows zero buckling length due to its flat arrangement of carbon atoms [15].

2.2 Electronic bands and energy gap

The electrical characteristics of graphene and silicene are comparable. Figure 2.2 (a) and (b) shows the theoretical band structures of graphene and silicene, respectively. From the figure, these two material systems possess Dirac points at the K points of the Brillouin zone. The Dirac point is the intersection of the valence and the conduction bands at the Fermi level [16]. Around the Dirac point, the charge carriers of graphene and silicene behave like massless electrons, and the bands of these systems cross each other linearly at the Fermi level, as shown in the figure [17]. This feature results in these material systems possessing a property of high electrical conductivity [18].
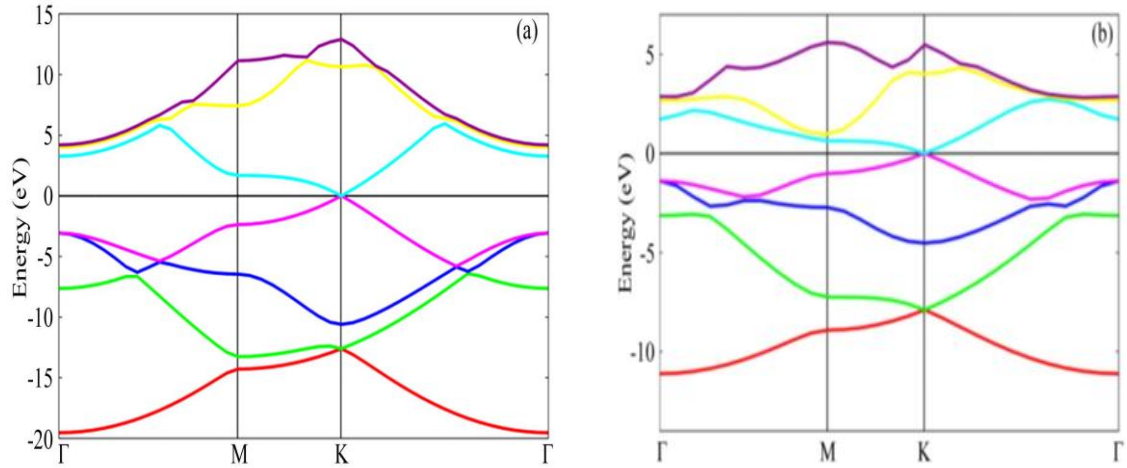
Figure 2.2: A comparison of the electronic band structure of (a) graphene, (b) silicene. Orbital colours: 1st sp^2 orbital (red), 2nd sp^2 orbital (green), 3rd sp^2 orbital (blue), unhybridized p_z orbital (pink), π^* orbital (cyan), σ^* orbitals (yellow and dark magenta). The zero energy is the Fermi level [4].

In graphene, this property is a result of the electrons in the unhybridized p_z orbital only, because the electrons of the hybridized s, p_x and p_y orbitals are deeply embedded in the valence band, and as such, makes no significant contribution to the electrical conductivity of graphene. This feature, renders graphene to be a semi-metal with a zero-band gap. However, in silicene, the electrical conductivity is mainly from the electrons of the p_z orbital. This means that the electrons due to the hybridization of the s, p_x, and p_y orbitals, with the p_z orbital, make a little contribution to the electrical conductivity of silicene. This feature, also renders silicene to be a semi-metal, though, with a tuneable band gap [4,6].

2.3 Potential applications of silicene

The potential applications of silicene are comparable to graphene's. For instance, graphene-based transistors may be regarded to be an established application, since this has been demonstrated. Also, silicene may be said to have an edge over graphene, because of its compatibility with the existing silicon nanotechnology [16]. Moreover, silicene possess a stronger spin-orbit coupling compared to graphene, which may establish the quantum spin Hall effect of silicene. Furthermore, silicene has a tuneable band gap which is a suitable feature in the realization of field-effect transistors. It also has a potential to be used as a material in spintronics and valleytronics. Silicene has been shown to be applicable as a material for chemical sensor, thermoelectric, and energy storage device [6]. Figure 2.3 shows the potential applications of silicene and its derivatives [19].
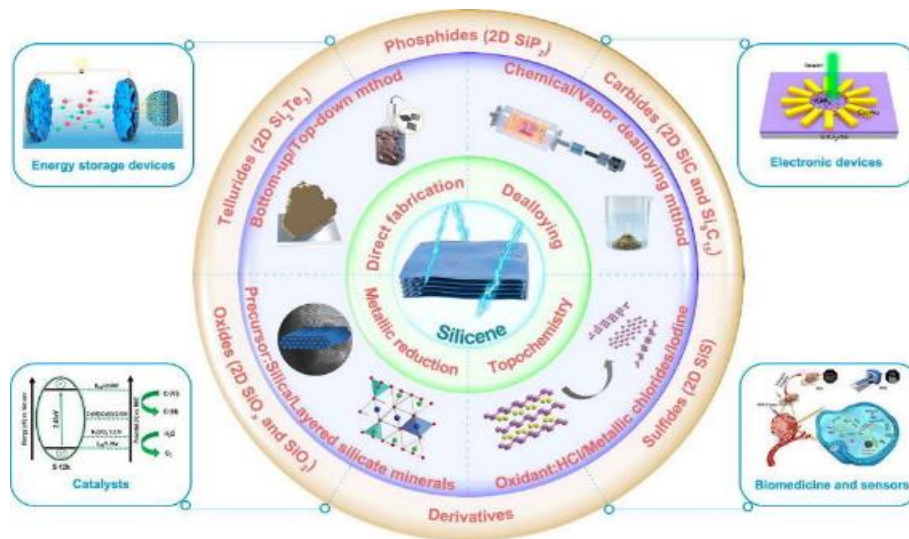
Figure 2.3: Potential applications of silicene and its derivatives [19].

2.4 Review of recent developments in silicene

2.4.1 Theoretical

The first theoretical studies on silicene sheet may be attributed to Takeda and Shiraishi [6,16,20], who predicted in 1994 that silicene has a buckled structure with a band structure featuring a Dirac cone, as shown in figure 2.2 (b). In 2007, another significant theoretical study on silicene sheet was conducted by Guzmán-Verri and Lew Yan Voon, who used both group theory and tight-binding model to show that silicene may be categorised as a semi-conductor with a zero-band gap [6,16,21,22]. In 2009, Cahangirov and his colleagues, theoretically showed that silicene is a stable, buckled material, that has a Dirac cone at the symmetric point K of the reciprocal lattice, and that, at this point of the Fermi level, the charge carriers behave as massless electrons [6,23]. The same results were independently obtained in the same year by Lebègue and Eriksson, when they were conducting silicene band structure calculations [17]. Furthermore, theoretical studies by Liu *et al.* [24] showed silicene to have a stronger spin-orbit coupling compared to graphene, and this feature, may lead to the realization of other phenomenon such as quantum valley Hall effect (QVHE), quantum spin Hall effect (QSHE) and quantum anomalous Hall effect (QAHE). These predicted quantum states serve as strong motivators among the experimentalists to explore the possibility of fabricating the silicene sheet.

2.4.2 Experimental

The theoretical studies on silicene charted a path for the experimentalists to begin to look into synthesizing silicene sheets. However, these efforts appeared to be difficult to realize, because silicon has no allotrope like graphite from which graphene may be mechanically stripped. Other methods such as chemical reduction method, which is used for the realization of graphene from graphene oxide, fails because silicon oxide is a hard insulator for silicene [6]. To date, it appears that the appropriate method for fabricating silicene sheets is through epitaxial growth on metal substrates. Other methods that are used to fabricate other two-dimensional materials failed when it came to silicene until 2012 [6]. However, on Ag (001) and Ag (110) substrates, silicene nanoribbons were successfully created [6,25-28]. Rachid Tchalala *et al.* also successfully grew silicene nanoribbons on Au (110) substrate later on [6,29]. Vogt *et al.* placed silicene on Ag (111) substrate and grew it successfully in 2012 [30]. Also in 2012, other experimentalists obtained Vogt *et al.* findings independently, by successfully synthesizing silicene on Ag (111) substrate [6,31-34].

Silicene was also successfully grown epitaxially on several substrates such as on metallic zirconium diboride [6,35], metallic zirconium carbide (111) [6,36], and iridium (111) [6,37]. As most experimentalists chose to epitaxially grow silicene on metallic surfaces, Chiappe *et al.*, chose to grow silicene epitaxially on a semi-conducting MoS_2 substrate, and this effort shows to preserve the properties of silicene [6,38]. The preceding assertions show that the epitaxial growth appears to be the main way in which silicene may be synthesized on substrates. Thus, together with employing different experimental techniques such as scanning tunnelling microscopy (STM), scanning electron microscopy (SEM), low-energy electron diffraction (LEED) and surface x-ray diffraction (SXRD), shows to be capable in assisting to determine the structure of silicene.

Our review of recent theoretical and experimental studies on silicene shows that there have been efforts to modify the intrinsic electronic and magnetic properties of silicene using structural and chemical modification approaches [39,40], including introducing defects into its structure such as point defects, of transition-metals and other non-metallic inclusions [41-46]. However, none of these studies probed the effect of environmental gases such as atomic and molecular hydrogen and oxygen gases. This is rather surprising since in the synthesis of impurity-doped silicene, these gases may be inadvertently introduced. The present study fills

this gap by considering the properties of metal-doped silicene having hydrogen and oxygen as co-adsorbates. We have used Vanadium-doped silicene as our model system.

Finally, we wish to state that there are fewer research studies on silicene compare to its graphene counterpart. This is partly because silicene deposition on a metal surface requires atomically clean conditions often obtained under ultra-high vacuum system. Silicene studies is thus an expensive process and time-consuming [39].

CHAPTER 3

Theoretical Methods and Implementation

3.1 Introduction

The knowledge about the properties of material systems is achieved through the determination of their quantum-mechanical total energy. It is the ground-state energy of the many-body system, and the subsequent minimisation of this energy that provides knowledge and understanding about the properties of these material systems. Several methods are being used to calculate this quantum-mechanical total energy of the many-body systems. However, since the exact total energy of these systems is not easily attained due to many-body interactions, lots of simplifications and approximations are being assumed in these methods to calculate this energy. In this thesis, a description of only two methods is given, among many others. These methods are the Born-Oppenheimer (BO) approximation and the Density Functional Theory (DFT).

3.2 Born-Oppenheimer approximation

The Born-Oppenheimer (BO) approximation involves the separation of the electronic and nuclear motions of molecules. It is based on the realization that since the nuclear motion is slow, then the fast-moving electrons have sufficient time to relax to a ground-state of the Hamiltonian of equation (3.1) given below. In other words, the electronic wavefunction becomes solvable by assuming that the nuclear degree of freedom is almost fixed compared to the electronic degree of freedom. The fixation of a range of these nuclear degrees of freedom results in the potential energy curve that actually traces the nuclei movement.

The time-independent, nonrelativistic Schrödinger equation for a many-body system is given by [47]:

$$\hat{H}\varphi = E\varphi \tag{3.1}$$

where $\hat{H}$ is the Hamiltonian operator and φ a set of solutions, or eigenstates of the Hamiltonian. The Hamiltonian operator is defined as the sum of the kinetic energy $\hat{T}$ and potential energy $\hat{V}$ respectively. That is [47]:

$$\hat{H} = \hat{T} + \hat{V} \tag{3.2}$$

The BO approximation simplifies the Schrödinger equation (SE) on the assumption that since the atomic nuclei is much more massive than the atomic electrons, then the nuclei should be perceived as being stationary relative to the fast-moving electrons. This approach renders the SE to be tractable for it is now expressed into separate nuclear and electronic Schrödinger equations [48].

The Hamiltonian of equation (3.2) is the total energy of the electronic-nuclei system and may be expressed (in atomic units) as follows [49,50]:

$$\hat{H} = \hat{T}_N(R) + \hat{T}_e(r) + \hat{V}_{eN}(r,R) + \hat{V}_{NN}(R) + \hat{V}_{ee}(r) \tag{3.3}$$

where

$\hat{T}_N = \dfrac{1}{2}\sum_i \nabla_i^2$, is the operator for the kinetic energy of the nuclei,

$\hat{T}_e = \dfrac{1}{2M_A}\sum_A \nabla_A^2$, is the operator for the kinetic energy of the electrons,

$\hat{V}_{eN} = \sum_{A,i} \dfrac{z_A}{r_{Ai}}$, is the operator for the potential energy due to electron-nuclear attraction,

$\hat{V}_{NN} = \sum_{A>B} \dfrac{z_A z_B}{r_{AB}}$, is the operator for the potential energy due to nuclear-nuclear repulsion,

and

$\hat{V}_{ee} = \sum_{i>j} \dfrac{1}{r_{ij}}$, is the operator for the potential energy due to electron-electron repulsion,

where A and B are the nuclei, i and j are the electrons, and $i > j$ prevents double counting in electron-electron interaction ($\hat{V}_{ee}$), otherwise, a factor ½ must be placed in front of the double sum for $i = j$ terms to prevent this double counting. The assumption that the nuclei are much more massive than the electrons, allows the fixing of the nuclear co-ordinates R so that in the electron wavefunction $\varphi_e(r,R)$ the co-ordinates R are just parametric. Moreover, this assumption also allows the disappearance of the term $\hat{T}_N(R)$ from equation (3.3). Thus equation (3.3) can be given as:

$$\hat{H}_{el} = \hat{T}_e(r) + \hat{V}_{eN}(r,R) + \hat{V}_{NN}(R) + \hat{V}_{ee}(r) \tag{3.4}$$

where $\hat{H}_{el}$ is the electronic Hamiltonian. This reduces the Schrödinger (with fixed nuclei) to:

$$\hat{H}_{el}\varphi(r, R) = E_{el}\varphi(r, R) \tag{3.5}$$

where E_{el} is the electronic eigenvalue.

The disappearance of the term $\hat{V}_{NN}(R)$ in equation (3.4) is allowed since it is just a constant that shifts the eigenvalue for R parametric. Hence equation (3.4) may be written as:

$$\hat{H}_e = \hat{T}_e(r) + \hat{V}_{eN}(r, R) + \hat{V}_{ee}(r) \tag{3.6}$$

where $\hat{H}_e$ is the electronic Hamiltonian without $\hat{V}_{NN}(R)$. Thus, equation (3.5) is reduced to:

$$\hat{H}_e\varphi_e(r, R) = E_e\varphi(r, R) \tag{3.7}$$

Equation (3.7) is referred to as the electronic Schrödinger equation, and E_e is the adiabatic electronic potential energy surface for a given set of nuclear co-ordinates. This means that varying the nuclear co-ordinates will result in a new electronic wavefunction $\varphi_e(r, R)$ that requires to be solved so that another adiabatic electronic potential energy surface may be obtained. Considering a total wavefunction $\varphi_T(r, R)$ that might be extended to include electronic wavefunction and a set of pre-selected nuclear wavefunctions may lead to a nuclear Schrödinger equation. That is:

$$\varphi_T(r, R) = \varphi_e(r, R)\varphi_N(R) \tag{3.8}$$

3.3 Density functional theory

Density Functional Theory (DFT) solves the Schrödinger equation of many-body systems by considering the electron density of the material system, which is a function of only three degrees of freedom. The electron density $n(r)$ at a particular position r in space of the system is related to the wavefunction of the system by the magnitude of the square of the wavefunction $\varphi(r)$. That is [36]:

$$n(r) = \sum_{i=1}^{N} |\varphi_i(r)|^2 \tag{3.9}$$

where $\varphi_i(r)$ is the single-electron wavefunction.

The relationship between the electron density and the energy of the system is contained in the Hohenberg-Kohn (HK) theorems. The neglect of the correlation of the electrons of the many-body system showed variations compared to experimental results. This anomaly caused Kohn-Sham to recast the intractable complex many-body system into a computationally solvable system consisting of single fictitious non-interacting electrons that are moving in an effective potential via the exchange-correlation functional. This exchange-correlation functional is approximate, however, it provides a thorough explanation of the many characteristics of the material systems.

3.4 Hohenberg-Kohn theorems

The statement of the first theorem of Hohenberg-Kohn is given as follows [51],

Theorem 1:

The external potential $V_{ext}(r)$, and hence the total energy $E[n(r)]$, is uniquely determined by the ground-state electron density $n_0(r)$.

The statement and proof of the second theorem of Hohenberg-Kohn is given, as follows [51],

Theorem 2:

The ground-state electron density obeys the variational principle: The electron density that minimises the total energy is the exact ground-state electron density.

The Hohenberg-Kohn total energy functional is given by:

$$E_{HK}[n(r)] = T[n(r)] + E_{ee}[n(r)] + \int V_{ext}(r)n(r)dr + E_{NN} \tag{3.10}$$

where E_{ee} is the electron-electron interaction energy, and E_{NN} is the nuclear-nuclear interaction energy.

Equation (3.10) may be written as:

$$E_{HK}[n(r)] = F_{HK}[n(r)] + \int V_{ext}(r)n(r)dr + E_{NN} \tag{3.11}$$

where $F_{HK}[n(r)]$ is the universal functional.

A universal functional is a functional that treats all electrons the same regardless of the external potential. In this case, since the kinetic energy and the energy that involves electron-electron interaction are expressed as functional of density only, then the universal functional $F_{HK}[n(r)]$ is given by:

$$F_{HK}[n(r)] = T[n(r)] + E_{ee}[n(r)] \tag{3.12}$$

Considering a system with the ground-state density $n_0^1(r)$ generated by the external potential $V_{ext}^1(r)$. The Hohenberg-Kohn total energy functional may be expressed as the expectation value of the Hamiltonian with wavefunction φ_0^1. That is:

$$E_0^1 = E_{HK}(n_0^1) = \left\langle \varphi_0^1 \middle| \hat{H}^1 \middle| \varphi_0^1 \right\rangle \tag{3.13}$$

Considering again, a system with a different ground-state density $n_0^2(r)$ generated by another external potential $V_{ext}^2(r)$ with a corresponding wavefunction φ_0^2. According to variational principle, the energy of the system considered second must be lower than the energy of the system considered first. That is:

$$E_0^1 = \left\langle \varphi_0^1 \middle| \hat{H}^1 \middle| \varphi_0^1 \right\rangle < \left\langle \varphi_0^2 \middle| \hat{H}^2 \middle| \varphi_0^2 \right\rangle = E_0^2 \tag{3.14}$$

Equation (3.14) asserts that the energy obtained by equation (3.11) for the correct ground-state density will be lower than the energy obtained by any other density.

The proof of Hohenberg-Kohn Theorem 2 was also shown by Levy and Lieb [51]. However, the proof of this theorem is based on densities that are N-representable. These are ground-state densities derived from wavefunctions φ_N of N electrons generated by unrestricted external potential $V_{ext}(r)$. This is also based on the minimisation of the total energy, however, with respect to a class of wavefunctions φ that have the same density $n(r)$. Thus, a unique lowest energy for that density is given by [51]:

$$E_{LL}[n(r)] = min_\varphi \left\{ \left\langle \varphi \middle| \hat{T} \middle| \varphi \right\rangle + \left\langle \varphi \middle| V_{ee} \middle| \varphi \right\rangle \right\} + \int V_{ext}(r)n(r)dr + E_{NN} \tag{3.15}$$

where $E_{LL}[n(r)]$ is the Levy-Lieb energy, $\hat{V}_{ee}[n(r)]$ is the electron-electron interaction, and E_{NN} is the nuclear-nuclear interaction.

Equation (3.15) may also be written as [51]:

$$E_{LL}[n(r)] = F_{LL}[n(r)] + \int V_{ext}(r)n(r)dr + E_{NN} \tag{3.16}$$

where $F_{LL}[n(r)]$ is the Levy-Lieb functional given by [51]:

$$F_{LL}[n(r)] = min_\varphi \left\{ \langle \varphi|\hat{T}|\varphi \rangle + \langle \varphi|V_{ee}|\varphi \rangle \right\}$$ (3.17)

which is a functional that gives the lowest kinetic and interaction energy that can be reached with all possible quantum states having a given density. Thus, the second theorem of Hohenberg-Kohn may also be stated as follows: The ground state energy of the system is obtained via minimization of the energy functional with respect to the electron density.

3.5 Kohn-Sham equations

From the Hohenberg-Kohn total energy functional $E_{HK}[n(r)]$ of many-body system, given by equation (3.10), Kohn-Sham expressed this energy equation for non-interacting electrons as follows [51]:

$$E_{KS}[n(r)] = T_s[n(r)] + E_H[n(r)] + \int V_{ext}(r)n(r)dr + E_{NN} + E_{XC}[n(r)]$$ (3.18)

where $T_s[n(r)]$ is the kinetic energy for a non-interacting electron system, $E_H[n(r)]$ is the Hartree or Coulomb energy, $E_{XC}[n(r)]$ is the exchange-correlation energy, which involves the effects of the exchange and correlation of electrons.

The kinetic energy $T_s[n(r)]$ is given by [51]:

$$T_s[n(r)] = -\frac{1}{2} \sum_{i=1}^{N} \int \varphi_i^*(r)\nabla^2 \varphi_i(r)dr$$ (3.19)

The Hartree energy $E_H[n(r)]$ as a functional of electron density is given by [51]:

$$E_H[n(r)] = \frac{1}{2} \iint \frac{n(r)n(r')}{|r-r'|} dr dr'$$ (3.20)

Comparison of the Hohenberg-Kohn and Kohn-Sham total energy functionals given by equations (3.10) and (3.18), defines the exchange-correlation energy $E_{XC}[n(r)]$ as [51]:

$$E_{XC}[n(r)] = T[n(r)] - T_s[n(r)] + E_{ee}[n(r)] - E_H[n(r)]$$ (3.21)

where $T[n(r)]$ and $E_{ee}[n(r)]$ are the real kinetic and electron-electron interaction energies for many-body systems, while $T_s[n(r)]$ and $E_H[n(r)]$ are the kinetic and electron-electron energies for independent-body systems.

Introducing the normalisation constraint on the electron density, given by the Lagrange multiplier μ so that the number of electrons N is conserved, that is, $\int n(r)dr = N$

results in [51]:

$$\frac{\delta}{\delta n(r)}\Big[E_{KS}n(r) - \mu\int n(r)dr - N\Big] = 0 \qquad (3.22)$$

Equation (3.22) may be simplified to:

$$\frac{\delta E_{KS}n(r)}{\delta n(r)} = \mu \qquad (3.23)$$

Putting equation (3.18) into equation (3.22) gives:

$$\frac{\delta T_s[n(r)]}{\delta n(r)} + V_{eff}(r) = \mu \qquad (3.24)$$

Equating equations (3.23) and (3.24) leads to:

$$\frac{\delta E_{KS}n(r)}{\delta n(r)} = \frac{\delta T_s[n(r)]}{\delta n(r)} + V_{eff}(r) \qquad (3.25)$$

where the effective potential $V_{eff}(r)$ is given by:

$$V_{eff}(r) = V_{ext}(r) + \int\frac{n(r')}{|r-r'|}dr' + V_{XC}(r) \qquad (3.26)$$

and the exchange-correlation potential $V_{XC}(r)$ is given by:

$$V_{XC}(r) = \frac{\delta E_{XC}[n(r)]}{\delta n(r)} \qquad (3.27)$$

The writing of equation (3.25) explicitly in terms of electron density of equation (3.9) leads to single-electron wavefunctions φ_i that minimise the Kohn-Sham energy functional and satisfy a set of N non-linear integro-differential equations. In other words, these single-electron wavefunctions φ_i are obtained from the self-consistent solutions of the Kohn-Sham equations that are given by [48]:

$$\Big[-\frac{1}{2}\nabla_i^2 + V_{eff}(r)\Big]\varphi_i(r) = \varepsilon_i\varphi_i(r) \qquad (3.28)$$

where ε_i is the Kohn-Sham eigenvalue, and φ_i is the single-electron wavefunction of electronic state i.

The Kohn-Sham theory is an exact method that determines the ground-state energy of a real many-body system provided that the exchange-correlation energy functional $E_{XC}[n(r)]$ was known exactly. However, since this energy functional is unknown, approximations to the exchange-correlation functional are needed to numerically solve the Kohn-Sham equations. The simplest exchange-correlation functional is the local density approximation (LDA).

Several more accurate exchange-correlation functionals have been developed over the years in an effort to accurately describe the properties of a wide range of materials. These include generalised-gradient approximation (GGA), the meta-GGA as well as the hybrid exchange functionals. A complete review of these can be found in Ref. [52]. Nevertheless, we give a brief overview of fundamentals of these functionals in the next section.

3.6 Exchange-correlation potential

The exchange-correlation energy $E_{XC}[n(r)]$ as defined by equation (3.21) is a contribution from the exchange and correlation parts. That is:

$$E_{XC} = E_X + E_C \qquad (3.29)$$

The exchange energy is a result of the Pauli exclusion principle. This principle forces the anti-symmetricity of wavefunctions so that electrons of the same spin do not occupy the same quantum state. Moreover, since electrons are charged particles, exert a repulsive interaction on each other. However, this spatial separation of the electrons results in the decrease of the total energy of the electron gas. The correlation energy is a result of the movement of the electrons in space. This means that the movement of a particular electron in space cannot be separated from the movement of all other neighbouring electrons. In other words, the movement of one particular electron is correlated to the movement of all other electrons in the midst. The exact value of this exchange-correlation energy functional is not known exactly, however, it may be approximated by assuming that the functional is local and is taken from a uniform electron gas. This assumption is derived from the fact that since the electron density of a real system varies smoothly in space, it may be equivalent to the uniform electron gas. This approximation is referred to as the local density approximation (LDA) which means that the exchange-correlation energy functional of an electron at a point r in space is approximated by the exchange-correlation energy functional of an electron in a uniform electron gas, which has the same density as the electron at a point r in space. That is [51]:

$$E_{XC}^{LDA}[n(r)] = \int \varepsilon_{XC}^{unif}[n(r)]n(r)dr \qquad (3.30)$$

where ε_{XC}^{unif} is the exchange-correlation energy per electron in a uniform electron gas, and is dependent on density only. Generally, equation (3.30) may be referred to as the local spin density approximation (LSDA) when expressed in terms of spin densities. That is [51]:

$$E_{XC}^{LSDA}[n^{\uparrow}(r), n^{\downarrow}(r)] = \int \varepsilon_{XC}^{unif}[n^{\uparrow}(r), n^{\downarrow}(r)]n(r)dr \qquad (3.31)$$

where $n^{\uparrow}(r)$ and $n^{\downarrow}(r)$ are spin-up and spin-down densities, respectively.

The local spin density approximation exhibited success in describing the properties of many material systems, however, it came short when material systems showed rapid density spatial variance around atoms. As a result, it was improved by making the functional to be dependent on both the density and the magnitude of the gradient of the density. This functional is referred to as the generalised gradient approximation (GGA). It is given by [51]:

$$E_{XC}^{GGA}[n^{\uparrow}(r),n^{\downarrow}(r)] = \int \varepsilon_{XC}^{GGA}[n^{\uparrow}(r),n^{\downarrow}(r),\left|\nabla n^{\uparrow}(r)\right|,\left|\nabla n^{\downarrow}(r)\right|]n(r)dr \qquad (3.32)$$

where $\left|\nabla n^{\uparrow}(r)\right|$ and $\left|\nabla n^{\downarrow}(r)\right|$ are the magnitudes of the gradient of the spin-up and spin-down densities.

The generalised gradient approximation showed some strides in describing the properties of material systems, however, the exchange potential lacked correct qualitative behaviour [53]. These inaccuracies, in both local density approximation and generalised gradient approximation, inspires a search for accurate functionals, hence there exist several flavours of these functionals for both local density approximation and generalised gradient approximation.

An improvement on GGA resulted in meta-GGA functionals. This functional involves higher order of the density derivatives. The information about the system is gathered from $n(r),\nabla n(r),\nabla^2 n(r)$. This means, the Laplacian of the density has the same physical description of the system as the kinetic energy density τ of the Kohn-Sham orbitals given by [47]:

$$\tau(r) = \tfrac{1}{2}\sum_{i}\left|\nabla\varphi_i(r)\right|^2 \qquad (3.33)$$

In other words, these functionals may use $\tau(r)$ in place of $\nabla^2 n(r)$. An example of a meta-GGA functional is a parameter-free functional referred to as Tao-Perdew-Staroverov-Scuseria (TPSS).

Another variation of the exchange-correlation function is the hybrid functional approximation [54]. This approximation is a combination of the orbital-dependent Hartree-

Fock energy and the DFT energies. That is, the hybrid functional can be given by a combination such as [55]:

$$E_{XC}^{half} = \tfrac{1}{2}(E_X^{HF} + E_{XC}^{DF}) \tag{3.34}$$

where E_X^{HF} is the Hartree-Fock exact exchange energy and E_{XC}^{DF} is the exchange-correlation energy of the Density Functional Theory. The Hartree-Fock exact exchange energy in terms of the orbitals is given by [54]:

$$E_X^{HF} = -\tfrac{1}{2} \sum_{ij\sigma} \iint \frac{\varphi_{i\sigma}^*(r)\varphi_{j\sigma}(r)\varphi_{j\sigma}^*(r')\varphi_{i\sigma}(r')}{|r-r'|} \, dr dr' \tag{3.35}$$

The most outstanding characteristic about the hybrid functionals is that they are non-local. That is, their evaluation is not at one specific spatial place. The most common and widely used hybrid functional is the B3LYP [54]. It is a combination of several energies that include the exchange-correlation of the local density approximation, Hartree-Fock exchange, Becke exchange, Lee-Yang-Parr (LYP) correlation, and Vosko-Wilk-Nusair (VWN) correlation. That is, this hybrid functional is expressed as follows [54]:

$$E_{XC}^{B3LYP} = (1-a)E_{XC}^{LDA} + aE_X^{HF} + bE_X^{Becke} + cE_C^{LYP} + (1-c)E_C^{VWN} \tag{3.36}$$

where a, b, and c are universal parameters. However, the B3LYP hybrid functional has a wide usage in the field of chemistry since it lacks accuracy for extended systems. Hence, the mostly used parameter-free hybrid functionals for material systems are Perdew-Wang 91 (PW91) and Perdew-Burke-Ernzerhof (PBE) functionals since they accurately approximate the exchange-correlation potential energy [47]. The PBE functional is a non-empirical functional with reasonable accuracy over a wide range of systems, while it is typically not the most accurate GGA functional for a given system, it is also not too far off either. The popularity of hybrid functionals emanates from their better approximation of the gap energy of many systems compared to both local density approximation and generalised-gradient approximation [54].

3.7 Treating the van der Waals (vdW) interaction

The van der Waals force may be defined as a weak force that exists in both finite and infinite material systems. It has a potential to influence the physical and chemical properties of these systems. It originates from the correlation of the electrons that are long-ranged, and have induced polarisation in the entities of the material system. However, other type of forces also exists between the entities of the material system, this may include forces such as the Keesom force, which is a force between two permanent dipoles; the Debye force, which is

a force between a permanent dipole and an induced dipole; and the London force, which is a force between two induced dipoles [56].

Density functional theory, as a technique that has successfully modelled the electronic structure of many material systems, fails to describe the effects of the van der Waals forces in these systems. This means, both the local density approximation and the generalised gradient approximation of the standard density functional theory treats weak interactions poorly [57]. This shortcoming, which may lead to inaccurate results of properties of material systems, may be overcome by developing approximate forms of the exchange-correlation energy that regards the effects of van der Waals forces.

Several functions have been developed to account for the effects of the van der Waals forces that are found between weak electron regions of the material systems. Popular vdW forces often employed to account for dispersion in DFT calculations include DFT-D, TS-vdW, Becke-Johnson, RPA and vdW-DF. The last one is called van der Waals density functional theory. The mathematical formulation of the aforementioned vdW functionals are described extensively in Ref. [56,58]. In this work, we have used the vdW-DF where necessary. In this method, the dispersion interactions are obtained directly from the electron density, not from predetermined input parameters [58]. Thus, the vdW-DF approach does not rely on empirical, semi-empirical, and special assumptions [56]. Another formulation of vdW-DF is known as vdW-DF2. The latter improves the description of binding in weak vdW systems. In this thesis, the vdW-DF method was used in the calculations involving the absorption of vanadium dimers on silicene sheet.

3.8 The planewave approach to solving density functional theory

3.8.1 Bloch's theorem

Bloch's theorem describes the periodicity of the crystal lattice. It informs that the probability of finding an electron is the same everywhere on the crystal lattice. In other words, it informs about the form of the electronic wavefunction when subjected to a periodic potential of the crystal lattice, which in turn, helps in the categorisation of material systems. The statement of the theorem is as follows [59]:

The eigenstates φ of the one-electron Hamiltonian is given by:

$$H = -\frac{\hbar^2 \nabla^2}{2m} + U(r) \tag{3.37}$$

where

$$U(r+R) = U(r) \tag{3.38}$$

for all R in the Bravais lattice.

3.8.2 Planewave basis set

A basis set is a set of functions that are linearly combined to create atomic orbitals around atoms. A planewave may be defined as waves whose wavefronts are parallel planes far away from the source [60]. Planewave basis set approach is one of the methods, among many others, that are used to solve Kohn-Sham (KS) equations. Solving KS equations using planewave approach is preferred due to the following reasons [55]:

- It is used with ease for extended systems with periodic boundary conditions.
- It uses complete, mutually orthogonal, and unbiased basis functions to any atom.
- It uses one criterion for a smooth and monotonic convergence.
- It allows integrals, derivatives, and other mathematical operations to be computed with ease in the reciprocal space.
- It is independent of atomic positions, and treats all regions of space equally.

However, the planewave basis set method also exhibits the following disadvantages against other approaches [55]:

- It requires a large number of planewaves to achieve accuracy.
- Its calculations are inclusive of empty space.

The planewave basis set is able to describe valence charge density when used with pseudopotentials. This is so because the core electrons produce very large electronic wavefunctions and density gradients around the nuclei that are difficult for the planewave basis set to describe [55].

Many extended material systems such as crystal structures and surfaces are periodic in nature. That is, these systems are comprised of infinite repeated unit cells. Hence, according

to Bloch's theorem, the charge density is periodic, thus making the calculation of the electronic wavefunction in a single unit cell to be sufficient. This electronic wavefunction $\varphi_{nk}(r)$, can be expressed as a product of a planewave and a periodic cell. That is:

$$\varphi_{nk}(r) = u_{nk}(r)e^{ik \cdot r} \tag{3.39}$$

where the first factor on the right-hand side of equation (3.39) is the periodic part with a periodicity of the lattice given by:

$$u_{nk}(r) = u_{nk}(r+R) \tag{3.40}$$

where R is a lattice vector. The second factor is the planewave part (phase factor) with a wavevector k that reside in the reciprocal lattice. This wavevector k specifies all possible states in the Brillouin zone.

The electronic wavefunctions at each k point can be expanded in terms of a discrete planewave basis set to a maximum of a reciprocal lattice vector G. That is [55]:

$$\varphi_{nk}(r) = \sum_{G=0}^{\infty} c_{nk}(G)e^{i(k+R) \cdot r} \tag{3.41}$$

where c_{nk} is the coefficient of the planewaves. The determination of these coefficients describes the electronic wavefunction. However, only coefficients with kinetic energies that are smaller than some particular cut-off energy E_{cut} are required. In other words, planewaves with energies higher than E_{cut} will have zero coefficients, and be rejected. This means that only planewaves with energies that satisfy the following condition will not be truncated [55]:

$$\tfrac{1}{2}\left|k+G\right|^2 \leq E_{cut} \tag{3.42}$$

A systematic increase in E_{cut} lead to a converged total energy of the system, which helps in avoiding an error in these computations [48].

When the periodic part of equation (3.39) is Fourier transformed, the wavefunctions have contributions associated to the reciprocal lattice vectors G, and the phase factor is incorporated into the definition of basis functions, which become dependent on the particular point in the Brillouin zone, then equation (3.41) may be written as,

$$\varphi_{nk}(r) = \sum_{G=0}^{\infty} c_{nk}(G)\phi_G^k(r) \tag{3.43}$$

where $\phi_G^k(r)$ are the basis functions.

However, for practical calculation of Kohn-Sham equations in an atomic basis, we define equation (3.28) as the single particle Hamiltonian, that is

$$H_s \varphi_i(r) = \varepsilon_i \varphi_i(r) \tag{3.44}$$

Putting equation (3.43) into equation (3.44), and multiplying the left of equation (3.44) by the complex conjugate of the basis functions, that is $\phi_G^{k^*}(r)$, and integrating over the region r, then equation (3.44) may be treated as an eigenvalue problem of the form,

$$(H_s - \varepsilon_i S_m) c_{nk} = 0 \tag{3.45}$$

where H_s are the elements of the Kohn-Sham Hamiltonian matrix, and S_m are elements of the overlap matrix. For purposes of integration in the irreducible wedge of the Brillouin zone, equation (3.45) is solved at each k-point. The Kohn-Sham orbitals may be represented by other several basis sets, such as the Linear Combination of Atomic Orbitals, Gaussians Type Orbitals and Slater Type Orbitals, however, in this thesis, planewave basis sets were used based on the advantages and disadvantages stated in this subsection.

3.8.3 k-point sampling in the Brillouin zone

The electronic wavefunctions of periodic material systems are allowed at certain sets of k-points. These sets of k-points are in the Brillouin zone (BZ) of the reciprocal lattice, and are dependent on the boundary conditions of the bulk solid. The density of these k-points is also dependent on the volume of the solid [48]. The Bloch's Theorem, which confirms the translational symmetry in periodic material systems, transforms the calculation of an infinite number of electronic wavefunctions to one of calculating a finite number of electronic wavefunctions at an infinite number of k-points in a single unit cell.

Considering the infinite number of calculations that needs to be done at different k-points in the Brillouin zone, makes this advancement to be of little value. However, the electronic wavefunctions that are at the k-points that are very close to each other appear alike [48]. The calculations of the properties of material systems, such as electronic energy bands, density of states, and projected density of states, takes the integration of all filled electronic wavefunctions in the Brillouin zone. However, this is not necessary, since it is possible to represent the electronic wavefunctions in the Brillouin zone with the wavefunctions at a single k-point. This means that these integrals may be replaced by a finite sample of k-points in the Brillouin zone, referred to as special points. In other words, the integration in the

Brillouin zone may be represented by a discrete sum over the chosen N_{kpt} k-points mesh, and is given by [61]:

$$\frac{\Omega_C}{(2\pi)^3}\int_{BZ}\Theta\left(E_F-\varepsilon_{kj}\right)dr = \frac{1}{N_{kpt}}\sum_k f_{kj} \qquad (3.46)$$

where Ω_C is the cell volume, $\Theta\left(E_F-\varepsilon_{kj}\right)$ is a filling factor that denotes the occupation of the state, f_{kj} are occupation numbers which are either one or zero, E_F is the Fermi level, ε is the eigenvalue, and k is the wavevector.

Monkhorst and Pack method, together with the Cohen and Chadi method [62], are some of the methods that are used to generate these fewest possible k points that give accurate approximation to the full integration of the k-points in the Brillouin zone. These k-points, when sufficiently sampled, may lead to an accurate approximation of the total energy of the material system. The uniform distribution of the sampled k-points in the Brillouin zone is asserted by a relation given by [63]:

$$k_j = x_{1j}b_1 + x_{2j}b_2 + x_{3j}b_3 \qquad (3.47)$$

where b_1, b_2 and b_3 are the reciprocal lattice vectors, while x_{ij} is given by [63]:

$$x_{ij} = \frac{\ell_i}{n_j} \qquad (3.48)$$

where ℓ_i is the reciprocal lattice vector length, and n_j is the number of special points.

As much as the converged results of the material system may be obtained by varying the density of the sampled k-points [62]. However, material systems such as semiconductors and insulators, need very few k-points sampling. Moreover, the computational cost is minimal, as this increases linearly with the number of k-points [62].

3.9 The pseudopotential method

The electronic wavefunctions may be expanded by planewave basis set according to Bloch's theorem [48]. However, the planewave basis set is not necessarily sufficient to expand the wavefunctions, because the expansion of the core electrons wavefunctions and the rapid oscillations of the valence electrons wavefunctions due to the strong ionic potential into the core electron space, requires lots of planewaves. The introduction of pseudopotential (PS)

approximation appears to overcome this challenge by using very few planewaves to expand the electronic wavefunctions.

The pseudopotential approximation involves the freezing of the core electrons and the nuclei. The freezing of the core electrons has no effect on the atom when placed in any environment, since these are chemically inert. The removal of the core electrons and the strong ionic potential is substituted by a weak pseudopotential that acts on pseudo-wavefunction instead of all electron wavefunctions. Within some core cut-off radius r_c, the pseudopotential approximation generates pseudo-wavefunction that have no radial nodes, and the pseudopotential that does not diverge at zero. However, outside the core cut-off radius r_c, the real electron wavefunctions, the pseudo-wavefunction, and the pseudopotential are the same. A pseudopotential with a larger core cut-off radius r_c, thus converging rapidly, is referred to as soft. This means, this is a pseudopotential that uses very few planewaves.

A pseudopotential is referred to as transferable provided that it may be used reliably regardless of the environment it is exposed to. Figure 3.1 shows the schematic illustration of the real potential and real wavefunction, and the corresponding pseudopotential and pseudo-wavefunction.
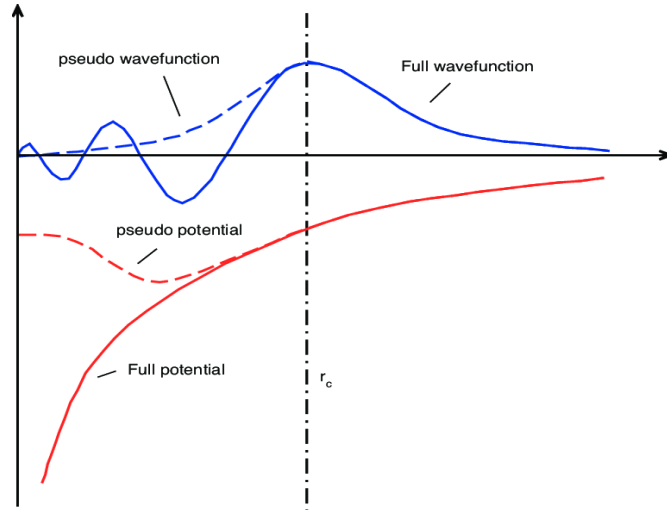
Figure 3.1: Depiction of real potential and real wavefunction, and the corresponding pseudopotential and pseudo-wavefunction [64].

The general form of the non-local (NL) pseudopotential is given by [48]:

$$V_{NL} = \sum_{\ell m} |\ell m > V_\ell < \ell m|$$

(3.49)

where ℓm are spherical harmonics and V_ℓ is the pseudopotential for angular momentum ℓ.

Equation (3.49) describes the decomposition of electron wavefunction into spherical harmonics, such that each of the spherical harmonics is multiplied by the necessary pseudopotential. Moreover, a local pseudopotential is, by definition [48], a potential that uses the same potential for all the angular momentum of the wavefunction. The existence of local and non-local pseudopotentials leads to different types of pseudopotentials such as norm conserving and ultrasoft pseudopotential (USPP). These different types of pseudopotentials are a result of the comparison of the unreal electron density with the real electron density, within and outside the core cut-off radius r_c.

3.9.1 Norm-conserving pseudopotential

Generating a pseudopotential that is both soft and transferable is no small feat [55]. This is so because a pseudopotential improvement on transferability requires the core cut-off radius r_c to be small, while an improvement on softness property requires that the core cut-off radius r_c to be large [61]. In order to achieve these properties, resulted in the following criteria for the construction of the norm-conserving pseudopotential [48]:

- The eigenvalues of the pseudo-wavefunction must be equal to those of the all-electron (AE) wavefunction.
- The radial pseudo-wavefunction must possess no nodes. Also, the core cut-off radius r_c must never be smaller than the outermost node of the all-electron wavefunction.
- The pseudopotential must satisfy the norm conservation condition. This means that inside the core cut-off radius r_c, both the all-electron and pseudo-wavefunctions must have the same norm to ensure equal generation of electron densities by both the all-electron and pseudo-wavefunctions outside the core cut-off radius r_c. That is [55]:

$$\int_0^{r_c} \left|\varphi^{PS}(r)\right|^2 dr = \int_0^{r_c} \left|\varphi^{AE}(r)\right|^2 dr \tag{3.50}$$

Equation (3.50) may also be written as:

$$\left\langle \varphi_{R,i} \middle| \varphi_{R,j} \right\rangle - \left\langle \varphi'_{R,i} \middle| \varphi'_{R,j} \right\rangle = 0 \tag{3.51}$$

where $\varphi_{R,i}$ and $\varphi'_{R,i}$ are all-electron wavefunction and pseudo-wavefunction of atom R, respectively.

- Both the normalised radial pseudo-wavefunction and the normalised all-electron wavefunction must be equal outside the core cut-off radius r_c.

When the full pseudopotential operator, $\hat{V}^{PS}$, is applied to any wavefunction it acts as a non-local operator, and gives [61]:

$$\hat{V}^{PS} = V_{loc}^{PS} + \sum_{\ell} V_{nl,\ell}^{PS}(r)\hat{P}_{\ell} \tag{3.52}$$

where $V_{loc}^{PS}(r)$ is the local pseudopotential of one specific angular momentum ℓ, the second term on the right side of equation (3.52) is defined as the non-local component of the pseudopotential, and $\hat{P}_{\ell}$ is the projector on to some angular momentum and radial state of the wavefunction. The non-local pseudopotential $V_{nl,\ell}^{PS}(r)$ is given as the difference between the original angular momentum depended pseudopotential and the local pseudopotential. That is:

$$V_{nl,\ell}^{PS}(r) = V_{\ell}^{PS}(r) - V_{loc}^{PS}(r) \tag{3.53}$$

The norm-conserving pseudopotential may be transferable to other environments. However, these are not as soft as desirable due to the required small core cut-off radius r_c [61].

3.9.2 Ultrasoft pseudopotential (USPP)

Many planewaves are required to accurately represent the wavefunction of the valence electrons that are localised within the core area, unfortunately, this requires ample computational time. Besides, the hardness of the norm conserving pseudopotentials due to a short core cut-off radius, resulted in the generation of Vanderbilt ultrasoft pseudopotentials [61]. This type of pseudopotentials involves the relaxation of the norm conserving constraint. That is, more complexity is put in the core by adding a smooth auxiliary function to the planewaves around each atom to represent the rapidly varying region of the density, thus permitting a larger core cut-off radius r_c. This approach results in the re-expression of an eigenvalue problem that is having a non-zero difference $Q_{R,ij}$ in norms compared to equation (3.51). That is:

$$\langle \varphi_{R,i} | \varphi_{R,j} \rangle - \langle \varphi'_{R,i} | \varphi'_{R,j} \rangle = Q_{R,ij} \tag{3.54}$$

According to equation (3.54), the electron density within the core cut-off radius r_c is different for both the all-electron and pseudo-wavefunction. However, outside the core cut-off radius

r_c, the all-electron wavefunction and pseudo-wavefunction are the same. Integration of this electron density and the usage of the orthonormality condition gives [55]:

$$\left\langle \varphi_i \middle| \hat{S} \middle| \varphi_j \right\rangle = \delta_{ij} \tag{3.55}$$

where $\hat{S}$ is a Hermitian operator, and is given by [55]:

$$\hat{S} = I + \sum_{R,ij} \middle| \hat{P}_{R,i} \right\rangle Q_{R,ij} \left\langle \hat{P}_{R,j} \middle| \tag{3.56}$$

where $\hat{P}_{R,i}$ are the projectors that are zero outside the core cut-off radius r_c, while within the core cut-off radius r_c, these projectors are forming dual basis with the reference pseudo-wavefunctions [55]. Figure 3.2 shows the relationship between the all-electron valence wavefunction and the pseudo-wavefunction of the Vanderbilt ultrasoft pseudopotential method [61].
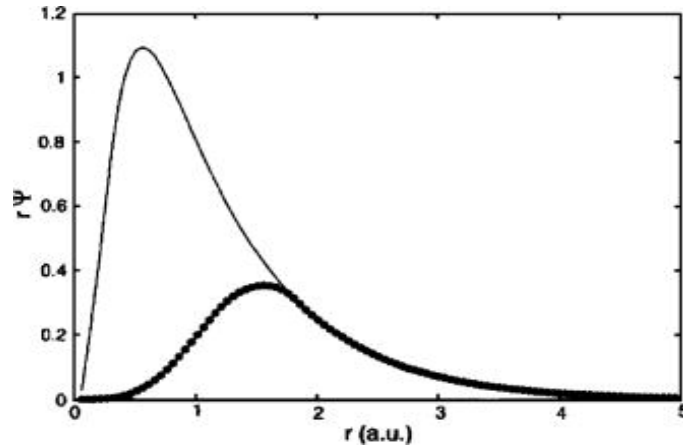
Figure 3.2: The relationship between the all-electron wavefunction (solid line) and the ultrasoft pseudo-wavefunction (dotted line) [65].

The criteria for constructing ultrasoft pseudopotentials is given as follows [55]:

- Outside the core cut-off radius r_c, the pseudo-wavefunctions and the all-electron wavefunctions must be the same, while inside the core cut-off radius r_c, the pseudo-eigenvalues and the all-electron eigenvalues must be equal.
- At each reference energy, correct scattering properties must be effected.
- The all-electron valence charge density must be equal to the modified valence charge density.

The advantage in adhering to these criteria result in the reduction of the number of planewaves used in effecting calculations. This is so because the Vanderbilt ultrasoft pseudopotential scheme uses only a small portion of the full valence wavefunctions to represent the planewaves [55], as indicated in figure 3.4. All calculations in this thesis used the ultrasoft pseudopotentials of the Vanderbilt type.

3.10 The supercell method

The task of modelling infinite material systems may be daunting, because these systems possess an infinite number of electrons. In order to simplify this daunting task, the supercell method is adopted to study the properties of these material systems. In this method, systems such as isolated atoms, point defects, voids, and dislocations are enclosed in a box, that is periodically extended in all spatial directions. However, each box, which represents a supercell, must be large enough so that the contents of each supercell do not interact with each other, otherwise this would result in the spurious interaction of the system with its periodic images. This interaction may occur in the following three ways; firstly, electronically, due to the overlapping of the system's wavefunctions; secondly, elastically, due to the atomic optimization around the system; and thirdly, due to Coulombic interactions between charged systems [66]. This means, from a region of a material system with an infinite number of electrons, a supercell was constructed, and periodic boundary conditions were applied to it, so that Bloch's theorem produces a supercell with a finite number of electrons. As a result of this method, properties of large material systems are being modelled and studied. However, the supercell method has some disadvantages. This includes, among others, that the artificial periodicity of the supercell may result in artificial interaction of the contents of the supercell. Secondly, the density used by the supercell method is finite and very lowly distributed, which may be construed as a misrepresentation of a true aperiodic physical material system. Lastly, this method shows to require a serious examination of the effects such as finite-size and periodicity [67].

3.11 Formation and binding energy of a defect

Defects have great potential in altering the properties of material systems. Hence, the calculation of defect formation and binding energies assists in determining preferred defect structures and the stability of given defect configurations in material systems, respectively. In this thesis, these energies were calculated using the supercell method within the density

functional theory technique. The defect formation energy may be calculated as follows [10,68-70]:

$$E_f = E_{defect} - E_{pris} - \sum n_i \mu_i + qE_F + E_{corr} \qquad (3.57)$$

where E_{defect} is the total energy of supercell containing the defect; E_{pris} is the total energy of pristine supercell, that is, without defect; n_i is the number of atoms of chemical species i, that are either added ($n_i > 0$) or subtracted ($n_i < 0$) from the supercell during defect creation, μ_i is the chemical potential of the species i, q is the charge of the defect, which are electrons that are either added ($q < 0$) or subtracted ($q > 0$) from the defected supercell, E_F is the Fermi energy, and E_{corr} is the correction term, that represents effects such as electrostatic interactions that result because of the usage of the supercell technique. The last two terms, that is, qE_F and E_{corr}, on the right-hand side of equation (3.57) are only relevant if the defect formation energy of charged systems are being considered, otherwise they are set to zero. A negative formation energy means that the material system is thermodynamically stable, while a positive formation energy means that the material system is unstable.

Also, binding energy may be defined as the difference between the energy of the system with defects and the sum of the components of the energy of isolated defects. That is [71]:

$$E_b = E_{defect} - \sum_{i=isol} E_i \qquad (3.58)$$

Here, E_{defect} is the total energy of a defect complex. The second term $\sum_{i=isol} E_i$ sums the total energy of isolated defects forming the defect complex whose energy is calculated by the first term on the right-hand side of equation (3.58). A negative binding energy suggests that the defect system is stable compared to the sum of the individual components of the isolated defects.

3.12 Magnetization energy

Magnetism may be defined as a phenomenon caused by the motion of electrons in an atom. The presence of a defect may introduce magnetization in an otherwise non-magnetic material. Also, a particular magnetization direction of the atoms may be preferred as the ground-state when a defect is present in the material. In collinear formalism, a

magnetization direction may be ferromagnetic (FM) or anti-ferromagnetic (AFM). In the former, the electrons spins are oriented in the same direction, while in the latter the electron orientations are in antiparallel direction. Both cases are shown in figure 3.3 (a) and (b), respectively:
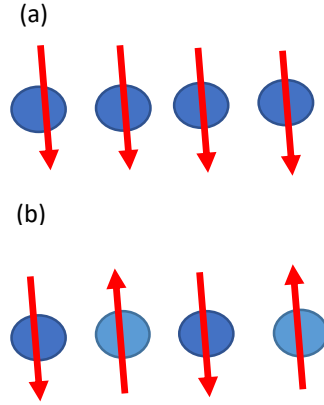
Figure 3.3: Schematic representation of magnetic orientation in an electron system. In the figure, (a) the ferromagnetic (FM) spin orientation, (b) antiferromagnetic (AFM) spin orientation. The blue sphere is the electron, while the red arrow shows the spin orientation.

The energy difference between the FM and AFM ordering state is referred to as the magnetic stabilisation energy, and it is given by [72,73]:

$$\Delta E = E_{FM} - E_{AFM} \tag{3.59}$$

where E_{FM} represent ferromagnetic energy, E_{AFM} represent anti-ferromagnetic energy. Positive ΔE means ferromagnetic ground state is preferred, and negative ΔE means anti-ferromagnetic ground state is preferred.

The parallel alignment of magnetic moments in ferromagnetic material systems is a result of a quantum mechanical effect referred to as exchange interaction [74]. This means, neighbouring magnetic moments influences one another to adopt a particular magnetic ordering state. In the case of ferromagnetism, the parallel alignment of magnetic moments is a result of Pauli's exclusion principle, which prohibits the occupation of the same orbital by electrons with the same spin. Hence, the two electrons with parallel spins, of the neighbouring magnetic moments, are compelled to move further apart due to Coulomb's repulsive interaction. Moreover, ferromagnetism takes place in systems that have nonzero total magnetic moment due to partially filled orbitals. That is, Hund's rule plays a role in increasing the total magnetic moment of ferromagnetic systems, for it allows the pairing of electron spins after the filling of one electron spin to each orbital.

As state above, antiferromagnetic behaviour in material systems may be perceived as the antiparallel alignment of spins of electrons of neighbouring magnetic moments of atoms. In other words, in this magnetic ordering, the magnetic moments are arranged in an alternating pattern with opposing spins. No magnetic field may result in antiferromagnetic material systems, for the magnetic moments cancel each other out, thus giving a zero total magnetic moment for the system. The antiferromagnetic property may disappear above the Néel temperature in these material systems due to thermal perturbations, and exist again below these temperatures. In the case of antiferromagnetism, the antiparallel alignment of magnetic moments respect Pauli's exclusion principle, which allows the occupation of the same orbital by electrons with different spins. Hence, the two electrons with antiparallel spins, of the neighbouring magnetic moments, are compelled to move closer together, thus enhancing Coulomb's interaction.

3.13 The quantum-ESPRESSO (QE) package

Quantum-ESPRESSO (QE) [75,76] is a high-performance code for first-principles electronic structure calculations. It implements planewave formalism to solve the density functional theory. Also, the code uses norm-conserving, ultrasoft, and projector-augmented waves (PAW) pseudopotentials as inputs to describe the interactions between the nuclei and the electrons. The QE code has the capability of executing the following computations, among many others [76]:

- Ground-state energies and single-electron Kohn-Sham orbitals of isolated and periodic systems.
- Complete structural optimization of atomic co-ordinates and unit cells using Hellmann-Feynman forces and stresses.
- Ground-state energies of magnetic or spin-polarised systems.

Quantum-ESPRESSO consists of several modules which performs various functions. Examples are [76]:

- Plane-Wave Self-Consistent Field (PWscf)- which calculates ground-state energy, Kohn-Sham orbitals, structural optimisation, etc.

34

- Post Processing (PostProc)- which calculates various quantities that helps in results analysis, such as density of states (DOS) and projected density of states (PDOS)

The code uses the XCrySDen (X Window Crystalline Structures and Densities) [77] program to visualise crystal structures with input data files from PWscf.

3.13.1 Band structure

Solids are composed of electrons interacting with nuclei. The nature of interacting electrons and nuclei gives materials its properties, such as metallic, semiconducting or insulating. Hence, an understanding of this behaviour by electrons will assist in the comprehension of properties of any material system. A way to understand the properties of material systems is by the construction of its band structure (BS). In other words, the arrangement of electrons in energy levels in a material system can be expressed as energy bands which determines its properties. The band structure of materials is formed by the allowance and non-allowance of the energy of the quantum mechanical wavefunction of an electron that is in a periodic lattice of the material system. That is, the band is the range of energies that the wavefunction of an electron is allowed to possess, while the energy gap or band gap is the range of energies that the electron wavefunction is not allowed to possess [78]. The band gap is actually the result of the Bragg reflection of the electron wavefunction in a material system after failing to satisfy the Bragg condition [78]:

$$2k \cdot G = G^2 \tag{3.60}$$

where k and G are the wavevector and lattice vector in reciprocal space, respectively.

The reciprocal lattice may be defined as the set of wavevectors that yield plane waves with the same wavelength corresponding to the periodicity of the direct lattice. Material systems have both direct and reciprocal lattices. The relationship between these two lattices is defined by the following equations [78]:

$$b_1 = 2\pi \frac{a_2 \times a_3}{a_1 \cdot a_2 \times a_3} \tag{3.61}$$

$$b_2 = 2\pi \frac{a_3 \times a_1}{a_1 \cdot a_2 \times a_3} \tag{3.62}$$

$$b_3 = 2\pi \frac{a_2 \times a_3}{a_1 \cdot a_2 \times a_3} \tag{3.63}$$

35

where a_1, a_2 and a_3 are the primitive vectors of the direct lattice, and b_1, b_2 and b_3 are the primitive vectors of the reciprocal lattice.

This indicates that the primitive direct and reciprocal lattice vectors have the property that [78]:

$$b_i \cdot a_j = 2\delta_{ij} \tag{3.64}$$

where $\delta_{ij} = 1$ if $i = j$ and $\delta_{ij} = 0$ if $i \neq j$

Any two direct lattice points are connected by the following set of vectors [78]:

$$T = u_1 a_1 + u_2 a_2 + u_3 a_3 \tag{3.65}$$

where u_1, u_2 and u_3 are integers. Similarly, any two reciprocal lattice points can be mapped by the following relationship [78]:

$$G = v_1 b_1 + v_2 b_2 + v_3 b_3 \tag{3.66}$$

where v_1, v_2 and v_3 are integers.

The real space primitive translation vectors of the hexagonal lattice such as silicene are given by [78]:

$$a_1 = \frac{\sqrt{3}a}{2}\hat{x} + \frac{a}{2}\hat{y} \tag{3.67}$$

$$a_2 = -\frac{\sqrt{3}a}{2}\hat{x} + \frac{a}{2}\hat{y} \tag{3.68}$$

$$a_3 = c\hat{z} \tag{3.69}$$

and the reciprocal space primitive translation vectors are given by [78]:

$$b_1 = \frac{2\pi}{\sqrt{3}a}\hat{x} + \frac{2\pi}{a}\hat{y} \tag{3.70}$$

$$b_2 = -\frac{2\pi}{\sqrt{3}a}\hat{x} + \frac{2\pi}{a}\hat{y} \tag{3.71}$$

$$b_3 = \frac{2\pi}{c}\hat{z} \tag{3.72}$$

while the volume of its primitive direct cell is given by [78]:

$$V = \frac{\sqrt{3}}{2}a^2 c \tag{3.73}$$

The band structure plots are accomplished through reciprocal lattice vectors and high symmetry points in the Brillouin zone (BZ). Brillouin zone is the primitive unit cell of the reciprocal lattice. It is a region in reciprocal space that is closer to the reference lattice point than any other reciprocal lattice point. The Brillouin zone of a material system is shown in figure 3.4. The Brillouin zone is the Wigner-Seitz cell of the direct lattice. It is also constructed by drawing lines that connect a particular lattice point of the reciprocal lattice, which is considered as a centre point to all nearby lattice points. The Bragg planes are then drawn at the midpoint and normal to these lines that are from the central point. All the k vectors that terminate at the Bragg planes satisfy the Bragg condition of equation (3.60). The first Bragg reflections and the first energy gap are occurring at the boundary $k = \pm\pi/a$ in one-dimension, where a is the primitive axis of the direct lattice.
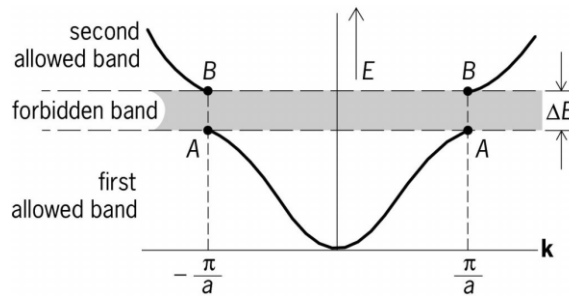
Figure 3.4: Energy bands of a material system [79].

The higher Brillouin zones, such as the nth Brillouin zone, are constructed from the original central lattice point of the first Brillouin zone to the crossing of the $(n-1)$ Bragg plane at the boundary $k = \pm n\pi/a$, where n is an integer. Thus, the band structure may be viewed as a map showing the allowance and non-allowance of the quantum mechanical wavefunctions of electrons in a periodic lattice of a particular material system following certain high symmetry paths within the Brillouin zone. These paths are joined by high symmetry points. Hence, within the Brillouin zone of the hexagonal reciprocal lattice such as silicene, the high symmetry points are labelled as follows [80]:

Γ – Centre of the Brillouin zone.
A – Centre of a hexagonal face.
H – Corner point.
K – Middle of an edge joining two rectangular faces.
L – Middle of an edge joining a hexagonal and a rectangular face.

M – Centre of a rectangular face.

These are shown in figure 3.5.
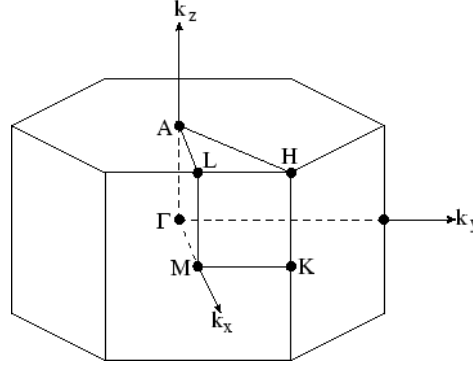
Figure 3.5: High symmetry points of the hexagonal reciprocal lattice such as silicene [80].

Examples of coordinates of high symmetry points of hexagonal reciprocal lattice, expressed in Cartesian co-ordinates are [81]:

$$\Gamma = \frac{2\pi}{a}[0,0,0] \tag{3.74}$$

$$M = \frac{2\pi}{a}\left[0,\frac{1}{\sqrt{3}},0\right] \tag{3.75}$$

$$K = \frac{2\pi}{a}\left[\frac{1}{3},\frac{1}{\sqrt{3}},0\right] \tag{3.76}$$

Thus, details of the reciprocal lattice vectors and high symmetry points are necessary to plot the band structure of a material system. This plot shows a relationship between the energy of an electron wavefunction and the wavevector. As examples, the band structures of graphene and silicene were shown in Figure 2.2 of Chapter 2, respectively. Thus, it can be construed that the properties of material systems are contained in the band structure and are described by the Brillouin zone. In the QE code, calculations of the BANDS are performed as follows:

- Self-consistent field (SCF) calculation where the executable "pw.x" is used.
- Bands calculation performed using the "pw.x".
- Plotting of bands using the "bands.x" executable.

3.13.2 Density of states and projected density of states

The electronic density of states (DOS) of a material system may be described as the number of different states that electrons may occupy at a particular energy level. In other words, this is the number of electron states per unit volume per unit energy. A high density of states at a particular energy level means a high number of states available for occupation by electrons at that particular energy level. On the other hand, this implies that, zero density of states means that no states are available for occupation by electrons. Moreover, it is observed that, in a symmetrical density of states, where the number of spin ups and downs is the same, implies zero total magnetic moment, thus the material system possesses no magnetism. However, in the case of an asymmetrical density of states, where the number of spin ups and downs are not the same, implies non-zero total magnetic moment, thus the material system possesses magnetism. This shows that, the density of states helps in determining the properties of material systems, such as metallicity, semi-conduction, and insulation.

Density of states are determined through the integration of the electronic density in the reciprocal space [47]. However, it is observed that these calculations require a large number of k points, and the energy is measured relative to Fermi energy instead of absolute energy during the plotting of graphs, that is, $E - E_f$. In the QE code, calculations of the DOS are performed as follows:

- Self-consistent field (SCF) calculation where the executable "pw.x" is used.
- Non-self-consistent field (NSCF) calculation performed using the "pw.x"
- Plotting of density of states using the "dos.x" executable.

Projected density of states (PDOS) may be described as the relative contribution of a particular atom or orbital to the total density of states. That is, it is the projection of the density of states of particular orbitals of particular atoms. Projected density of states also helps in further understanding of properties of material systems, such as hybridization of orbitals of atoms in a material system, and its magnetization. In the QE code, the PDOS calculations is performed as follows:

- Self-consistent field (SCF) calculation with the "pw.x" executable.

- Non-self-consistent field (NSCF) calculation with the "pw.x" executable
- Plotting of projected density of states with the "projwfc.x" executable.

3.13.3 Description of density functional theory calculations

The computational procedure in calculating the total energy of a material system is shown in the flow chart of figure 3.6. The procedure starts by guessing an initial electronic charge density $n_0(r)$ that will give the Hartree potential and exchange-correlation potential. These potentials enable the solving of the Kohn-Sham equations with the initial electronic charge density $n_0(r)$ so that the single-electron wavefunctions may be obtained. These single-electron wavefunctions will generate a new electronic charge density $n(r)$. The new electronic charge density $n(r)$ is compared to the initial electronic charge density $n_0(r)$. When the two electronic charge densities are the same, this would mean that the ground-state electron density has been found, and as such, the ground-state total energy of the material system can be calculated. However, when the two electronic charge densities are different, the procedure is re-started with another guess of the electronic charge density until these two electronic charge densities are self-consistent. In this thesis, density functional theory was used that solved the Kohn-Sham equations through the plane-wave pseudopotential approach, as implemented in the Quantum Espresso code.
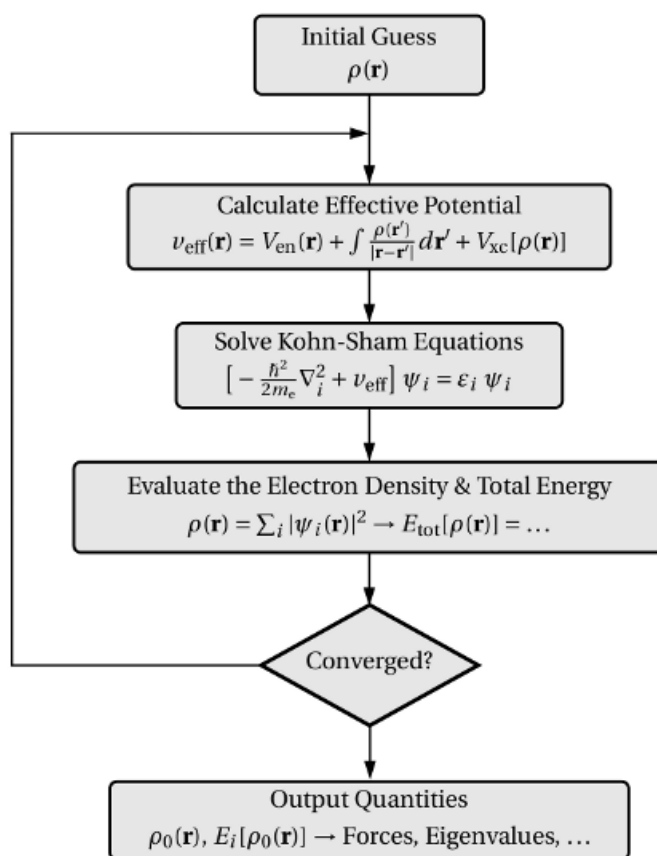
Figure 3.6: A flow chart of the iteration scheme [82].

3.14 Successes and failures of density functional theory

Density functional theory has successfully made significant strides in a variety of fields, such as in catalytic processes, transportation of electrons, conversion of solar energy, and designing of drugs for medicinal purposes [83]. The successes and failures of density functional theory are based on the exchange-correlation functional. That is, if this functional was exactly known, then the quantum mechanics of any system would be perfectly described. However, since this functional is approximated in order to find the ground-state total energy of systems, renders the application of this theory to systems to have limitations.

The density functional theory calculates bond lengths of molecular systems to less than 2% accuracy compared to experimental data, while the vibrational frequencies of these systems are overestimated by less than 5% [48]. The simplest exchange-correlation functional, the local density approximation, overbinds molecules by about 1eV/bond, which is too large an error for applications. An improved version of local density approximation, that depends on the gradient of the density, the generalised gradient approximation, overbinds molecules

by about 0.3eV/bond. The third standard approximation, the hybrid functionals, that mixes the exact exchange energy with generalised gradient approximation, improves this overbinding in molecules by another factor of 2. Using hybrid functionals, the density functional theory estimates the ionisation and affinity energies to around 0.2 eV compared to experimental data [54].

The density functional theory underestimates the band gaps of semiconductors and insulators, however, hybrid functionals give better estimates compared to experimental data. Since generalised gradient approximation largely reduces overbinding, hence, it is recommended for absorption energy calculations [48]. Density functional theory fails to perfectly treat systems with strong electron-electron correlation. Moreover, the density functional theory also fails to treat weak interacting systems of materials, because the effect of van der Waals forces are not catered for in the exchange-correlation functionals [83].

CHAPTER 4

Pristine silicene: structural and electronic properties

The fundamental structural, electronic and magnetic properties of pristine silicene are determined here. However, prior to that we present convergence studies wherein we determined calculation parameters such as the kinetic energy of the wave function, energy and charge density cut-offs. The convergence studies are performed with a 2-atom unit cell of silicene. The Vanderbilt ultrasoft pseudopotentials (USPP) [84] have been used to describe the nuclei of silicon, while the generalised gradient approximation (GGA) of the type given by Perdew, Burke and Ernzerhof (PBE) [51,85] is used for the exchange-correlation potential. The choice for this parameter-free functional is based on the accuracy that it gives in producing both structural and electronic properties for a wide range of systems [86]. In the present work, the USPP [84] used for silicon was taken from the original quantum-ESPRESSO pseudopotentials library [76] and is named "Si.pbe-n-van.UPF". All the atomic systems were geometrically relaxed using the Broyden-Fletcher-Goldfarb-Shanno (BFGS) method [87-90], with the total energy convergence threshold of 1 meV, while the Brillouin zone (BZ) was sampled using the Monkhorst-Pack (MP) grid k-points. The Marzari-Vanderbilt-Devita-Payne cold smearing method [91] was used as a smearing scheme. For most of the post-processing calculations involving non-self-consistent field calculations such as the density of states (DOS) and the projected density of states (PDOS), MP grid of higher density (that is, relative to the converged values) was used. Also, the tetrahedron method was used for the BZ integration [92]. We have used a smearing width of 0.03 eV throughout, for the DOS and PDOS. Furthermore, the XCrySDen (X Window Crystalline Structures and Densities) software [77] was used for the visualization of geometrical structures of all the atomic systems.

4.1 Convergence studies

The purpose of convergence studies in DFT calculations is to determine the appropriate value of parameters which shall enable the accuracy and quick convergence of our calculations. Such parameters include k-point grid, energy, charge density cut-off and smearing. The convergence studies were conducted using a 2-atoms silicene unit cell with theoretical lattice constant of 3.86 Å [20]. This configuration was used to obtain the

convergence of the kinetic energy cut-off (E_{cut}) and the k-point grid (n_k). Figure 4.1 (a) shows the result of convergence test for E_{cut}. This figure shows that the energy does not change by more than 1 meV beyond 50 Ry (680 eV) kinetic energy cut-off. Also, figure 4.1 (b) shows the convergence test for k-points grid. The n_k selected for the plot was 18×18×1.
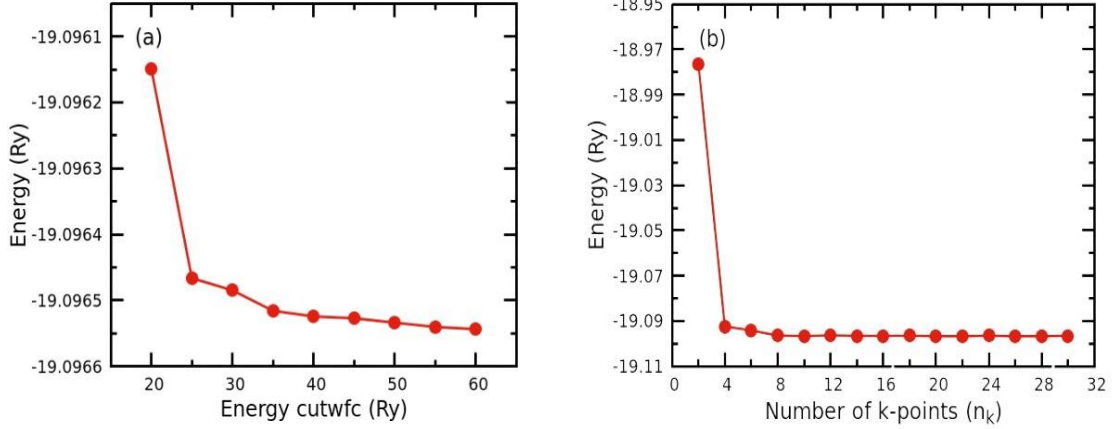
Figure 4.1: (a) Convergence test for kinetic energy cut-off, (b) Convergence test for k-points grid. The connecting lines are guide to the eye.

4.2 Basic structural parameters of pristine silicene

Figure 4.1 (c) shows the calculation of the lattice parameters of silicene using the obtained converged E_{cut} and n_k, which are 50 Ry and 18×18×1, respectively. In this figure, it is observed that the equilibrium lattice constant of 3.88 Å gives the minimum energy, which is 0.52% greater than the value of 3.86 Å obtained in theoretical studies by Takeda and Shiraishi [20]. The difference in the values may be attributed to the difference in calculation parameters used such as the pseudopotential, exchange-correlation potential energy and plane waves kinetic energy cut-off. Ref. [20] used the norm-conserving pseudopotential of Hamann, Schluter and Chiang [93], and of Bachelet, Hamann and Schluter [94], while we used Vanderbilt ultrasoft pseudopotential. Also, Ref. [20] used local density approximation with a functional form given by Ceperley and Alder [95], but parametrized by Perdew and Zunger [96] as the exchange-correlation potential energy, while we used generalized gradient approximation given by Perdew, Burke and Ernzerhof as the exchange-correlation potential energy. Furthermore, Ref. [20] used planes waves with a kinetic energy cut-off of 12.25 Ry, while we used 50 Ry as the plane wave kinetic energy cut-off. Table 4.1 shows the comparison of our calculated structural parameters with other values obtained in the literature.
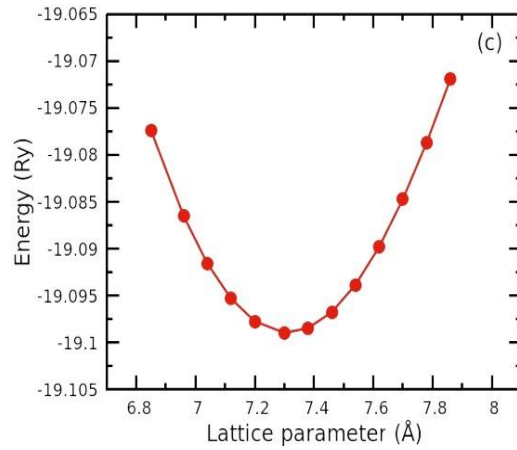
Figure 4.1(c): Calculated lattice parameter of silicene obtained using the converged E_{cut} = 50 Ry and k-grid points of 18x18x1.

Table 4.1: Calculated parameters of pristine silicene: lattice parameter a, bond length between adjacent silicene atoms $d_{Si\text{-}Si}$, bond angle between three adjacent silicene atoms $<S_iS_iS_i>$, buckling length, h.

Pristine silicene	a (Å)	$d_{Si\text{-}Si}$ (Å)	< $S_iS_iS_i$> (°)	h (Å)	Method
Theory (this work)	3.88	2.30	117	0.45	GGA
Theory (others)	3.88[a]	2.27[a]	117[a]	0.41[a]	GGA
	3.87[b]	2.28[b]	120[b]	0.44[b]	GGA
	3.87[c]	2.28[c]	116[c]	0.46[c]	GGA
Experiment		2.30[d]			

[a]Reference [4]
[b]Reference [97]
[c]Reference [98]
[d]Reference [99]

We found a good agreement between the experimental, our calculated values and other theoretical studies.

4.3 Electronic properties of pristine silicene

The electronic properties of pristine silicene are shown in Figures 4.2. Specifically, figure 4.2 (a) shows the calculated band structure of pristine silicene.
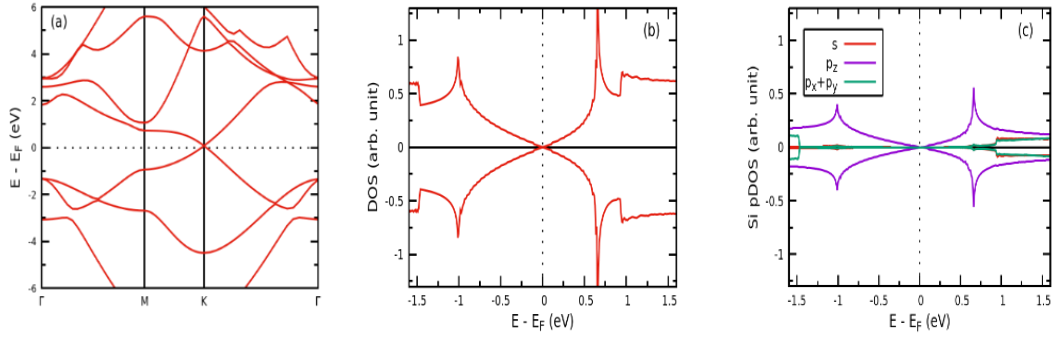
Figure 4.2: (a) Band structure of pristine silicene, (b) Density of states of pristine silicene, and (c) Projected density of states showing the *s* and *p* orbital of silicene atom. Fermi level is set at zero as shown by the black dashed line.

A prominent feature in this band structure is the presence of the valence and conduction bands that crosses one another quadratically at the Dirac point, which is the point of intersection of the K high symmetry point and the Fermi level (E_F). The crossing of π and π^* bands at this point in Figure 4.2 (a) indicates the absence of the band gap, thus rendering pristine silicene semi-metallic, mainly due to the contribution of the p_z electrons [97,98].

Figure 4.2 (b) shows pristine silicene to have zero density of states (DOS) at the Dirac point. It is also at this point that the electrons behave like massless Dirac-Fermions, thus giving pristine silicene to have a unique electron conductivity. Moreover, this figure also shows that the density of spin up states are the same as the density of spin down states. This suggest that partially filled orbitals are absent in silicene, hence the observed zero total magnetic moments, that is, a non-magnetic material. Also, figure 4.2 (c) is the spin-polarized projected density of states (PDOS) of silicene. As expected, the similarity in the spin-up and spin-down DOS confirms non-magnetism in silicene. Furthermore, figure 4.2(c) shows that the hybridization of silicene orbitals leans towards sp^2 rather than sp^3, thus giving sp^2/sp^3 mixed hybridization which results from buckling. Buckling makes the overlapping area of the p_z orbitals to be less [4].

4.4 Pristine silicene supercell

In the supercell approach, we repeated the primitive unit cell seven times along the *x* and *y* direction in order to minimize defect-image interaction. The size of the supercell used in this study therefore may be written as $7a \times 7a$ where *a* is the calculated silicene lattice

46

parameter of 3.88 Å. This supercell consists of 98 silicon atoms. Figure 4.3 (a) and (b) shows the top view and the side view of the supercell. This supercell is large enough to ensure that the interactions between periodic replicas of defects are minimized. This is based on the knowledge that, for neutral defects, the interaction between the periodic replicas decreases fairly quickly with increasing supercell size.
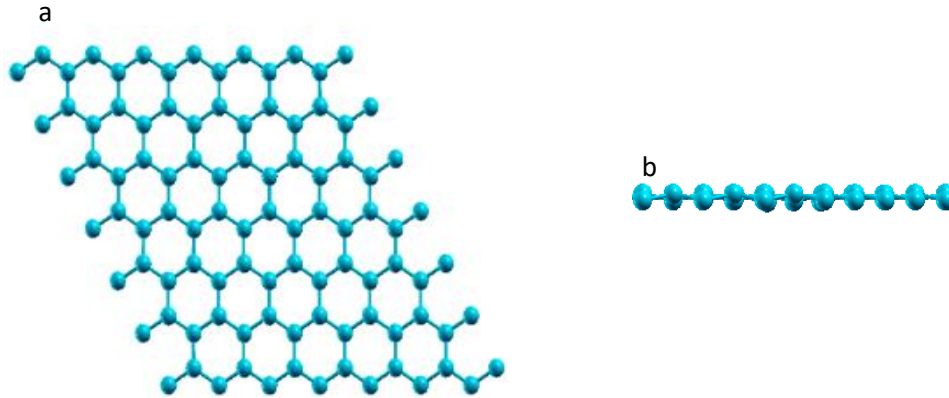
Figure 4.3: (a) Top view (b) Side view of relaxed spin-polarised configuration of pristine silicene. The blue spheres represent the silicene atoms.

To summarize, our calculations of the electronic and magnetic properties of pristine silicene are in excellent agreement with findings in the literature [4,16,98,100].

CHAPTER 5

Native defects in silicene

In the following, we determine the structural, electronic and magnetic properties of silicene containing:

•   Single and double vacancies.

•   Vacancy-vacancy complex.

For all the defect calculations, we have used the supercell of size $7a$ x $7a$ where a is the optimized lattice parameter of silicene unit cell as described in the previous chapter.

5.1 Single vacancy

5.1.1 Energetics and structural properties

A single vacancy silicene was considered and its electronic and magnetic properties were obtained as illustrated in figure 5.1.
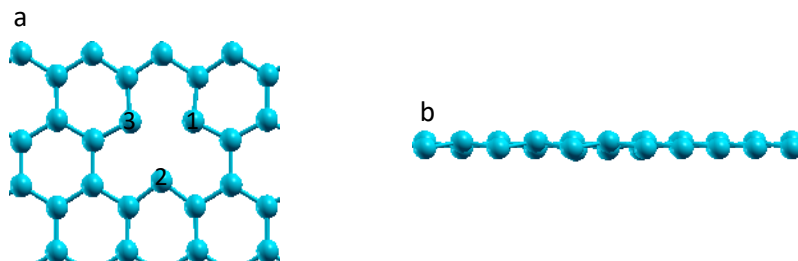
Figure 5.1: (a) Top view (b) Side view of relaxed spin polarised configuration of silicene with a single vacancy. The blue spheres represent the silicene atoms. Silicon atoms numbered '1', '2', and '3' are those carrying the dangling bonds, and are regarded as Si1, Si2 and Si3, as explained in the main text.

A vacancy is created by removing one silicene atom from the pristine 98-atoms silicene structure shown in Figure 4.3. A vacancy introduces three dangling bonds to the silicene lattice and these are indicated by numbers '1', '2', and '3' in figure 5.1. We determine the formation energy of single vacancy as well as its structural parameters which are summarized in table 5.1.

The formation energy, E_f, needed to create a vacancy in a system may be defined as [101-103]:

$$E_f = \frac{1}{n}\left[E_n - \left(\tfrac{N-n}{N}\right)E_{pris}\right] \tag{5.1}$$

where a positive formation energy means that the system is less stable, while a negative formation energy means that the system is more stable. The first term on the right-hand side of equation (5.1) represents the total energy of relaxed silicene with a single vacancy, the second term represents the total energy of relaxed pristine silicene, N is the total number of atoms in relaxed pristine silicene supercell, and n is the number of vacancies in a relaxed silicene supercell. In the case of a single vacancy $n = 1$.

Table 5.1: Calculated parameters of a single vacancy in silicene: Formation energy E_f, the shortest bond lengths between the nearest neighbour silicene atoms around the vacancy (d_{Si-Si}) and induced total magnetic moments per unit cell (μ_m). The calculated distance d is with reference to figure 5.1(a) where the silicon atoms numbered '1', '2', and '3' are those carrying the dangling bonds, and are regarded as Si1, Si2 and Si3, as explained in the main text.

Single Vacancy	E_f (eV)	$d_{Si1-Si2}$(Å)	$d_{Si1-Si3}$(Å)	$d_{Si2-Si3}$(Å)	μ_m/cell(μ_B)
Theory (this work)	3.52	3.55	3.50	3.50	2.02
Theory (others)	2.47 – 4.30[a,b,c,d,e]	2.74[b]	2.74[b]	2.74[b]	2.33[d]

[a]Reference [104].
[b]Reference [105].
[c]Reference [106].
[d]Reference [102].
[e]Reference [107].

For a single vacancy, the calculated formation energy is 3.52 eV, which falls within the range 2.47 to 4.30 eV as reported in previous studies [102,104-107]. However, the positive value of formation energy means that vacancy is not readily or easily formed via thermodynamic equilibrium techniques and may require external perturbation to create, such as ion or electron bombardment [108]. Figure 5.1 shows the relaxed vacancy structure. In describing the relaxed structure, we focus on the three nearest atoms to the vacancy, tagged '1', '2', and '3' in the figure. These are the nearest-neighbour silicene atoms with dangling bonds around the single vacancy, and are referred to as Si1, Si2, and Si3. Upon relaxation, the atoms around the single vacancy are displaced slightly towards the centre of the single vacancy such that the bond length between atoms Si1 and Si2 is 3.55 Å, while the bond lengths between atoms Si1 and Si3, and that between atoms Si2 and Si3 are the same with a smaller value of 3.50 Å each. This means, the bond lengths between these atoms have decreased compared to that of unrelaxed structure which is 3.87 Å.

5.1.2 Magnetic and electronic properties

Table 5.1 also shows the total magnetic moment obtained for silicene with a single vacancy to be 2.02 μ_B per unit cell, which is very close to the value obtained by other theoretical studies [90], of 2.33 μ_B. The magnetic moment of Si3 atom is 0.14 μ_B, while those of Si2 and Si1 atoms are 0.13 μ_B each. Thus, the remaining atoms surrounding the vacancy contribute a total magnetic moment of 1.61 μ_B. In figure 5.2, we show the magnetization (M_s) plot obtained for a silicene containing a vacancy. The figure has been obtained using the formula:

$$M_s = \rho_\uparrow - \rho_\downarrow \tag{5.2}$$

where $\rho_\uparrow$ and $\rho_\downarrow$ are density of spin-up and spin-down electrons, respectively. It is evident from the figure that the majority of the magnetization reside on the silicene atoms nearest to the vacancy centre (that is, atoms marked as 1, 2, 3) and the magnetization decreases farther away from the vacancy. It should be recalled that the silicene atoms 1, 2, 3 carry dangling bonds and thus unfilled orbitals which are responsible for the induced magnetization. Thus, they carry more magnetic moments.
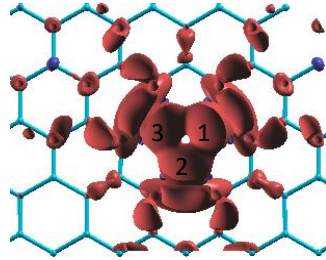
Figure 5.2: Magnetization density in silicene containing a single vacancy atom in silicene. Atoms marked as '1','2' and '3'are the nearest-neighbour atom to the vacancy. Red and blue colours, respectively, correspond to the spin up and spin down densities, with isovalue of 4×10^{-4} electron/Å^3.

The inducement of magnetic moment on silicene sheet by a single vacancy is a result of the localised σ and π dangling states [102]. Also, the introduction of a single vacancy on silicene sheet destroys the Dirac point at the *K* high symmetry point, as shown in the band structure, that is, figure 5.3(a). The destruction of the linearly crossing π and π' bands at the *K* high symmetry point induces a band gap, thus rendering this material system to acquire semiconductor characteristics. In other words, the π and π' bands, and σ and σ' bands of the pristine silicene hybridizes with the vacancy orbitals, thus resulting in a number of bands in both the valence and conduction bands [106].
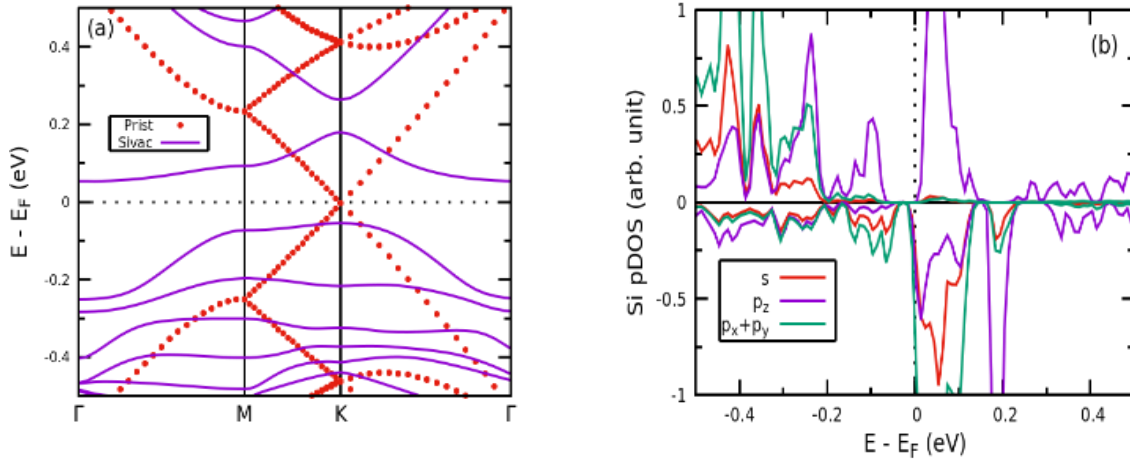
Figure 5.3: (a) Band structure of single vacancy, (b) Projected density of states of silicene atom. The red dot line is the band for pristine silicene, while the purple line represents the bands for single vacancy configuration. The Fermi level is set at zero as shown by the black dashed line.

Figure 5.3(b) is orbital-resolved DOS otherwise known as projected density of states. This figure shows the hybridization of *s* and *p* orbitals of the nearest silicene atom to the single vacancy at the Fermi level. This figure further shows that the inducement of magnetization is a contribution from all the orbital states.

In summary, we conclude that a silicene monolayer with a vacancy may be obtained via external perturbation. Such a defective silicene structure is semiconducting and has finite magnetic moment, thus making it a low-dimensional magnetic material.

5.2 Double vacancy

5.2.1 Energetics and structural properties

This sub-section explores the structural configuration and stability of a double vacancy as indicated in figure 5.4. The parameters of this structure are shown in table 5.2, while the magnetic and electronic properties are shown in figure 5.5.

Figure 5.4: Top view of (a) Pre-relaxed and (b) relaxed spin polarised configuration of silicene with a double vacancy. The blue spheres represent the silicene atoms.

A simple divacancy is created by removing two silicene atoms from the pristine 98-atoms silicene system (Figure 4.3). The relaxed divacancy has no dangling bonds, as shown in figure 5.4 (b). Equation 5.1 with $n = 2$ was used to determine the formation energy of this defect. For the divacancy, the first term on the right hand of equation 5.1 corres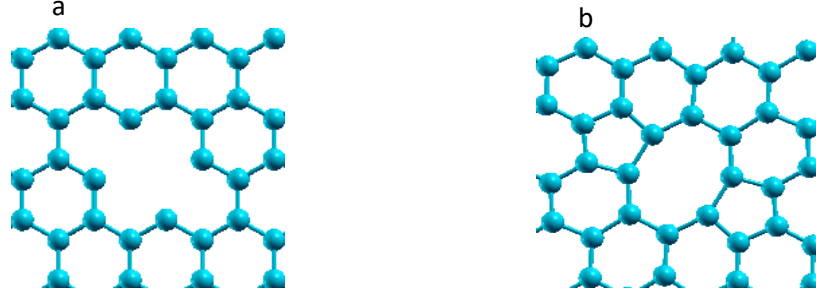ponds to the total energy of relaxed double vacancy in silicene, the second term represent the total energy of relaxed pristine silicene supercell, and N is the total number of atoms in relaxed pristine silicene supercell. Since binding energy serves the purpose of giving insight into the stability of a structure by quantifying the energy needed to overcome all interactions holding the structure together, we calculate the binding energy of double vacancy as [71]:

$$E_b = E_D - E_{pr} - 2E_V \tag{5.3}$$

where the first term on the right hand side of equation (5.3) represents the total energy of relaxed double vacancy in silicene, the second term represent the total energy of relaxed pristine silicene supercell, and the last term represent the total energy of relaxed silicene with single vacancy.

Table 5.2: Calculated parameters of a double vacancy in silicene: formation energy E_f, binding energy E_b, the shortest bond length between the nearest neighbour silicene atoms around the double vacancy (d_{Si-Si}), induced total magnetic moments per unit cell(μ_m).

Double vacancy	E_f (eV)	E_b (eV)	d_{Si-Si} (Å)	μ_m/cell(μ_B)
Theory (this work)	2.13	-2.79	2.37	0.00
Theory (others)	3.70[a,b,c] , 1.61[d]		2.32[e]	0.00[e]

[a]Reference [104].
[b]Reference [106].
[c]Reference [105].
[d]Reference [107].
[e]Reference [109].

The formation energy for a double vacancy is calculated to be 2.13 eV which is in agreement with the previous theoretical values, of 1.61-3.70 eV [103-106]. However, similar to the

case of a single vacancy, the positive value of formation energy means that in order to create the double vacancy, an external perturbation is needed such as electron irradiation of appropriate energy. Figure 5.4 (b) shows that the relaxed silicene configuration after the creation of a divacancy. Notably, an octagon and a pentagon is created along with the silicene's hexagonal ring and there are no dangling bonds in the silicene lattice. This type of defect is referred to as 5-8-5 defect. The average bond length in the 5-side pentagon is 2.35 Å, while for the 8-side octagon is 2.45, the average Si-Si bond length is 2.30 Å. These values are to be compared with 2.30 Å which is the optimized Si-Si bond length in pristine silicene. Finally, we observe that it is easier to create a double vacancy (Table 5.2) than a single vacancy (Table 5.1) judging from the lower formation energy of the former, that is, 2.13 eV as against 3.52 eV of the latter. This is because a pre-existing vacancy creates a weak bonding in the silicene lattice thus enabling easier formation of another vacancy, that is, double vacancy. Thus, a double vacancy is more easily formed than a single vacancy.

5.2.2 Magnetic and electronic properties

A double vacancy retains the zero magnetization found in pristine silicene which agrees well with the value acquired in Ref. [109]. It should be recalled that in contrast, a single vacancy introduces a finite magnetization in silicene. The absence of magnetization in double vacancy is due to absence of dangling bonds (that is, unlike single vacancy). In other words, the Si atoms making up the core 5-8-5 defect structure all have saturated bonds. From the band structure, one can see that the introduction of a double vacancy on silicene sheet destroys the Dirac point at the high-symmetry K-point as shown in figure 5.5 (a). This, results in the emergence of several bands in both the valence and conduction bands. But, the nearly flat band comes close to the Fermi level at the K high symmetry point. The disappearance of the Dirac point implies a band gap of ~0.13 eV, which confers semiconductor characteristics to the silicene monolayer.
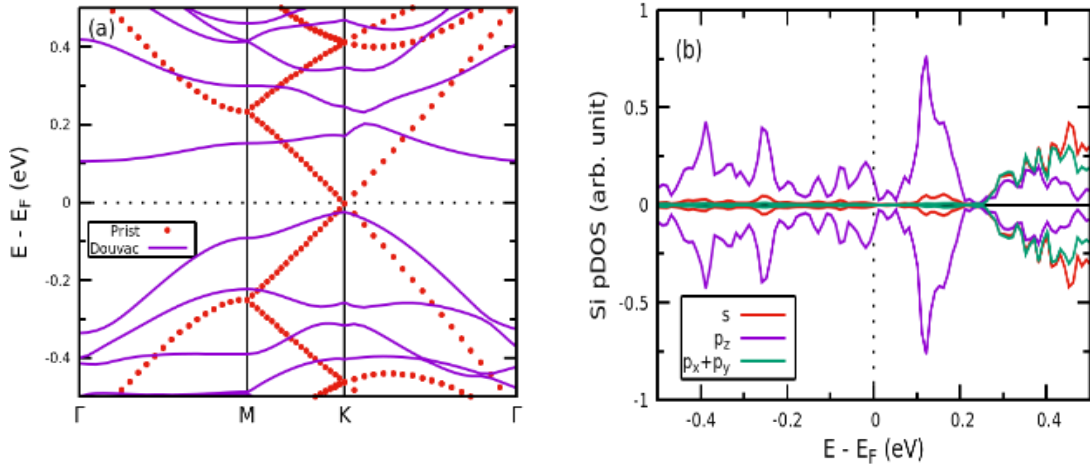
Figure 5.5: (a) Band structure of double vacancy, (b) projected density of states of silicene atom. The red dot line is the band for pristine silicene, while the purple line represents the bands for double vacancy configuration. The Fermi level is set at zero as shown by the black dashed line.

Figure 5.5 (b) shows the non-hybridization of s and p_x+p_y orbitals with the p_z orbital of the nearest silicene atom to the double vacancy at and near the Fermi level. This figure further shows that the double vacancy induces no magnetisation in silicene. In general, a double vacancy renders silicene to be less stable (compared to pristine silicene), semi-conducting, and non-magnetic material system.

5.3 Vacancy-vacancy interaction

We further extend our study of the double vacancy in silicene to the interactions between two vacancies separated at varying atomic distances. Due to the bipartite nature of the silicene lattice, divacancies are not at the same sub-lattice type when they are separated. In figure 5.6, we show a typical 98-atom supercell we used to study the divacancy. The numbering on the Si atom indicates the Si atoms that will be removed to create the divacancy. Creating the divacancy proceeds by removing Si atoms designated as 0 and 1, 0 and 2, and so on. The divacancy configuration wherein 0 and 1 atoms are removed will be termed *v0-v1*. When atoms 0 and 2 are removed, then we have *v0-v2*, until *v0-vn* where $n = 8$. For each divacancy configuration, we obtain the formation energy, binding energy, magnetization, and electronic properties. The formation energy, E_f^{v-v} is calculated using equation (5.1).
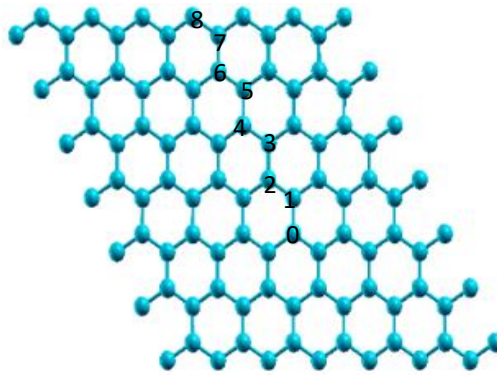
Figure 5.6: Top view of relaxed spin polarised configuration of pristine silicene with numbered atoms that are removed in turn. The blue spheres represent the silicene atoms.

5.3.1 Energetics and structural properties

The formation energies of eight different vacancy-vacancy (*v-v*) interactions are shown in figure 5.7. It should be recalled that *v0-v1* vacancy-vacancy complex of figure 5.6 is the double vacancy defect presented in Section 5.2 above together with its structural, electronic and magnetic properties.
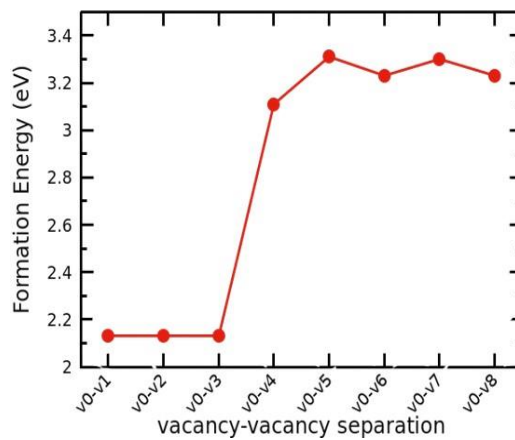
Figure 5.7: Formation energy as a function of vacancy-vacancy interaction. Data points represents the calculated formation energy, while the connecting line is a guide to the eye.

Figure 5.7 shows that the formation energies of these configurations are all positive. This suggest that external perturbation process is needed to induce *v-v* divacancy. The formation energy is the same when there are ≤ 3 atoms in between the divacancy, beyond which, the formation energy increases dramatically. The *v-v* defect on a similar sublattice have similar formation energy.

5.3.2 Magnetic and electronic properties

The magnetic moment and magnetization density plots of these configurations are shown in figures 5.8 and 5.9, respectively. Figure 5.8 shows that when the *v-v* separation is ≤ 3 atoms, the total magnetic moment of these configurations equals zero. At *v0-v4*, that is, when there are four atoms between the vacancy pair, the total magnetic moment increases slightly, to 0.1 μ_B. In general, when the *v-v* defects are on a different sublattice type, they have zero total magnetic moment as has been shown by *v0-v1*, *v0-v3*, *v0-v5* and *v0-v7* vacancy pair configurations. Also, when the vacancy pair are on a similar sublattice such as in *v0-v4*, *v0-v6* and *v0-v8* configurations, silicene has finite total magnetic moments, however, the total magnetic moments decrease with increasing *v-v* separation. The variation in the magnetic moments due to varying distance between the vacancies can be explained by different interactions between the electrons of silicene as the separation between the vacancies changes. It is further observed that these finite total magnetic moments are negative, meaning that per unit cell there are more electrons with spin-down orientation than with spin-up orientation.
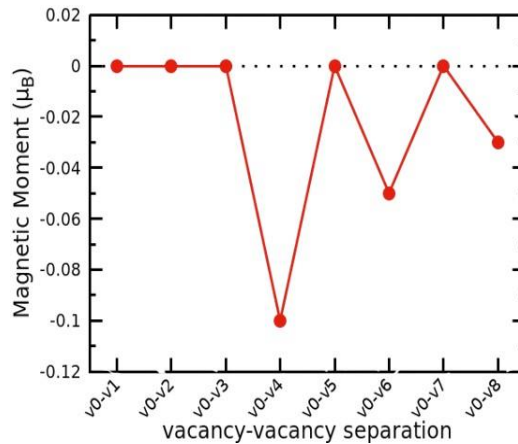
Figure 5.8: Magnetic moment as a function of vacancy-vacancy interaction. The connecting line is guide to the eye.

Figures 5.9 (a), (b) and (c) respectively, shows the magnetization density plots for the *v0-v1*, *v0-v2* and *v0-v3* configurations, that is, zero magnetization. Similarly, (d), (e), (f), (g) and (h) show the magnetization density plots of configurations *v0-v4*, *v0-v5*, *v0-v6*, *v0-v7* and *v0-v8*, respectively. It appears from the plots that when the vacancies are on the same sublattice type such as in *v0-v4*, *v0-v6* and *v0-v8*, the magnetization on the Si atoms is more delocalized compared to the more localized magnetization in the *v0-v5* and *v0-v7*

56

configurations, where the magnetization is more localized and around the vacancy, the variation in magnetic densities is due to electronic spin alignment.
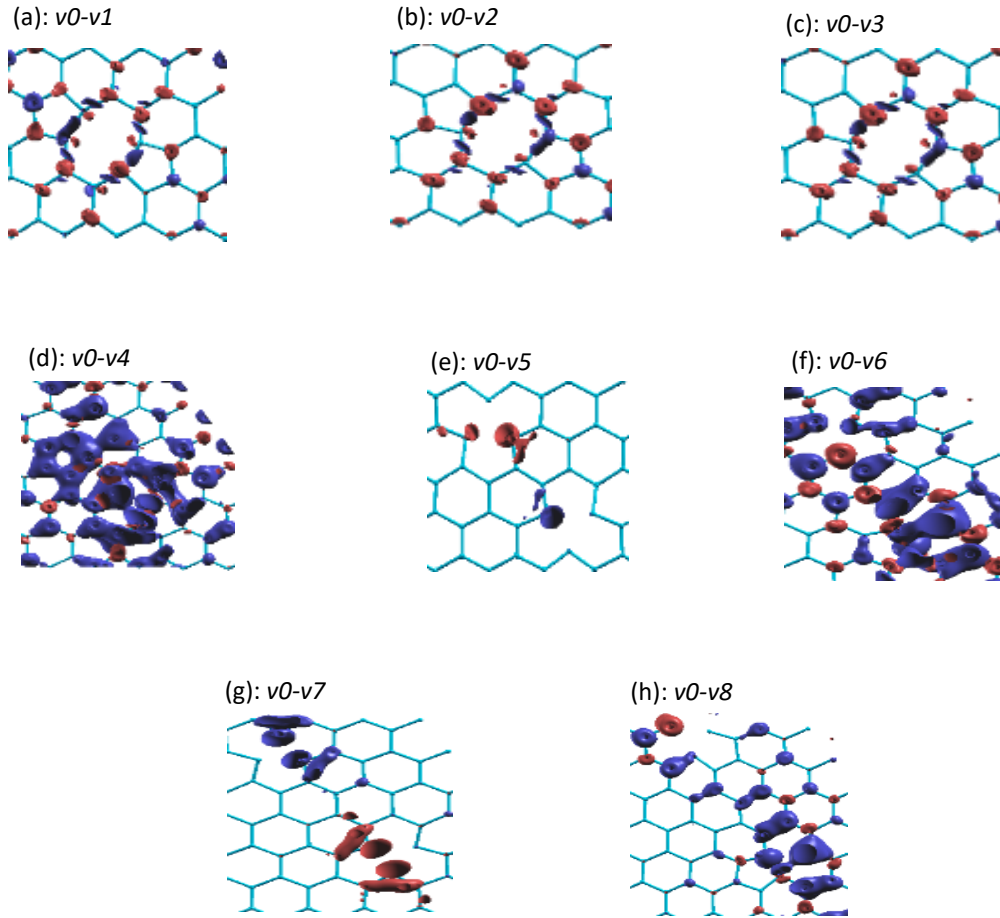
Figure 5.9: Magnetization density in silicene for vacancy-vacancy interaction of (a) $v0$-$v1$, (b) $v0$-$v2$, (c) $v0$-$v3$, (d) $v0$-$v4$, (e) $v0$-$v5$, (f) $v0$-$v6$, (g) $v0$-$v7$, (h) $v0$-$v8$. Red and blue colours, respectively, correspond to the spin up and spin down densities, with isovalues of 10^{-7} electron/Å^3 for (a), (b), and (c); 10^{-6} electron/Å^3 for (e); 10^{-5} electron/Å^3 for (d), (f), (g), and (h).

The band structures of eight different vacancy-vacancy (v-v) separations are shown in figure 5.10.

57
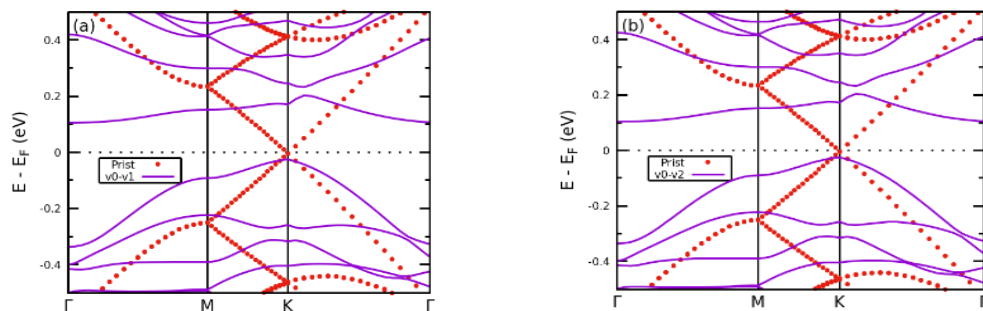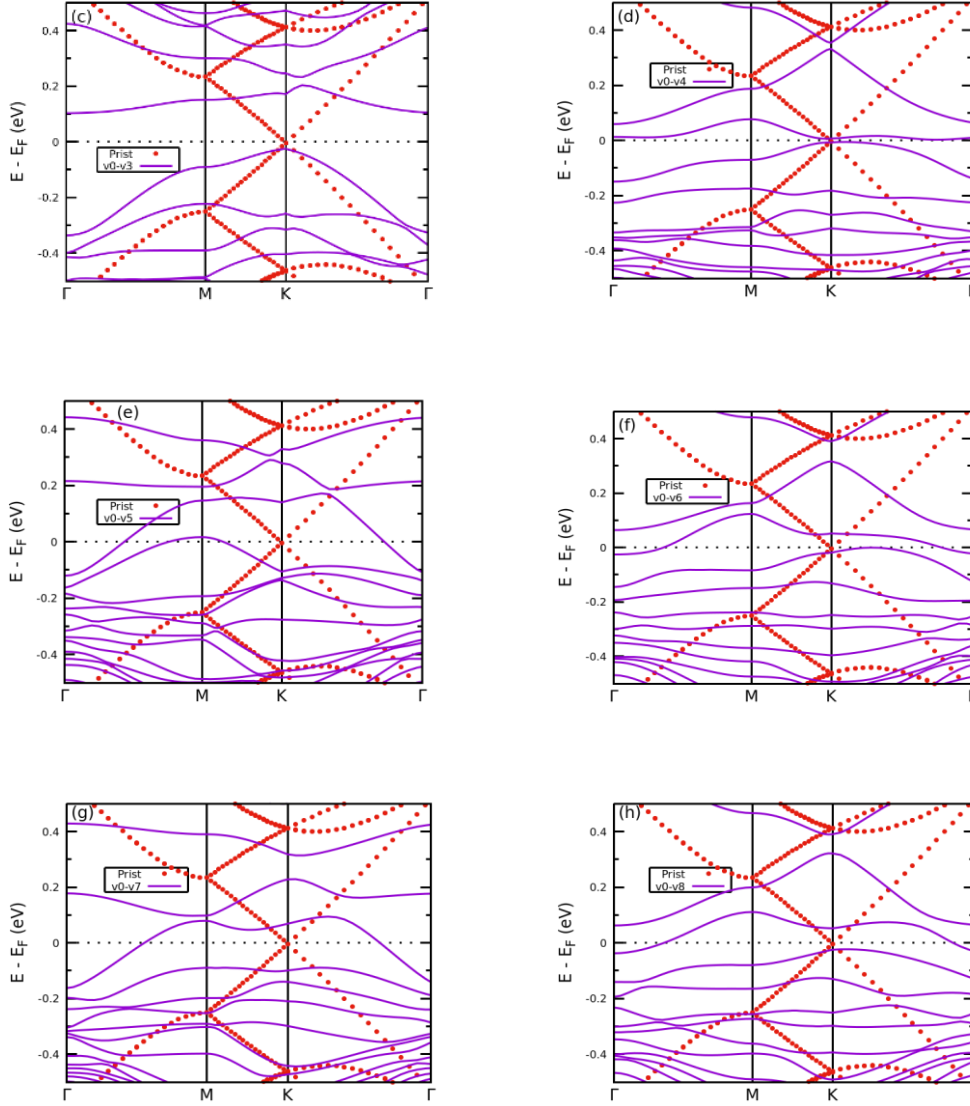
Figure 5.10: Band structures of vacancy-vacancy interaction of (a) v0-v1, (b) v0-v2, (c) v0-v3, (d) v0-v4, (e) v0-v5, (f) v0-v6, (g) v0-v7, (h) v0-v8. The red dot line is the band for pristine silicene, while the purple line represents the bands for vacancy-vacancy configurations. The Fermi level is set at zero as shown by the black dashed line.

Figures 5.10 (a)-(c) shows the electronic band structures of silicene containing divacancy configurations v0-vn (n = 1,2,3) respectively. Clearly, these divacancy configurations introduce two separate bands which run across the Brillouin zone. The Dirac point disappears and thus a band gap is created, that is, a semiconducting property is introduced into the silicene lattice due to the presence of the specific divacancy configurations, of v0-vn (n = 1,2,3). The origin of the two bands is the splitting of the p bands, that is, the valence bands. It should be recalled that we have shown in figure 4.2 (section 4.3) that the dominant band in silicene density of states is the p bands. Furthermore, in figures 5.10 (d)-(h), the band structures show that the introduction of divacancy configurations v0-vn (n = 4, 5, 6, 7,

8) leads to the persistence of the two new bands, but which now cross the Fermi level, and thus introducing metallicity into the silicene lattice. We may thus conclude that vacancy engineering of silicene structure may result in a material with a variety of properties such as non-magnetic or semiconducting property as well as magnetic or metallic property, depending on the spatial distribution or location of the vacancies.

CHAPTER 6

Vanadium doped silicene

Here, we introduce vanadium (V) atom into the silicene lattice. We investigate the energetics of insertion, that is, the formation and binding energy as well as electronic and magnetic properties of silicene containing V atoms. We remark that Vanadium is a BCC transition metal as its ground-state with a bulk crystal magnetic moment of 3.00 μ_B [110,111] and atomic radius of 2.62 Å [112]. However, we also study V defect complexes consisting of substitutional V and vacancy combinations as well as small V atom clusters in the form of vanadium dimers at different separation from each other.

6.1 Single substitutional vanadium

6.1.1 Energetics and structural properties

Figure 6.1 shows the ground state vanadium atom substituted in a silicene sheet. This structural configuration was achieved by removing one atom of silicene and replacing it with a vanadium atom and the structure was relaxed.
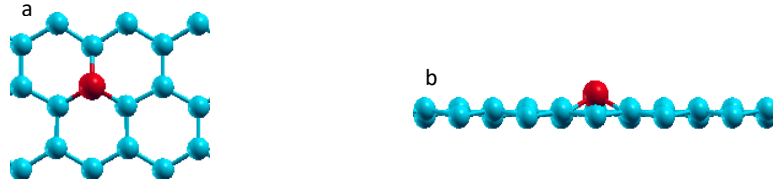
Figure 6.1: (a) Top view (b) side view of relaxed spin polarised configuration of vanadium-doped silicene. The blue spheres represent the silicene atoms, while the red sphere represent the vanadium atom.

The binding energy E_b^{vac-V} of a single substitutional V to the silicene surface may be defined as [101]:

$$E_b^{vac-V} = E_{vac-V} - E_{vac} - E_V \tag{6.1}$$

where E_{vac-V} represents the energy of substitutional vanadium atom in relaxed silicene supercell, E_{vac} represents the total energy of relaxed silicene with single vacancy, and E_V represents the total energy of isolated vanadium atom. Equation 6.1 was used to determine the binding energy of this system, and its magnitude and structural parameters are

summarized in table 6.1. Also, the formation energy, $E_f(Vs)$, of substitutional vanadium may be defined as:

$$E_f(Vs) = E_{V-Si} + \mu_{si} - E_{pr} - \mu_V \qquad (6.2)$$

where E_{V-Si} represents the total energy of relaxed vanadium-doped silicene, μ_{si} represents the chemical potential of silicene atom, E_{pr} represents the total energy of relaxed pristine silicene, μ_V represents the chemical potential of vanadium atom.

Table 6.1: Calculated parameters of vanadium-doped silicene: binding energy E_b, formation energy E_f, the shortest bond length between the nearest neighbour silicene atom and substitutional vanadium atom d_{Si-V}, induced magnetic moment on substitutional vanadium atom μ_{m-V}, induced total magnetic moment per unit cell μ_m.

Vanadium-doped silicene	E_b (eV)	E_f (eV)	d_{Si-V} (Å)	μ_{m-V} (μ_B)	μ_m/cell (μ_B)
Theory (this work)	-6.08	1.37	2.43	1.30	2.61
Theory (others)	-5.40[a]		2.39[a]	1.00[a]	1.60[a]

[a]Reference [12].

Table 6.1 shows a binding energy of a single substitutional vanadium atom to silicene with a large value of ~ -6 eV. This implies that this substitutional V is strongly binded in silicene. Our calculated values of E_b^{vac-V} is fairly in agreement with a previous theoretical value of - 5.40 eV [12]. The difference in theoretical values of binding energies may be attributed to differences in computational parameters, such as pseudopotential, periodic supercell size and plane-wave cut-off. The table also shows that the relaxed V-Si distance, that is, the relaxed distance of V to each of the nearest-neighbour (NN) Si atom is ~ 2.43 Å. This distance is to be compared with 2.30 Å for Si-Si length in pristine silicene. Since the radius of vanadium atom is larger than the radius of silicene atom, the surrounding silicene atoms experience a strained environment in the form of outward push of the NN silicene atoms, hence the larger V-Si separation compared to the Si-Si separation.

6.1.2 Magnetic and electronic properties

We found the magnetic moment of V when substituted in silicene as 1.30 μ_B, however, the whole supercell has a total magnetic moment of 2.61 μ_B. This suggests the rest of the silicene atoms contributes 1.31 μ_B to the supercell magnetization. This is in qualitative agreement to Ref. [12] where 1.00 μ_B is obtained as the magnetic moment on the vanadium atom and 1.60 μ_B as the total magnetic moment on the silicene supercell containing the vanadium atom. The difference in the values of the magnetic moment may be due to the difference in

the supercell size where in our calculations, we have used 98 atom supercell (1.02 atomic %) whereas in Ref. [12], a smaller supercell cell size of 72 atoms (1.39 atomic %) was used. It appears therefore, vanadium induced magnetization in silicene may be concentration dependent. Figure 6.2 shows the magnetization density plot for the substitutional V supercell. This figure shows that the bulk of magnetization density is on vanadium atom. As seen from the figure, the vanadium atom and the nearest-neighbour silicene atoms are in opposite spins direction. Away from the vanadium atom, the silicene atoms are coupled in opposite spins direction relative to the nearest neighbour silicene atoms. The magnetization density on the vanadium atom also shows the shape of the d orbital of the vanadium atom. This confirms the origin of the magnetization to be of the d orbital of the vanadium atom.
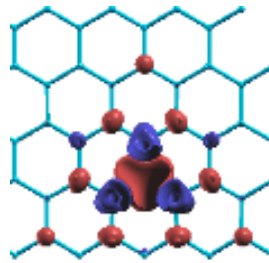
Figure 6.2: Magnetization density in vanadium-doped silicene. Red and blue colours, respectively, correspond to the spin up and spin down densities at the isovalue of 10^{-3} electron/$Å^3$.

Furthermore, substituting a silicene atom with a single vanadium atom in a pristine silicene result in the destruction of the Dirac point, as shown in the band structure plot, that is, figure 6.3 (a). This results in the emergence of several bands in both the valence and conduction bands. Figure 6.3 (a) also shows bands that are crossing the Fermi level, which consequently renders the material system to acquire a metallic character.
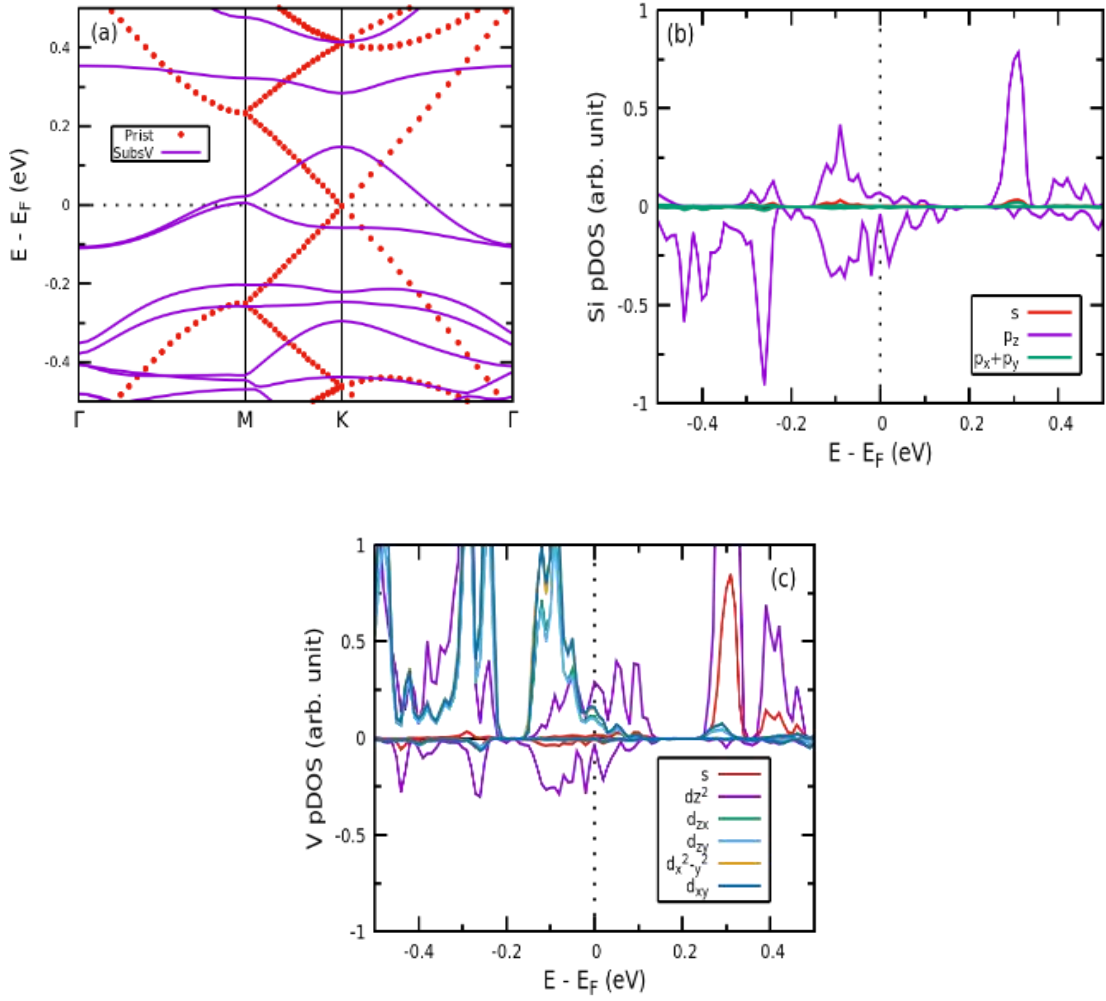
Figure 6.3: (a) Band structure of substitutional vanadium in silicene, (b) Projected density of states of silicene atom in vanadium-doped silicene, (c) Projected density of states of vanadium atom in vanadium-doped silicene. The red dot line is the band for pristine silicene, while the purple line represents the bands for substitutional vanadium configuration. Fermi level is set to zero as shown by the black dashed line.

Figure 6.3 (b) shows the plot of *s* and *p* orbitals of the nearest silicene atom to the vanadium atom. Figure 6.3 (c) also show the *d* orbital of the vanadium atom. It can be seen from the two plots that there is overlapping of the orbitals within the energy range shown in the plot. The overlapping of the orbital is evidence of hybridization between the silicene and vanadium electron states which results in bonding between the two atoms and hence the stability of vanadium at the substitutional site.

6.2 Vacancy-vanadium interaction

Here, we consider the interaction between a single vacancy (*v0*) and a single substitutional vanadium (*Vsn*) atom. The vacancy (*v0*)-vanadium (*Vsn*) configuration is such that a vanadium atom is placed at a varying atom distance from a single vacancy. Thus, using

figure 6.4 as an illustration, a typical *v0-Vsn* configuration will consist of a vacancy and a substitutional vanadium atom at position '3' in the figure, that is, *v0-Vs3*. Another configuration such as *v0-Vs5* will consist of a single vacancy and a vanadium atom at the lattice site '5'. Thus, we can determine how the sublattice type position of the V atom affects the electronic and magnetic properties of the silicene structure. Eight different *v0-Vsn* configurations have been considered. Below, we present the binding energy, electronic and magnetic properties of the configurations.
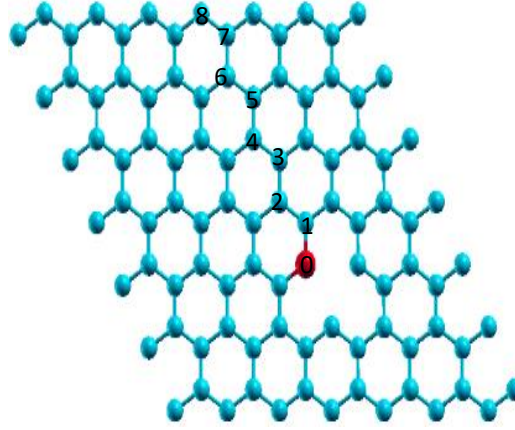
Figure 6.4: Top view of pre-relaxed spin polarised configuration of vanadium atoms placed at positions 1 to 8 in turns interacting with a vacancy at position 0 in silicene. The blue spheres represent the silicene atoms, while the red sphere represent the vanadium atom.

6.2.1 Energetics and structural properties

The binding energy of *v-V* combinations has been obtained using [71,101]:

$$E_b^{v-V} = E_{v-V} + E_{pr} - E_v - E_{V-Si} \tag{6.3}$$

where E_{v-V}, represents the total energy of relaxed vacancy-vanadium interaction in silicene, E_{pr} symbolize the total energy of relaxed pristine silicene, E_v represent the total energy of relaxed silicene with a single vacancy, E_{V-Si} represents the total energy of relaxed vanadium-doped silicene.

As stated earlier, a total of eight *v0-Vsn* interactions were investigated. Figure 6.5 (a) shows the binding energy between the silicon atom and the substitutional vanadium. This figure shows a very strong binding energy of E_b^{v-V} = -2.79 eV when a single V atom is captured by a double vacancy, that is, *v0-Vs1* configuration, as shown in Figure 6.5 (b).

Figure 6.5: (a) Pre-relaxed (b) relaxed structure of silicene containing nearest-neighbour vacancy-vanadium defect complex, *v0-Vs1*. The blue spheres represent the silicene atoms, while the red sphere represent the vanadium atom.

Of all the *v0-Vsn* (n = 1, 2, 3, … ,8) configurations investigated, the *v0-Vs1* may be considered as the most stable as illustrated in Figure 6.6. The E_b^{v-V} for the *v0-Vs1* when compared to that of single substitutional vanadium *Vs* of -6.08 eV, suggest V atom is less stable in a double vacancy (that is, *v0-Vs1*). This may be due to less bonding (compared to *Vs*) between the nearest-neighbour silicene atoms and the V atom (due to larger hole created by the double vacancies) in the *v0-Vs1*. The difference in the binding energy between the *Vs* and *v0-Vs1* may be due to induced bond strain in the silicene lattice containing the defect. The nearest-neighbour silicon-vanadium distance in the *v0-Vs1* is about 2.64 Å which is longer than 2.30 Å for the Si-Si bond in pristine defect-free silicene and 2.43 Å for the *Vs* atom. Thus, the Si bond with the V atom in the *v0-Vs1* is more strained (relative to the Si-Si bond in pure silicene) compared to that of the *Vs* atom. Thus, the *v0-Vs1* has lower binding energy compared to *Vs* atom.
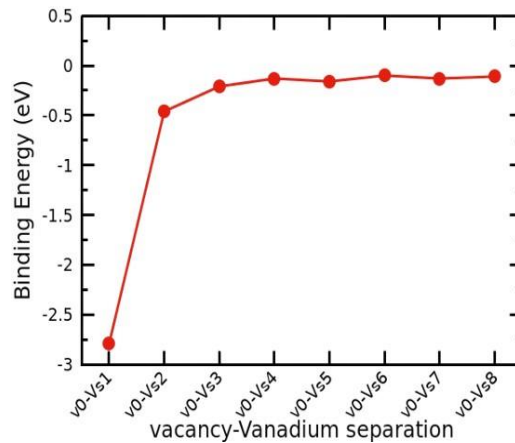

Figure 6.6: Binding energy as a function of vacancy-vanadium interaction in silicene. The connecting line is guide to the eye.

6.2.2 Magnetic and electronic properties

Figure 6.7 show the total magnetization in the supercell and the induced magnetization on the V atoms as the separation between the vacancy and V atom increases. From the figure,

it is clear that the V-induced magnetization in silicene is the highest, that is 2.69 μ_B, when both the V atom and vacancy are nearest-neighbours. When this value of magnetic moment is compared to that of supercell containing a single vacancy, that is 2.02 μ_B, it may be inferred that V atom induces higher magnetization in silicene. Also, beyond the nearest-neighbour v-V, that is, when the vacancy (v) and the V atom are separated by one silicene atom, the cell magnetization falls rapidly and then rise again when the v-V are separated by more than two atoms. The increasing magnetization as the v-V increases is such that the total magnetization on the silicene supercell approaches that of single vacancy or single substitutional V atom. This is intuitive in the sense that as the separation increases, the interaction between the v and V atom decreases and thus, the induced magnetization in silicene is determined by either of the two defects. The total magnetization approaches that of either of the two defects in the limit of much larger supercell size or infinite separation of the two defects. The magnetization density plots of Figure 6.8 illustrate this observation.
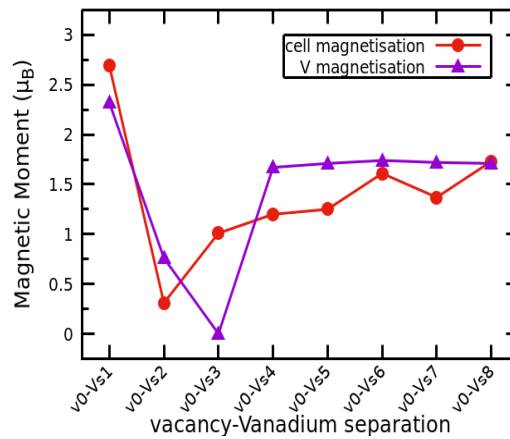

Figure 6.7: Total magnetic moment in the supercell and on V atom as a function of vacancy-vanadium separation in silicene. The connecting line is guide to the eye.

(a): *v0-Vs1*

(b): *v0-Vs2*

(c): *v0-Vs3*

(d): *v0-Vs4*

(e): *v0-Vs5*

(f): *v0-Vs6*
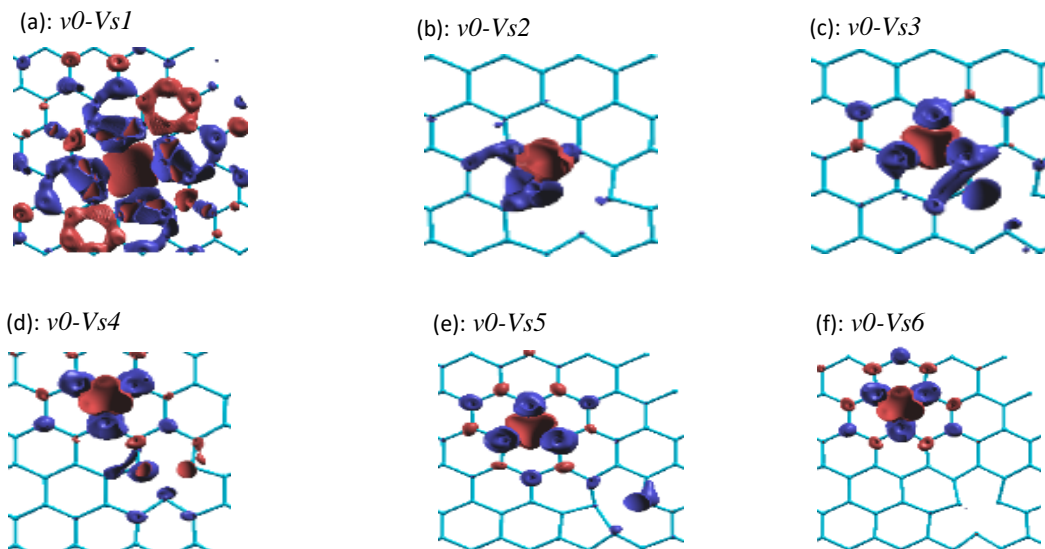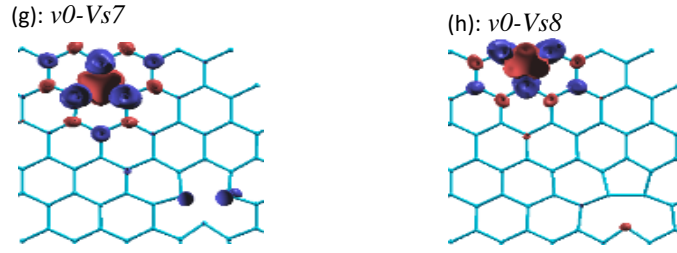
(g): *v0-Vs7*   (h): *v0-Vs8*

Figure 6.8: Magnetization density in silicene for vacancy-vanadium interaction of (a) *v0-Vs1*, (b) *v0-Vs2*, (c) *v0-Vs3*, (d) *v0-Vs4*, (e) *v0-Vs5*, (f) *v0-Vs6*, (g) *v0-Vs7*, (h) *v0-Vs8*. Red and blue colours, respectively, correspond to the spin up and spin down densities, with isovalues of 10^{-4} electron/Å^3 for (a); and 10^{-3} electron/Å^3 for (b), (c), (d), (e), (f), (g), and (h).

Figure 6.9 shows the band structures of *v0-Vsn* vacancy-vanadium complex. Clearly, in Figure 6.9 (a) the presence of the two defect types annihilates the Dirac point of the silicene lattice such that a tiny 0.06 eV gap appears which separates the valence and the conduction bands. Below the Fermi level, there appears several bands which originates from the *d*-bands of vanadium atom, thus rendering *v0-Vs1* configuration to possess semiconducting characteristics. However, all other *v0-Vsn* vacancy-vanadium complex, shows metallic behaviour from (b) to (h) of Figure 6.9.
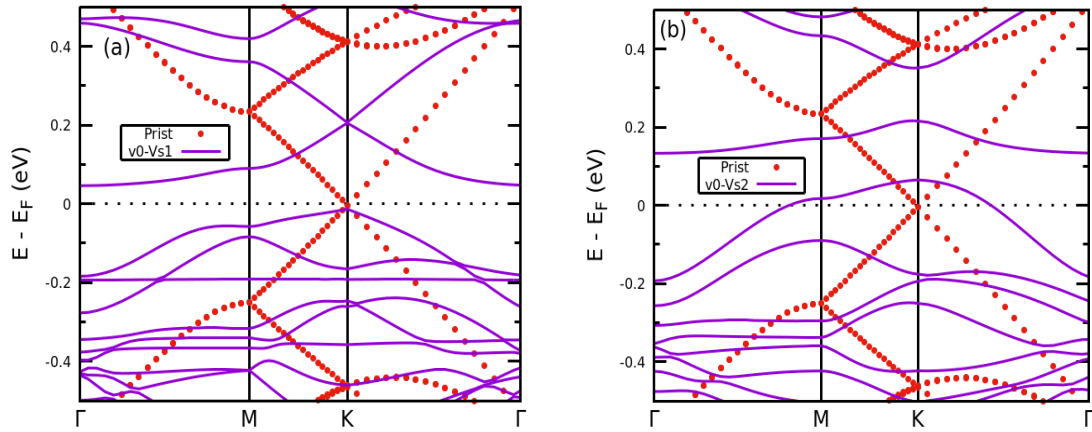
Figure 6.9: Band structures of vacancy-vanadium interaction of (a) *v0-Vs1*, (b) *v0-Vs2*, (c) *v0-Vs3*, (d) *v0-Vs4*, (e) *v0-Vs5*, (f) *v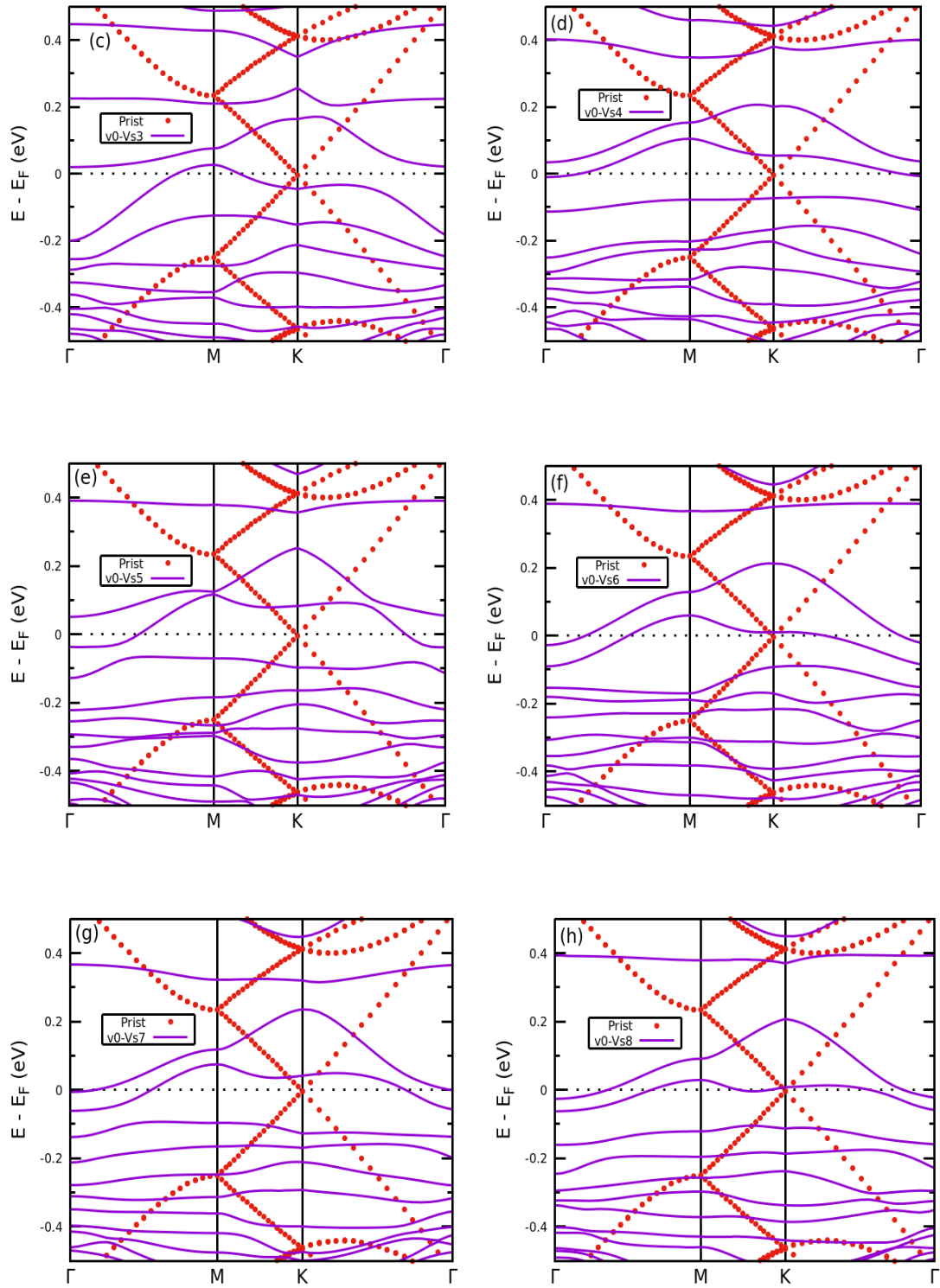0-Vs6*, (g) *v0-Vs7*, (h) *v0-Vs8*. The red dot line is the band for pristine silicene while, the purple line represents the bands for vacancy-vanadium configurations. Fermi level is set to zero as shown by the black dashed line.

6.3   Small vanadium clusters

The previous section dealt with the small defect cluster consisting of a vacancy and substitutional vanadium atom at varying separations. Here, we examine a small vanadium cluster, that is, a dimer consisting of two vanadium atoms located at the high symmetric lattice points of the silicene lattice. In each of the dimer configurations, the atoms are either coupled in ferromagnetic (FM), antiferromagnetic (AFM) or non-magnetic (NM) orientations. In general, we have investigated three different types of vanadium dimers while exploiting the symmetric points of the silicene lattice. Below is the description of the dimer configurations:

(a) Two vanadium atoms separated by at least 2 Å around the hexagon of the silicene lattice. The hexagon has been chosen since it offers the largest space for the dimer. A total of eight (8) configurations have been examined. These are named as (i) *tri-u*; (ii) *tri-b*; (iii) *bridge-u*; (iv) *bridge-b*; (v) *hollow-uu*; (vi) *hollow-ud;* (vii) *top-hor*; and (viii) *top-vert*. The description of each of the configurations are shown in table 6.2.

(b) Two vanadium atoms arranged in such a way that each of the V atom occupies the substitutional site (*s*) but are separated by intermediate silicene atoms. These configurations are named *V2s-nSi*, that is two vanadium atoms at substitutional sites separated by n (n = 0, 1, … ,7) silicene atoms.

(c) Two vanadium atoms occupying the interstitial hole sites (*h*), but their separation varies. We have named these configurations *V2h-nh*, where n = 0, 1, … ,4 is the number of interstitial hole sites separating the vanadium atoms.

6.3.1 Vanadium dimer on silicene

6.3.1.1 Energetics and structural properties

Figure 6.10 shows the binding energy of each of the vanadium dimers on silicene as described in table 6.2.
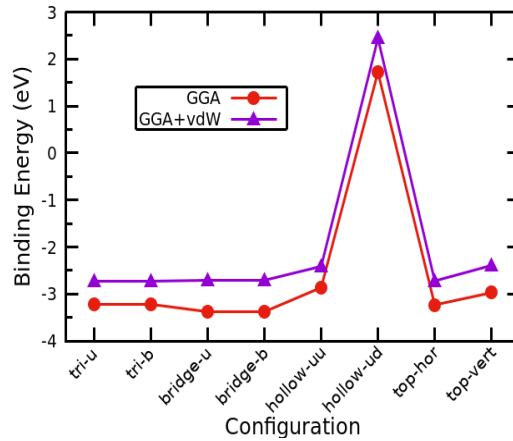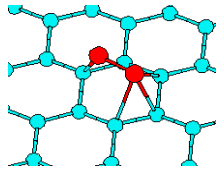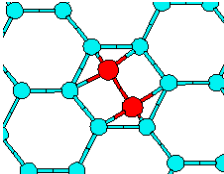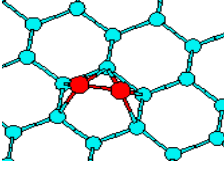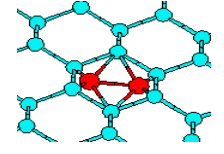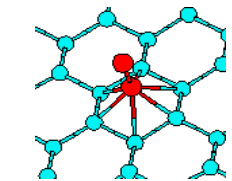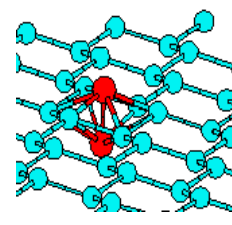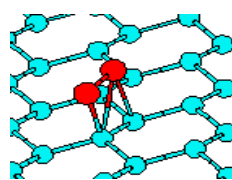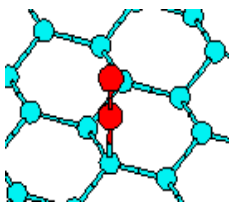
Figure 6.10 Binding energy as functions of structural configuration using generalised gradient approximation and the van der Waals correction. The connecting line is guide to the eye.

Table 6.2: Description of V dimer on silicene configurations, that is, two vanadium atoms separated by at least 2 Å around the hexagon of the silicene lattice.

Configuration number	Configuration	Reference figure	Description
1	*tri-u*	6.11 (a)	Each of the atom at the edge of the two triangles formed by silicene hexagon such that each of the V atom are at a height of 2.70 Å.
2	*tri-b*	6.12 (a)	Similar to *tri-u* but the two V atoms are at the same plane as the silicene layer.
3	*bridge-u*	6.13 (a)	The two V atoms are located close to two bridge sites which are directly opposite to each other. However, in this pre-relaxed configuration, each of the V atoms are at a height of 2.47 Å.
4	*bridge-b*	6.14 (a)	Similar to *bridge-u*, however, the two V atoms are at the same plane as the silicene layer.

5	*hollow-uu*	6.15 (a)	The V dimer are located at the hole position above the silicene layer but separated by 2.00 Å with the closer V atom at a height of 2.60 Å above the silicene layer.
6	*hollow-ud*	6.16 (a)	Similar to *hollow-uu* but the V atoms are such that one is above the plane and the other below at a height of 1.00 Å and -1.00 Å respectively.
7	*top-hor*	6.17 (a)	Each of the V atoms are located at the top site of two nearest-neighbour silicene atoms such that the V atoms are at height of 2.47 Å above the top site in a horizontal orientation.
8	*top-vert*	6.18 (a)	The V dimer is located at the top site on the silicene atom in vertical orientation with the V dimer separated by 2.00 Å. The nearest V atom to the silicene layer is at a height of 2.45 Å directly above the silicene atom.

The binding energy E_b^{Si-dim} is calculated as:

$$E_b^{Si-dim} = E_{Si-dim} - E_{Si} - E_{dim} \qquad (6.4)$$

where E_{Si-dim} symbolizes the total energy of the relaxed silicene and vanadium dimer complex, the second term E_{Si} symbolize the total energy of relaxed pristine silicene sheet, and the last term E_{dim} is the total energy of a relaxed isolated vanadium dimer. The E_{dim} is obtained by putting the exact dimer configuration in a cubical box of dimension 28.35 Å. In equation (6.4) above, a negative value of E_b^{Si-dim} suggests that a dimer is more stable when binded on the silicene lattice than as isolated dimer. Also, the more negative the E_b^{Si-dim}, the larger the binding and thus the greater the stability of the configuration. Furthermore, the binding energy has been obtained using the total energy values obtained from the standard GGA and GGA+vdW correction. It should be noted that the values of E_b^{Si-dim} given by the GGA+vdW are larger than that of the standard GGA as shown in figure 6.10.

However, both functionals give negative binding energies of E_b^{Si-dim} for all the dimer configurations on silicene except for the *hollow-ud*, that is, where the orientation of V atoms is such that one is above the plane while the other is below. The strongest binding is of V dimer of *bridge* configuration, that is, *bridge-u/bridge-b* with E_b^{Si-dim}= -3.38 eV as given by the GGA. The GGA+vdW functional gives the *tri-u/tri-b* and *top-hor* as the most stable with E_b^{Si-dim}= -2.72 eV. However, this binding energy value is similar to E_b^{Si-dim}= -2.70 eV obtained for the *bridge-u/bridge-b* configurations. It is safe therefore to state that of all the dimer configurations considered as shown in figure 6.10, the *bridge* configuration is the most stable. The similarity in the stability of the *bridge* and *tri-u/tri-b* configurations is not entirely surprising. This is because at equilibrium (that is, the final relaxed), the configurations of the two structures are similar as shown in figure 6.11 (b), 6.12 (b), 6.13 (b), and 6.14 (b), respectively. However, for future consideration, such as the analysis of the electronic structures, we shall focus on the *bridge* configuration as obtained from the GGA since it has the largest E_b^{Si-dim}. Moreover, for the structures calculated with the GGA+vdW, the same *bridge* configuration has similar E_b^{Si-dim} as the *tri-u/tri-b* configurations, that is, the latter only bind stronger to the silicene surface by 0.02 eV (cf. figure 6.10). Nevertheless, the fact that all the structures have negative E_b^{Si-dim} except the *hollow-ud* configuration, suggest that they and their corresponding dimer configuration are feasible. The V-V atom separation at equilibrium is about 1.24 Å, and in the case of *bridge-u* configuration, each of the V atoms are approximately at a height 2.65 Å above the silicene surface. For the *bridge-b* configuration, the V atoms are below the plane of the silicene as shown in figure 6.14 (b).

Figure 6.11 (a) Pre-relaxed *tri-u* configuration as described in table 6.2; (b) relaxed structure of the same configuration based on the GGA functional; (c) relaxed structure based on the vdW functional. The blue sphere is the silicene atom, while the red sphere is the vanadium atom.
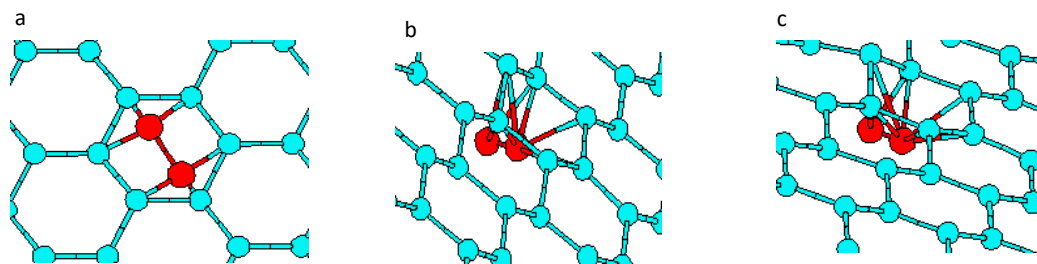
Figure 6.12 (a) Pre-relaxed *tri-b* configuration as described in table 6.2; (b) relaxed structure of the same configuration based on the GGA functional; (c) relaxed structure based on the vdW functional. The blue sphere is the silicene atom, while the red sphere is the vanadium atom.
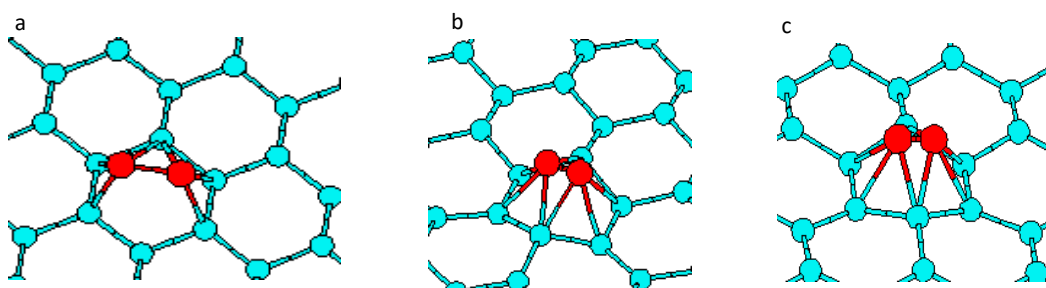
Figure 6.13 (a) Pre-relaxed *bridge-u* configuration as described in table 6.2; (b) relaxed structure of the same configuration based on the GGA functional; (c) relaxed structure based on the vdW functional. The blue sphere is the silicene atom, while the red sphere is the vanadium atom.
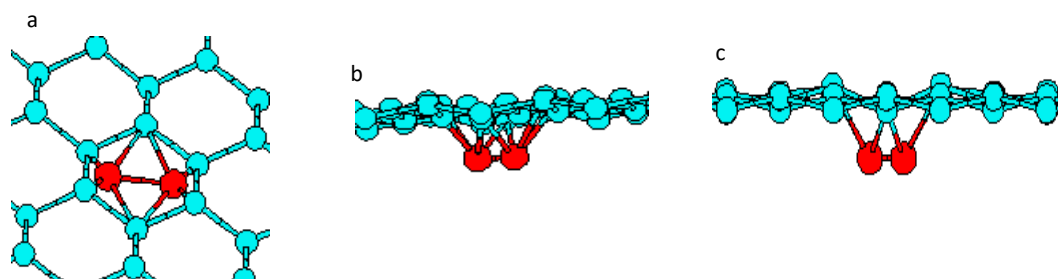
Figure 6.14 (a) Pre-relaxed *bridge-b* configuration as described in table 6.2; (b) relaxed structure of the same configuration based on the GGA functional; (c) relaxed structure based on the vdW functional. The blue sphere is the silicene atom, while the red sphere is the vanadium atom.
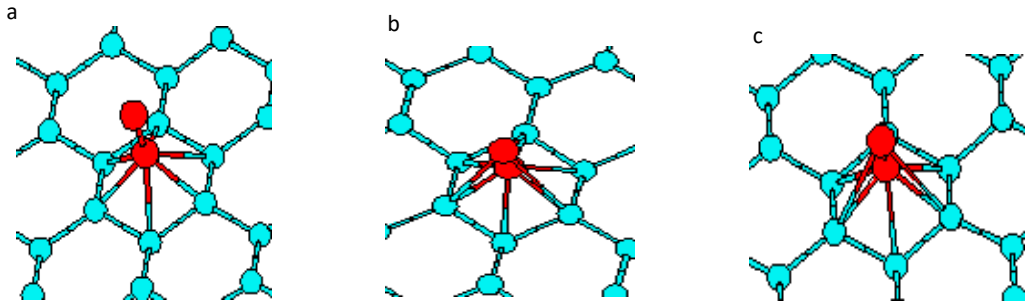
Figure 6.15 (a) Pre-relaxed *hollow-uu* configuration as described in table 6.2; (b) relaxed structure of the same configuration based on the GGA functional; (c) relaxed structure based on the vdW functional. The blue sphere is the silicene atom, while the red sphere is the vanadium atom.
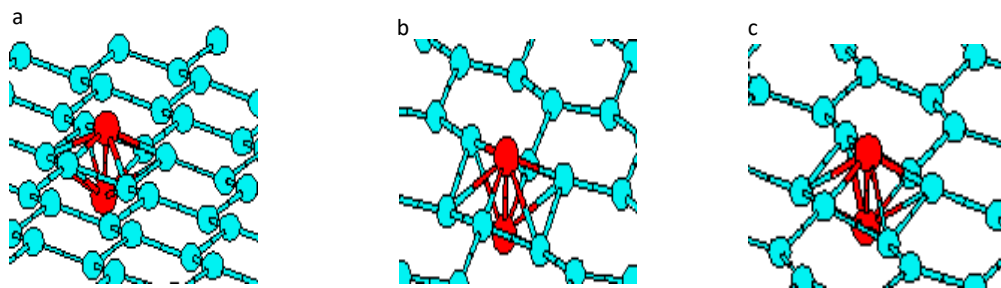
Figure 6.16 (a) Pre-relaxed *hollow-ud* configuration as described in table 6.2; (b) relaxed structure of the same configuration based on the GGA functional; (c) relaxed structure based on the vdW functional. The blue sphere is the silicene atom, while the red sphere is the vanadium atom.
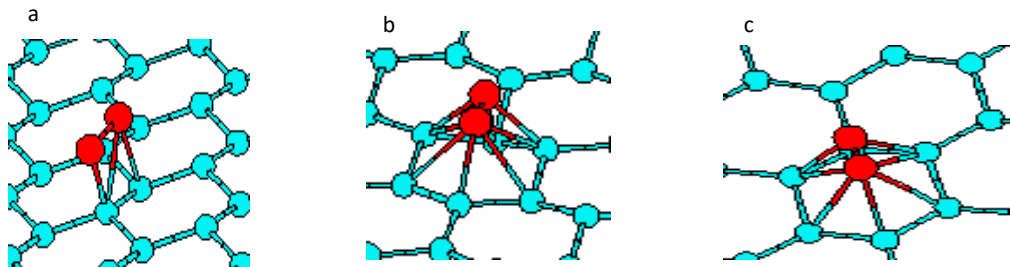
Figure 6.17 (a) Pre-relaxed *top-hor* configuration as described in table 6.2; (b) relaxed structure of the same configuration based on the GGA functional; (c) relaxed structure based on the vdW functional. The blue sphere is the silicene atom, while the red sphere is the vanadium atom.
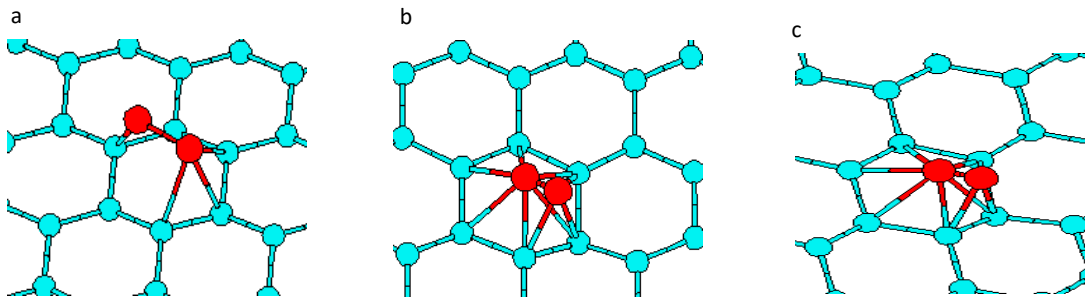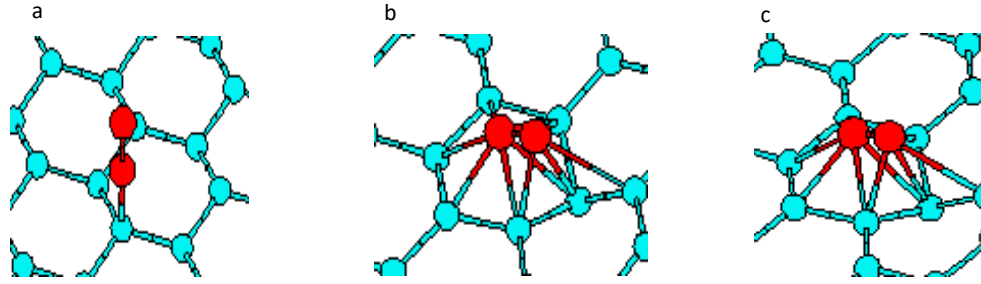
Figure 6.18 (a) Pre-relaxed *top-vert* configuration as described in table 6.2; (b) relaxed structure of the same configuration based on the GGA functional; (c) relaxed structure based on the vdW functional. The blue sphere is the silicene atom, while the red sphere is the vanadium atom.

6.3.1.2 Magnetic and electronic properties

To obtain a better understanding of the *bridge* configuration, that is, *bridge-u*, we have plotted the corresponding band structure and the projected density of states of silicene and vanadium atoms with the generalised gradient approximation in figure 6.19.
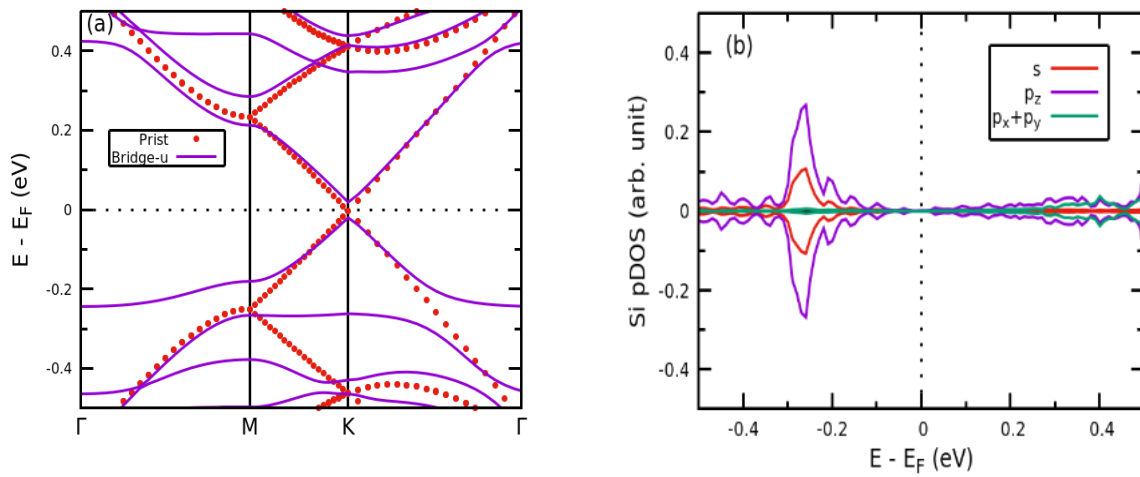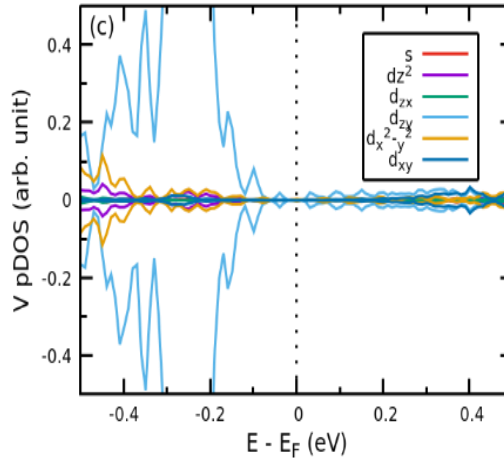
Figure 6.19: *Bridge-u* configuration with GGA functional (a) Band structure, (b) Projected density of states of Si atom, and (c) Projected density of states of V atom. The red dot line is the band for pristine silicene, while the purple line represents the bands for *Bridge-u*. Fermi level is set to zero as shown by the black dashed line.

It is easily seen from the band structure that the presence of vanadium dimer opens a band gap in the silicene monolayer. The projected density of states for silicon and vanadium atoms shows that the band gap opening is due to the hybridization of p_z and d_{zy} orbitals of silicene and vanadium atoms, respectively.

The total magnetic moments in all the vanadium dimer configurations, including the *bridge-u* is zero. Figure 6.20 shows the exchange energy ΔE, that is, the difference in energy between the FM and the AFM configurations, for all the configurations. From the figure, two configurations should be particularly noted, that is *tri-u* and *top-vert*, the structures of which are described in table 6.2, and are illustrated in figures 6.11 and 6.18, respectively. Both have negative binding energy of -3.22 eV and -2.97 eV, but also an exchange energy of -2.45 meV and -2.41 meV, respectively. This suggests that the ferromagnetic (FM) configuration of vanadium dimer is relatively more stable than the antiferromagnetic (AFM) configuration.

76
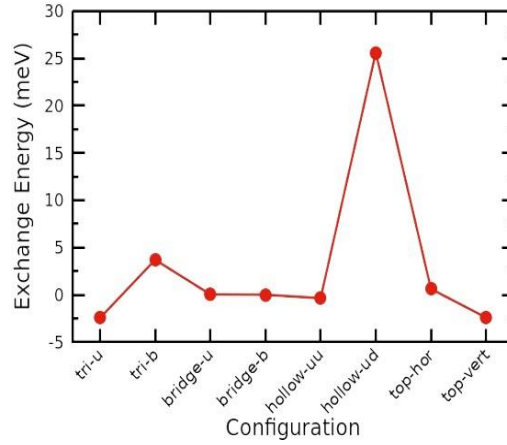
Figure 6.20: Exchange energy as a function of structural configuration with GGA functional. The connecting line is guide to the eye.

6.3.2 Substitutional vanadium dimer in silicene

6.3.2.1 Energetics and structural properties

Here we consider the vanadium dimer that is placed at substitutional positions on the silicene lattice. As explained earlier, each of the dimer is separated by n number of Si atoms as the separation between the dimer increases. The binding energy of these configurations is obtained from [71]:

$$E_b = [E_{V-V} + E_{pr}] - 2E_V \qquad (6.5)$$

where E_{V-V} represents the total energy of the relaxed substitutional vanadium dimer in silicene, E_{pr} is the total energy of relaxed pristine silicene, E_V represents the total energy of a single vanadium atom at the substitutional site. Table 6.3 shows the difference in energy (ΔE) between the FM and the AFM configurations of V-V pair as their separation increases, calculated binding energy E_b, as well as the total magnetic moment of the supercell containing the V-V pair μ_m. It should be emphasized that for each of the V-V pair, the AFM and FM configurations are considered. From the table, the *V2s-0Si* configuration wherein the V atoms are the nearest-neighbour substitutional sites, has the most negative binding energy of -6.43 eV which implies highest stability. Figure 6.21 shows the pre-relaxed and relaxed structure of the most stable substitutional V-V pair in silicene, that is, *V2s-0Si*. The relaxed configuration is such that the atoms shift from their respective initial lattice sites and sit atop each other in a vertical orientation. In this configuration, the V-V distance between the atoms is ~1.27 Å.
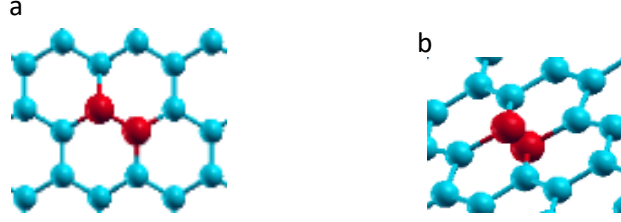
Figure 6.21: (a) pre-relaxed (b) relaxed structure of the most stable substitutional V-V pair, that is, *V2s-0Si*. The blue sphere represents the silicene atom while the red sphere is the vanadium atom.

Furthermore, in all the other configurations, the V-V pair are binded by $\leq \sim 0.1$ eV. Notably, when the V-V atoms pair are separated by more than one Si atom, the binding energy becomes positive with a very low binding energy. The V-V atoms thus prefers to exist as individual V atoms on their respective substitutional sites when they are separated by more than one Si atom along the zig-zag direction.

Table 6.3: Calculated parameters of substitutional vanadium-vanadium interaction at varying distances of separation in silicene; *n-d/s* is the number *n* of Si separating the V-V pair, the latter is either in the different (*d*) or same (*s*) sublattice. E_{min} is the minimum energy configuration between the ferromagnetic (FM) and the antiferromagnetic (AFM) configuration of the V-V pair, ΔE is the energy difference between the FM and the AFM configuration of the V-V pair, E_b is the binding energy of the corresponding minimum energy configuration. When ΔE is positive, the AFM is the more stable configuration whereas when it is negative the FM is the more stable. Induced magnetic moment per unit cell is μ_m in Bohr magneton.

n-d/s	V-V configuration	E_{min}	$\Delta E = E_{FM} - E_{AFM}$ (meV)	E_b(eV)	μ_m/cell (μ_B)
0-d	*V2s-0Si*	AFM	0.17	-6.43	-0.00
1-s	*V2s-1Si*	AFM	158.80	-0.03	0.01
2-d	*V2s-2Si*	FM	-77.81	0.01	2.84
3-s	*V2s-3Si*	AFM	45.37	0.11	0.00
4-d	*V2s-4Si*	FM	-40.83	0.00	3.27
5-s	*V2s-5Si*	AFM	27.71	0.02	-0.01
6-d	*V2s-6Si*	FM	-54.27	0.01	3.75
7-s	*V2s-7Si*	AFM	26.05	0.02	-0.01

6.3.2.2 Magnetic and electronic properties

Table 6.3 also show the energy difference, or the exchange energy ΔE between the AFM and the FM configurations of the V-V pair as they are separated in silicene layer as well as the corresponding total magnetization. What is clear from the table and figure 6.22 is the flipping of the stable magnetic states as the positions or the sublattice site of the V atom changes. Specifically, when the V-V dimer are on a similar sublattice type, they prefer to couple together antiferromagnetically. However, when they are on a different sublattice type, V-V prefer to be in FM configuration. This is more aptly shown in the plot of exchange energy versus V-V separation which shows flipping or zigzag feature, as shown in figure 6.22.
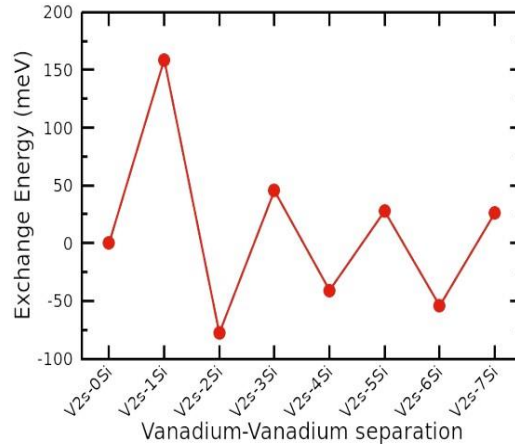
Figure 6.22: Plot of exchange energy of V-V pair configuration as the separation between the pair and the number of atom separating the pair increases.

From the table, the configuration denoted as *V2s-1Si* has the highest positive exchange energy ΔE, while *V2s-2Si* has the most negative ΔE. In other words, the former is the most stable AFM V-V configuration, while the latter is the most stable FM V-V substitutional pair. The small value of ΔE between the FM and AFM suggests that either of the two magnetic configuration is stable for this particular V-V pair. Table 6.3 also show the value of the magnetic moment per supercell. The magnetic moments for the FM configurations varies between ~3 μ_B and 4 μ_B. These spin moments are contributed by the embedded V atoms.

It should be recalled that the AFM *V2s-0Si* is the most stable V-V substitutional pair configuration with a binding energy of ~6.4 eV. Therefore, this configuration has been selected to gain an insight into the electronic interactions between the V-V pair.
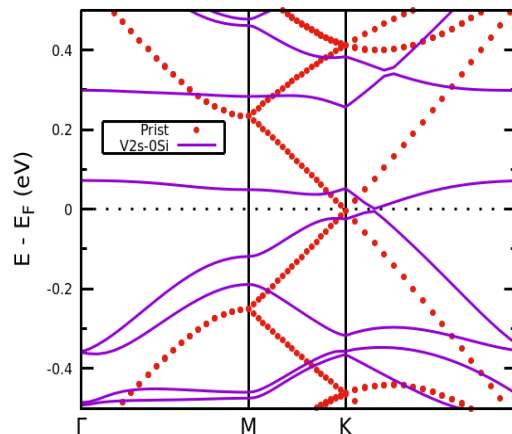
Figure 6.23: Band structure of *V2s-0Si* configuration. The red dot line is the band for pristine silicene while the purple line represents the bands for the V-V-embedded silicene. Fermi level is set to zero as shown by the black dashed line.

Figure 6.23 shows the band structure of this configuration. The most significant change to the electronic bands is the annihilation of the Dirac point such that a small band gap of ~0.08 eV is created at K point. Nevertheless, the bands still cross the Fermi level along the Γ-K direction which makes the system metallic. The significant modification of the bands due to presence of V-V suggests strong electronic interaction between the V atom and the Si atoms of silicene layer.

6.3.3 Interstitial hole vanadium dimer in silicene

6.3.3.1 Energetics and structural properties

The preceding section considered the interaction of V-V atom pairs at substitutional positions in monolayer silicene. This section focuses on the interaction of V-V pair at interstitial hole positions in a monolayer silicene. Similar to the case of substitutional V-V, the V-V pair are relaxed when they are coupled in FM or AFM magnetic orientations. Non-magnetic coupling of the V atoms was also considered. The binding energy of these configurations is obtained using [71]:

$$E_b = [E_{V-V} + E_{pr}] - 2\mu_V \tag{6.6}$$

where E_{V-V} represents the total energy of the relaxed interstitial hole vanadium dimer in silicene, E_{pr} represent the total energy of relaxed pristine silicene, μ_V represents the chemical potential for the vanadium atom.

Table 6.4 shows the difference in energy ΔE, between the FM and the AFM configurations of the interstitial V-V pair as their separation increases, the calculated binding energy E_b, as well as the total magnetic moment of the supercell containing the V-V pair. From the table, it is seen that the interstitial hole V-V are most strongly binded when both are nearest neighbours, that is, at the centre of two adjacent hexagonal holes, with a E_b = ~-0.5 eV. When the V atoms are separated farther apart, the E_b reduces drastically to less than 0.01 eV. We may deduce therefore that two- or three-dimensional clustering of V atoms may occur at the interstitial holes, but only when the atoms are closest together. Figure 6.24(b) shows the relaxed structure for the most stable configuration. Each of the atom relaxes to a height of 1.25Å above the silicene plane. Unlike the nearest-neighbour substitutional V-V where the V atoms are perturbed from their substitutional sites, the V atoms are located within the silicene hexagon, but are elevated to the aforementioned height.
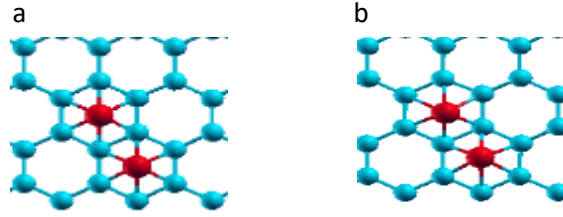
Figure 6.24: (a) Pre-relaxed (b) relaxed structure of interstitial hole V-V pair. The blue sphere represents the silicene atom while the red sphere is the vanadium atom.

Table 6.4: Calculated parameters of interstitial hole vanadium-vanadium interaction at varying distances of separation in silicene, E_{min} is the minimum energy configuration between the ferromagnetic (FM) and the antiferromagnetic (AFM) configuration of the V-V pair, ΔE is the energy difference between the FM and the FM configuration of the V-V pair, E_b is the binding energy of the corresponding minimum energy configuration. When ΔE is positive, the AFM is the more stable configuration whereas when it is negative the FM is the more stable. Induced magnetic moment per unit cell is μ_m in Bohr magneton.

V-V configuration	E_{min}	$\Delta E = E_{FM} - E_{AFM}$ (meV)	E_b(eV)	μ_m/cell (μ_B)
V2h-0h	AFM	343.70	-0.52	0.00
V2h-1h	AFM	23.64	0.00	0.00
V2h-2h	FM	-1.52	0.01	9.52
V2h-3h	FM	-3.94	0.01	9.52
V2h-4h	AFM	23.65	0.00	0.01

6.3.3.2 Magnetic and electronic properties

Table 6.4 also show the energy difference or the exchange energy ΔE between the AFM and the FM configurations of the V-V pair as they are separated in silicene layer. This is also illustrated in figure 6.25. The figure shows drastic change to the ΔE as the atoms separates. Beyond the nearest-neighbour interstitial hole V-V configuration, the ΔE reduces drastically. Configuration *V2h-0h* has the highest positive exchange energy of ~0.34 eV, which implies that the antiferromagnetic orientation of the V-V pair is stable against the FM. In general, in all the configurations considered, the AFM V-V pair presents a more positive absolute ΔE compared to the FM. The table also shows total magnetization per unit cell for each of the configurations. From the table, the FM V-V orientations, have total magnetization per unit cell of 9.52 μ_B, that is, *V2h-2h* and *V2h-3h*, which is about twice the value of magnetization per a single V atom in interstitial hole site, that is, -4.68 μ_B. Thus, magnetic moments are contributed by the embedded V-V atom pair.
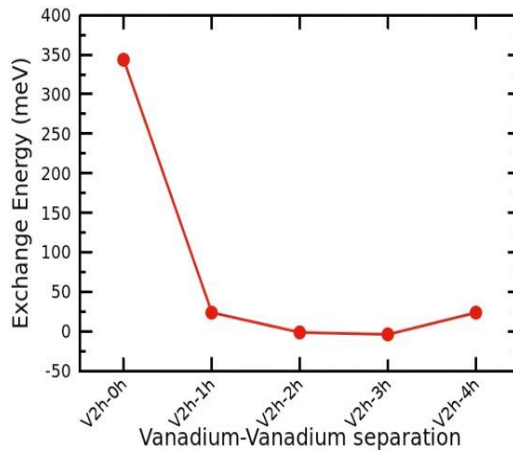
Figure 6.25: Plot of exchange energy of V-V pair configuration as the separation between the V-V pair in interstitial hole increases. Configuration *V2h-0h* is where the V-V are closest and there is no separating Si hexagon between them. In *V2h-4h*, the V-V pair is separated by four hexagons formed by Si atoms.

Figure 6.26 shows the band structure for the most stable interstitial V-V pair, that is, *V2h-0h*.
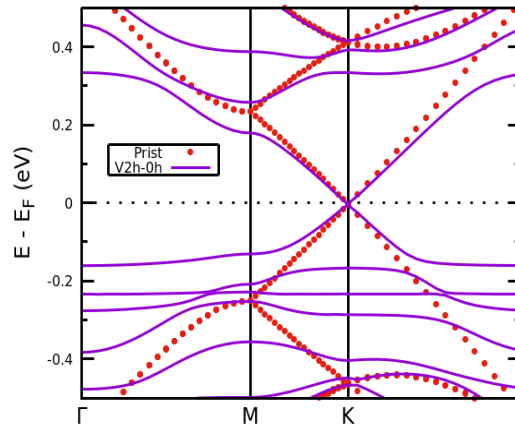
Figure 6.26: Band structure of *V2h-0h* configuration. The red dot line is the band for pristine silicene while the purple line represents the bands for the V-V-embedded silicene. Fermi level is set to zero as shown by the black dashed line.

Here, the Dirac point is preserved, that is, at K point, renders this system to acquire metallic characteristics. The figure also shows few additional bands that have been introduced by the embedded V atoms. For completeness, we have shown the band structures for the relatively stable FM configurations in Figure 6.27, that is, *V2h-2h* and *V2h-3h*. Here, the Dirac point is preserved but with a small opening. Also, the point is shifted such that a band crosses the Fermi level thus making the system metallic.
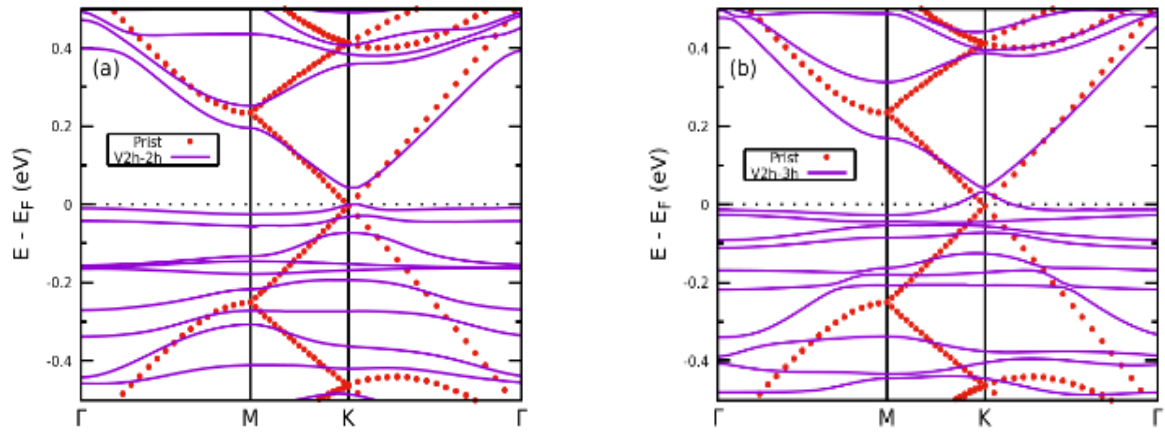
Figure 6.27: Band structures of FM (a) *V2h-2h* (b)*V2h-3h*. The red dot line is the band for pristine silicene, while the purple line represents the bands for V-V-embedded silicene. The Fermi level is set at zero as shown by the black dashed line.

CHAPTER 7

Vanadium-doped silicene: Effect of oxygen and hydrogen impurities

This section deals with the effects of oxygen and hydrogen impurities on vanadium-doped silicene. Oxygen(O) and hydrogen(H) are ubiquitous gases that are introduced into a material sample during synthesis protocols and thus, their effect cannot be neglected. Therefore, we have considered a model system consisting of vanadium in substitutional site with O and H at nearby lattice position. With regards to the latter, eight different configurations of silicene containing V-O and V-H defect impurity complexes have been considered. These configurations are described in table 7.1 while the corresponding atomic structures are shown in figures 7.1–7.8. We performed spin-polarized (sp) and non-spin polarized (nsp) structural relaxation in order to obtain the V-doped silicene containing V-O and V-H impurity defect complexes.

Table 7.1: Naming convention and description of vanadium-doped silicene containing H and O impurity atoms.

Serial	Configuration	Description	Illustration
1	Si-VO_2	Substitutional V atom with O_2 molecule attached to the V atom.	Fig. 7.1 (a)
2	SiO_2-V	Substitutional V atom with O_2 molecule attached to the nearest-neighbour Si atom to the V atom.	Fig. 7.2 (a)
3	SiO-V	Substitutional V atom with O atom attached to the nearest-neighbour Si atom to the V atom.	Fig. 7.3 (a)
4	Si-VO	Substitutional V atom with O atom attached to the V atom.	Fig. 7.4 (a)
5	Si-VH_2	Substitutional V atom with H_2 molecule attached to the V atom.	Fig. 7.5 (a)
6	SiH_2-V	Substitutional V atom with H_2 molecule attached to the nearest-neighbour Si atom to the V atom.	Fig. 7.6 (a)
7	Si-VH	Substitutional V atom with H atom attached to the V atom.	Fig. 7.7 (a)
8	SiH-V	Substitutional V atom with H atom attached to the nearest-neighbour Si atom to the V atom.	Fig. 7.8 (a)
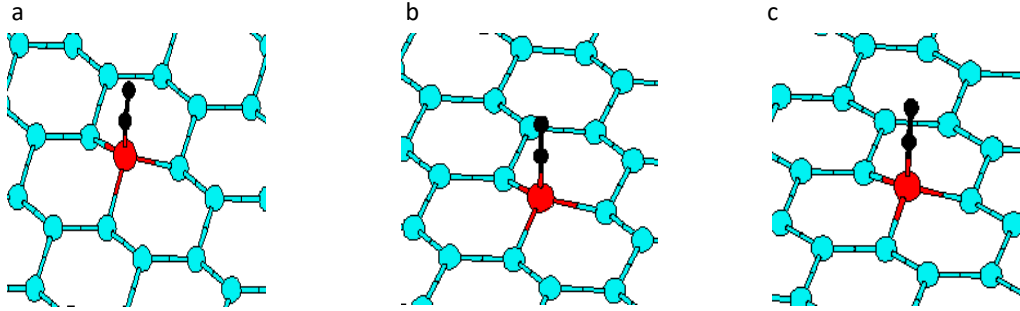
Figure 7.1 (a) Pre-relaxed *Si-VO₂* configuration; (b) relaxed spin-polarized (*sp*) *Si-VO₂* configuration; (c) relaxed non-spin polarized (*nsp*) *Si-VO₂* configuration. Blue sphere is the silicene atom, the red sphere is the vanadium atom, and the black spheres is the oxygen molecule.

Figure 7.2 (a) Pre-relaxed *SiO₂-V* configuration; (b) relaxed *sp SiO₂-V* configuration; (c) relaxed *nsp SiO₂-V* configuration. Blue sphere is the silicene atom, the red sphere is the vanadium atom, and the black spheres is the oxygen molecule.

Figure 7.3 (a) Pre-relaxed *SiO-V* configuration; (b) relaxed *sp SiO-V* configuration; (c) relaxed *nsp SiO-V* configuration. Blue sphere is the silicene atom, the red sphere is the vanadium atom, and the black sphere is the oxygen atom.

Figure 7.4 (a) Pre-relaxed *Si-VO* configuration; (b) relaxed *sp Si-VO* configuration; (c) relaxed *nsp Si-VO* configuration. Blue sphere is the silicene atom, the red sphere is the vanadium atom, and the black sphere is the oxygen atom.
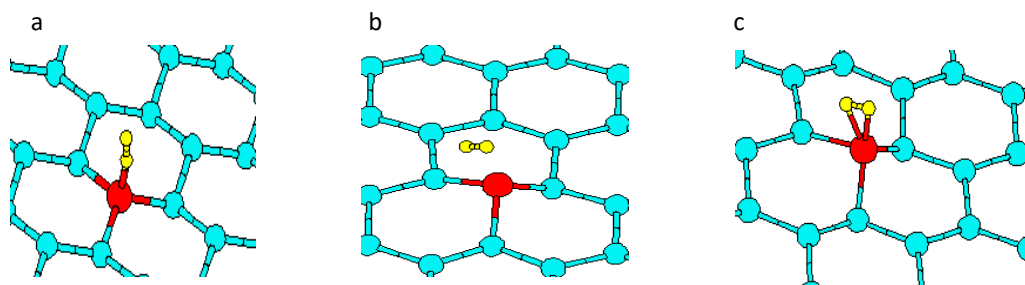
Figure 7.5 (a) Pre-relaxed *Si-VH₂* configuration; (b) relaxed *sp Si-VH₂* configuration; (c) relaxed *nsp Si-VH₂* configuration. Blue sphere is the silicene atom, the red sphere is the vanadium atom, and the yellow spheres is the hydrogen molecule.
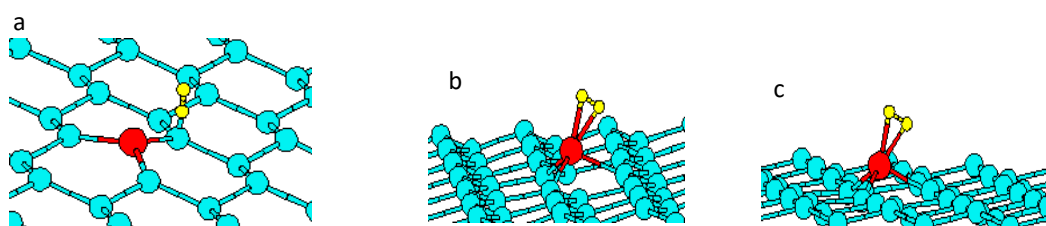
Figure 7.6 (a) Pre-relaxed *SiH₂-V* configuration; (b) relaxed *sp SiH₂-V* configuration; (c) relaxed *nsp SiH₂-V* configuration. Blue sphere is the silicene atom, the red sphere is the vanadium atom, and the yellow spheres is the hydrogen molecule.
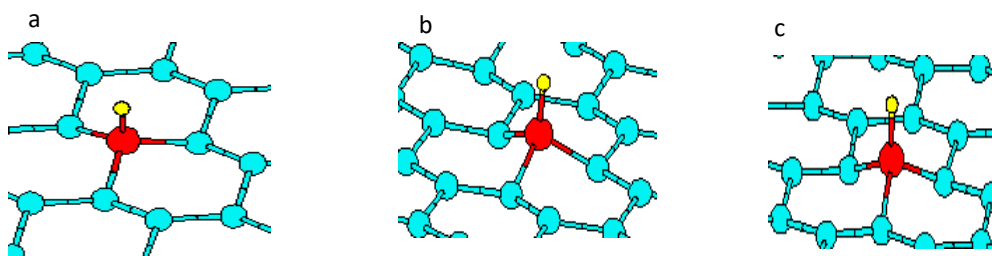
Figure 7.7 (a) Pre-relaxed *Si-VH* configuration; (b) relaxed *sp Si-VH* configuration; (c) relaxed *nsp Si-VH* configuration. Blue sphere is the silicene atom, the red sphere is the vanadium atom, and the yellow sphere is the hydrogen atom.
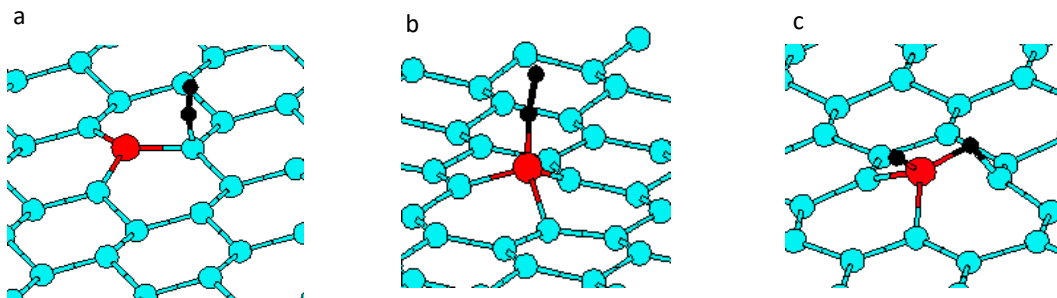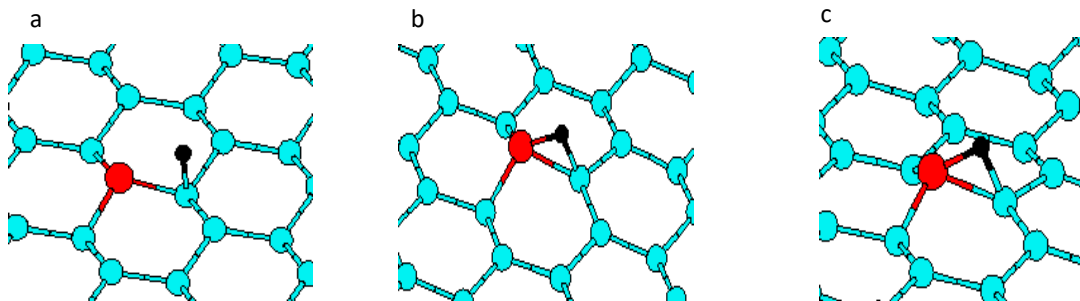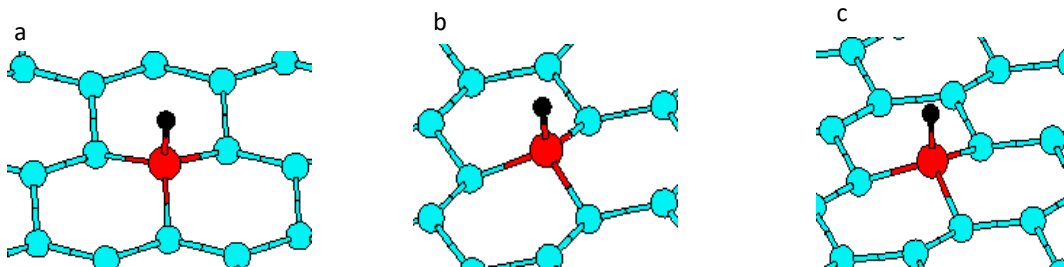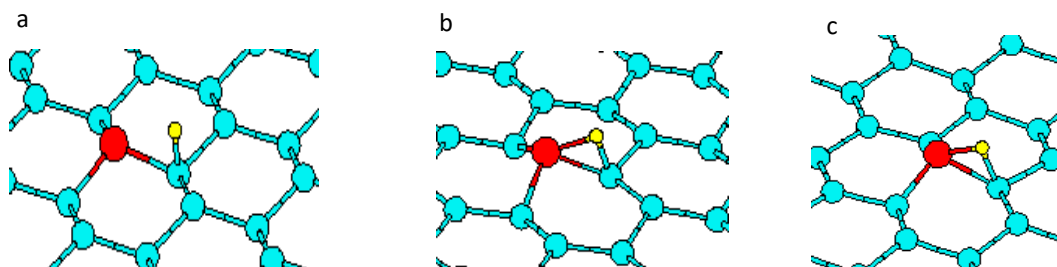

Figure 7.8 (a) Pre-relaxed *SiH-V* configuration; (b) relaxed *sp SiH-V* configuration; (c) relaxed *nsp SiH-V* configuration. Blue sphere is the silicene atom, the red sphere is the vanadium atom, and the yellow sphere is the hydrogen atom.

7.1 Energetics and structural properties

Vanadium-doped silicene monolayer containing O and H defects were relaxed with and without spin-polarization. As described in table 7.1, the initial configuration of O-adsorbed V-doped silicene consist of O atom or molecule attached atop the nearest-neighbour silicene atom to the V atom, as shown in figures 7.2(a) and 7.3(a). The initial O-O bond length is 1.25 Å. Upon relaxation, the O atom drifts away from the initial top site position on the silicene atom and attaches itself directly to the V atom. Interestingly, when the initial configuration of the O atom is such that it is located on the V atom, the O remains in position. Therefore, one may conclude that the V atom attracts the O atom in a stable V-O or V-O_2 orientation. These are illustrated in figures 7.1(b), 7.2(b), 7.3(b) and 7.4 (b) for *Si-VO₂*, *SiO₂-V*, *SiO-V*, and *Si-VO*, respectively. It should be noted the relaxed spin-polarized (*sp*) and non-spin polarized (*nsp*) are similar except for the *SiO₂-V* where the O_2 molecule appears to have dissociated for the *nsp SiO₂-V* (figure 7.2 (c)) compared to the *sp* structure (figure 7.2(b)). The O-O bond length in the former is now 3.02 Å compared to the non-dissociated structures (figures 7.1(b-c) and 7.2(b)). Also, the relaxed V-O bond length is 1.73 Å (figure 7.2(b)) as compared to 1.60 Å in figure 7.2 (c). Furthermore, figures 7.3 (b-c) and 7.4 (b-c) show the relaxed configurations for the O atom on V-doped silicene. There is no difference between the relaxed *sp* (figures 7.3(b) and 7.4(b)) and relaxed *nsp* (figures 7.3(c) and 7.4(c)) configurations. The relaxed V-O bond length is 1.77 Å for both *sp* and *nsp SiO-V* (figure 7.3(b) and 7.3(c)).

The initial configurations of H-adsorbed V-doped silicene are similar to those of V-doped silicene with adsorbed O, as shown in figures 7.5(a), 7.6(a), 7.7(a) and 7.8(a). The respective relaxed configurations are such that the H atom or molecule attach itself to the V atom, away from the top site position on the nearest-neighbour Si atom to the substitutional V atom. Also, these are clearly shown for *Si-VH₂*, *SiH₂-V*, *Si-VH*, *SiH-V* in figures 7.5(b-c), 7.6(b-c), 7.7(b-c) and 7.8(b-c), respectively. One may conclude therefore that substitutional V atom attracts H and O to itself in stable *V-H*, *V-H₂*, *V-O* and *V-O₂* configurations. However, the relaxed configurations of certain *V-O* and *V-H* defect complexes deserve further consideration. As an example, for the *Si-VH₂*, that is, the relaxed H_2 molecule is oriented so that it lies parallel to the silicene surface but directly on top of the V atom. It should be emphasized that the initial orientation (before relaxation) is such that the H_2 molecule lies vertically on the vanadium atom. This is shown in figure 7.5 (a) for the initial configuration

and figure 7.5 (b) for the final relaxed configuration. However, even when the H_2 molecule initial orientation is vertical on the nearest-neighbour silicene atom to the V atom, the final relaxed configuration is such that the H_2 molecule lies on top of the V atom but in horizontal orientation and parallel to the silicene surface. One may conclude therefore that the V atom attracts H_2 molecule in a stable *V-H_2* configuration wherein the H_2 molecule lies in parallel orientation to the surface atop the V atom. Also, deserving of mentioning is the O_2 molecule. The relaxed configurations clearly show that the molecule attaches itself to V atom as *V-O* defect complex, and not as *V-O_2* complex, if the initial configuration is such that the O_2 molecule sits atop the nearest-neighbour silicene atom, that is *SiO_2-V*, as illustrated in figure 7.2 (a). However, if the initial configuration is such that the O_2 molecule is located atop the V atom, that is *Si-VO_2*, the O_2 attaches itself to the V atom as a molecule in a vertical orientation as shown in figure 7.1 (b).

We have also calculated the formation energy (E_f) of the defect complex as:

$$E_f^{Si-V-ad} = E_{Si-V-ad} + \mu_{Si} - [E_{Si} + \mu_V + \mu_{ad}] \tag{7.1}$$

where $E_{Si-V-ad}$ is the total energy of a defect complex made up of vanadium atom and adsorbate (*ad*) (*ad* = O, O_2, H or H_2) in the silicene layer, while E_{Si} is the total energy of pristine or adsorbate-free silicene layer. Also, μ_{Si}, μ_V and μ_{ad}, respectively, are the chemical potentials for the silicon atom (of silicene), vanadium atom and the adsorbate (O, O_2, H or H_2). The formation energy gives an indication of ease of formation of a particular defect structure it has been computed for. Based on the convention adopted for the equation above, the more negative its value, the more readily a particular defect is able to be formed when it is compared to other defect configurations.

Table 7.2 show the computed $E_f^{Si-V-ad}$ for all the defect configurations as described in table 7.1 and shown in figures 7.1–7.8. The table contains the formation energy obtained with and without the spin-polarization. It is clear from the table that when the spin-polarized and spin-unpolarized $E_f^{Si-V-ad}$ of the same structure are compared, the latter is more negative or less probable than the former. This suggest that, of all the configurations of V-substituted silicene with adsorbate, that is $Si - V - ad$, the spin-polarized structures are the most likely to be found in silicene. Therefore, we focus on the spin-polarized $Si -V- ad$ defect complexes. Here, the configuration *SiO_2-V*, that is, where the O_2 attaches directly to the silicon atom (Figure 7.2 (a)), has the least formation energy of -0.64 eV. However, this is similar to the $E_f^{Si-V-ad}$ = -0.66 eV obtained for the *Si-VH*, that is, the configuration where

the H atom attaches directly to the V atom (Figure 7.7 (a)). It should be noted however, that the $E_f^{Si-V-ad}$ for *Si-VH₂* is +0.96 eV, which makes it unstable or its formation highly unlikely. Similarly, the configuration *Si-VO₂*, where the O₂ molecule binds directly to the V atom (Figure 7.1 (a)), has $E_f^{Si-V-ad} = -0.72$ eV which also is similar formation energy compared to *Si-VH* and *SO₂-V*. Worthy of comparison is the $E_f^{Si-V-ad} = -5.48$ eV for *Si-VO*, that is, atomic O attached to the V atom (Figure 7.4 (a)). It appears therefore that molecular O, that is O₂, are more easily formed in V-substituted silicene layer. In the case of hydrogen atom however, $E_f^{Si-V-ad} = -1.15$ eV and +1.03 eV for *SiH-V* and *SiH₂-V*, respectively. When this is compared with the $E_f^{Si-V-ad}$ for *Si-VH* (-0.66 eV) and *Si-VH₂* (+0.96 eV), it means H atom is more easily formed in V-substituted silicene layer.

Table 7.2: Calculated parameters of spin and non-spin polarised vanadium-doped silicene with adsorbed adsorbate (*ad*) of O₂, O, H₂, or H: adsorption energy, E_{ads}; formation energy, E_f; the shortest bond length between the adatom and the silicene atom, d_{ad-Si}; the shortest bond length between the adatom and the vanadium atom, d_{ad-V}; and total magnetic moment per unit cell, μ_m.

	spin (*sp*)					non-spin (*nsp*)			
	E_{ads} (eV)	E_f (eV)	d_{ad-Si} (Å)	d_{ad-V} (Å)	μ_m (μ_B)	E_{ads} (eV)	E_f (eV)	d_{ad-Si} (Å)	d_{ad-V} (Å)
Si-VO₂	-2.09	-0.72	3.37	1.69	-0.02	-3.80	-3.84	3.37	1.69
SiO₂-V	-2.00	-0.64	2.99	1.73	0.82	-9.32	-9.36	1.67	1.60
SiO-V	-7.18	-5.82	1.74	1.77	-1.07	-9.07	-9.11	1.74	1.77
Si-VO	-6.85	-5.48	3.34	1.59	0.64	-8.97	-9.00	3.34	1.59
Si-VH₂	-0.41	0.96	2.62	1.91	0.00	-0.59	-0.63	2.49	1.80
SiH₂-V	-0.33	1.03	2.60	1.92	1.36	-0.55	-0.59	2.49	1.82
Si-VH	-2.02	-0.66	3.47	1.67	0.00	-3.62	-3.65	3.47	1.67
SiH-V	-2.52	-1.15	1.66	1.81	2.03	-3.80	-3.84	1.73	1.74

The adsorption energy of an adsorbate, that is O; O₂; H or H₂, to the silicene containing substitutional V is calculated using the formula:

$$E_{ads}^{Si-V-ad} = E_{si-V-ad} - [E_{Si-V} + E_{ad}]$$ (7.2)

where $E_{si-V-ad}$ is the total energy of a defect complex made up of vanadium atom and adsorbate (ad) (ad = O, O₂, H or H₂) in the silicene layer. Also, E_{Si-V} is the final relaxed energy of silicene containing substitutional V atom, while E_{ad} is the energy of isolated adsorbate, that is, O; O₂; H or H₂. A negative E_{ads} indicate that the defect complex consisting of an adsorbate on V-substituted silicene (*Si-V*) is more stable than the individual defect components making up the defect complex, that is, V-substituted silicene and the

adsorbate. Also, the more negative the E_{ads}, the more stable it is relative to similar defect complexes. Furthermore, Table 7.2 reveals that the adsorption energy of non-spin polarized systems of Si-V-ad (*ad* = adsorbate of O, O_2, H or H_2) is more negative (higher stability) than the spin-polarized counterparts. This observation may be explained as due to the fact the adsorbate interact with the V orbitals states (that is, the source of induced magnetization in V-doped silicene) in such a way that the unpaired V orbital electrons are paired with adsorbate electrons. The pairing with electrons, of previously unpaired V orbitals leads to zero magnetization, that is, stable non-spin polarized system.

The adsorption energy for the relaxed *SiO₂-V* and *Si-VO₂* of -2.00 eV and -2.09 eV, respectively, shows that both final configurations of O_2 molecule on V-doped silicene are feasible. However, a single O atom attaches itself to the V atom with a much greater energy of adsorption of ~-7.0 eV as shown in Table 7.2. Therefore, the O atom adsorbs more strongly to the V atom when the latter is in substitutional position, while the O_2 molecule is less adsorbed as aforementioned. Similar conclusion can be reached for the H atom. Here, the H atom adsorbs to the V atom with E_{ads} of ~-2.02 eV and -2.52 eV, which is order of magnitude higher than ~0.3–0.4 eV for the H_2 molecule on V-doped silicene.

Table 7.3: Calculated parameters of spin-polarised silicene monolayer without vanadium atom but containing adsorbate of O, O_2, H or H_2; adsorption energy, E_{ads} and induced magnetic moment per unit cell, μ_m. The adsorbates *pSi-X* (*X = Si-O, Si-O₂, Si-H* and *Si-H₂*) are *X* molecules on a pristine silicene monolayer. These are different from *SiO-V, SiO₂-V, SiH-V* and *SiH₂-V* in Table 7.2 which are molecules adsorbed on V-doped silicene layer.

Configuration	E_{ads} (eV)	μ_m/cell (μ_B)
pSi-O	-6.03	0.00
pSi-O₂	-0.37	1.64
pSi-H	-2.05	0.62
pSi-H₂	-0.00	0.00

It is important to compare the adsorption of the O, O_2, H or H_2 adsorbates with and without the presence of substitutional vanadium. In Table 7.3, we show the adsorption energies of spin-polarised silicene monolayers without substitutional vanadium atom but with O, O_2, H or H_2 adsorbate. We have denoted these configurations without V atom as *pSi-O, pSi-O₂, pSi-H*, and *pSi-H₂*, where the '*pSi-O*' for example indicates pristine (*p*) silicene (*Si*) with adsorbed O atop the Si atom. The same notation meaning applies to the other three configurations. A comparison of the energy of adsorption of the aforementioned four pristine structures with similar structures but with substitutional V, reveals that the presence of V atom enhances the adsorption of the O, O_2, H or H_2 adsorbates. As an illustration, the

E_{ads} of the *pSi-O*, of ~-6.0 eV is less than that of *SiO-V* and *Si-VO*, which has E_{ads} = ~-7.2 eV and ~-6.9 eV (table 7.2), respectively. It should be remembered that in the structure *SiO-V*, the O atom is attached to the silicene atom next to the V substitutional atom (figure 7.3 (a)), whereas in the case of *Si-VO*, the O atom is directly attached to the substitutional V atom (figure 7.4 (a)). Similar enhancement of adsorption due to the presence of V atom is observed for the *pSi-O₂* configuration. In this case, its E_{ads} of -0.37 eV is significantly less than that of ~-2.0 eV obtained for *Si-VO₂* and *SiO₂-V* (table 7.2). The same trend continues with *pSi-H₂* configuration, the adsorption energy of which should be compared with that of *Si-VH₂* and *SiH₂-V*. In the same vein, the E_{ads} of *pSi-H* should be compared to those of *Si-VH* and *SiH-V*, which also show that the presence of V atom enhances the adsorption of the H atom. To summarize, we can say that substitutional V atom enhances the adsorption of O, O_2, H or H_2 adsorbates on silicene, as demonstrated when tables 7.2 and 7.3 are compared for the aforementioned structures. The enhanced H adsorption properties of V-doped silicene could be significant in possible application of the material as hydrogen storage medium.

7.2 Magnetic and electronic properties

Here, we consider the effect of adsorbates O, O_2, H and H_2 on the electronic properties and magnetization in vanadium-doped silicene layer. We focus on the relaxed structures shown in figures 7.1 (b) to 7.8 (b). The values of magnetic moments for the spin-polarized systems are also given in table 7.2. We recall that both O and H atoms as well as their molecular forms, that is O_2 and H_2 respectively, are adsorbed on silicene via the V atom or on the nearest-neighbour (*NN*) silicene atom to V atom. We consider firstly the O and O_2. The effect of their adsorption on silicene is such that when the O_2 molecule is adsorbed on the V atom, it annihilates the magnetization in the V-doped silicene. It would be recalled that the magnetization on the latter is ~2.61 μ_B. However, if the O_2 is adsorbed on the nearest-neighbour silicene atom to the substitutional V atom, the magnetization in the system is retained at 0.82 μ_B.

The behaviour of O atom is different in the sense that whether it is located on the V atom or on the *NN* silicene atom, it retains the magnetization in the V-doped silicene system, although to a smaller value of 0.64 μ_B in the case of O atom adsorbed directly on the V atom (figure 7.4 (a)). In the case of H and H_2 adsorption, we learnt from table 7.2 that both species

when adsorbed on V atom results in zero magnetization. On the contrary, their adsorption on the *NN* silicene atom to V atom retains the magnetization in V-doped silicene. In actual fact, in the case of H adsorption, that is, *SiH-V* (figure 7.8(a)), the magnetization of 2.03 μ_B obtained for this system approaches ~2.61 μ_B for the H-free V-doped silicene layer.

To summarize, H_2 and O_2 molecules when adsorbed on V atom in V-doped silicene annihilates the latter's magnetization. On the other hand, when they are adsorbed on the *NN* silicene atom to the V atom, they retain the magnetization in the V-doped silicene layer. Also, when the adsorbates of H_2, H, O_2 and O are adsorbed on the *NN* silicene atom, the magnetization in the V-doped silicene is retained as can be seen for *SiH$_2$-V*, *SiH-V*, *SiO$_2$-V*, and *SiO-V* configurations. It should be emphasized, however, that the *Si-VH$_2$* has a positive formation energy of 0.96 eV, which makes its formation highly unlikely in V-doped silicene.

Here, we outline the electrical properties of V-doped silicene layer containing the adsorbates of O, O_2, H and H_2. Also, we compare the aforementioned with the V-doped system without the adsorbate. We recall that the V-doped silicene containing O_2 and O are named *Si-VO$_2$*, *SiO$_2$-V*, *Si-VO* and *SiO-V*, while the V-doped silicene containing H_2 and H are named *Si-VH$_2$*, *SiH$_2$-V*, *Si-VH*, *SiH-V*, as stated in Table 7.1. Figure 7.9 shows the band structure of vanadium-doped silicene layer.
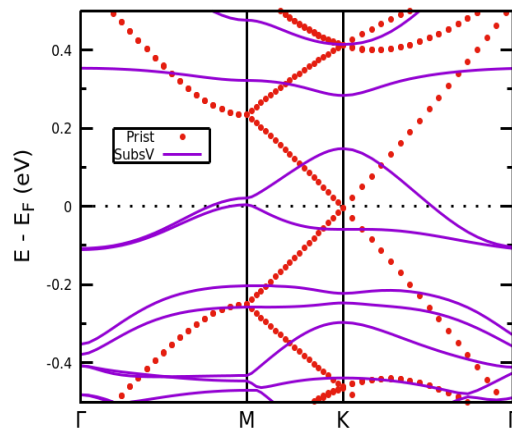
Figure 7.9: Band structure of substitutional vanadium in silicene. The red dot line is the band for pristine silicene, while the purple line represents the bands for substitutional vanadium in silicene. The Fermi level is set at zero as shown by the black dashed line.

Figure 7.10: Band structures of V-doped silicene with O_2 adsorbates (a) *Si-VO₂* and (b) *SiO₂-V*. The red dot line is the band for pristine silicene, while the purple line represents the bands for *Si-VO₂* and *SiO₂-V*, respectively. The Fermi level is set at zero as shown by the black dashed line.
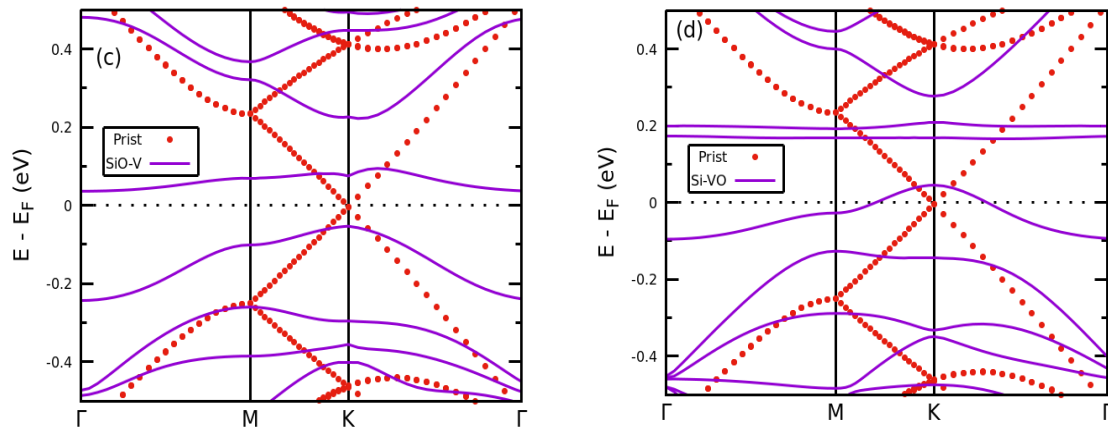
Figure 7.11: Band structures of V-doped silicene with O adsorbates (c) *SiO-V* and (d) *Si-VO*. The red dot line is the band for pristine silicene, while the purple line represents the bands for *SiO-V* and *Si-VO*, respectively. The Fermi level is set at zero as shown by the black dashed line.
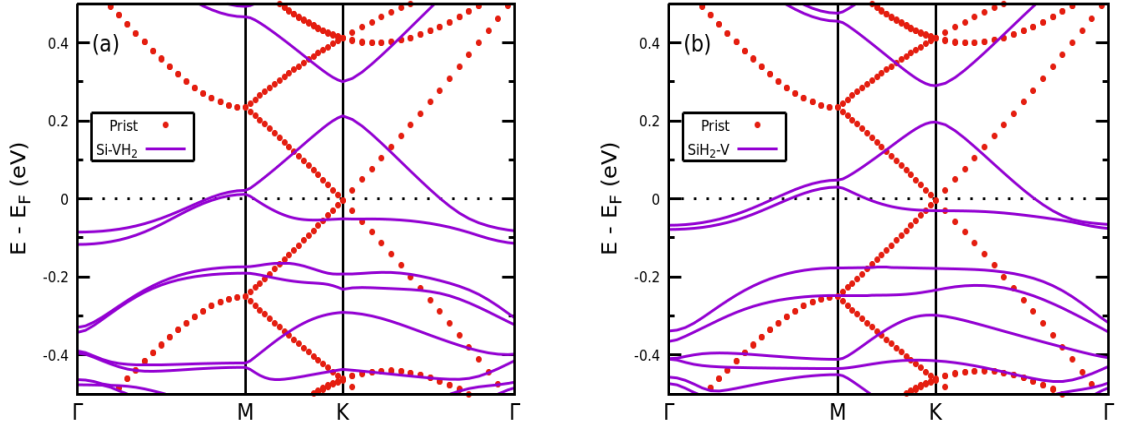
Figure 7.12: Band structures of V-doped silicene with H_2 adsorbates (a) *Si-VH₂* and (b) *SiH₂-V*. The red dot line is the band for pristine silicene, while the purple line represents the bands for *Si-VH₂* and *SiH₂-V*, respectively. The Fermi level is set at zero as shown by the black dashed line.

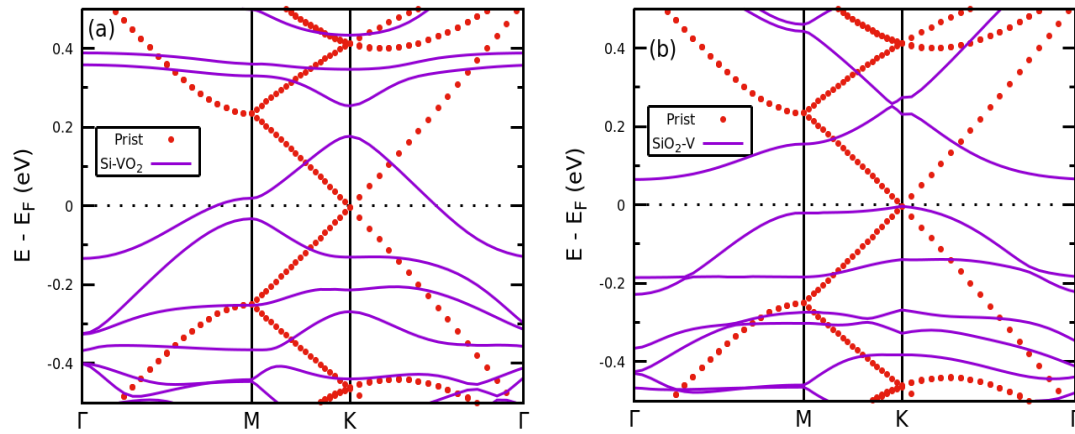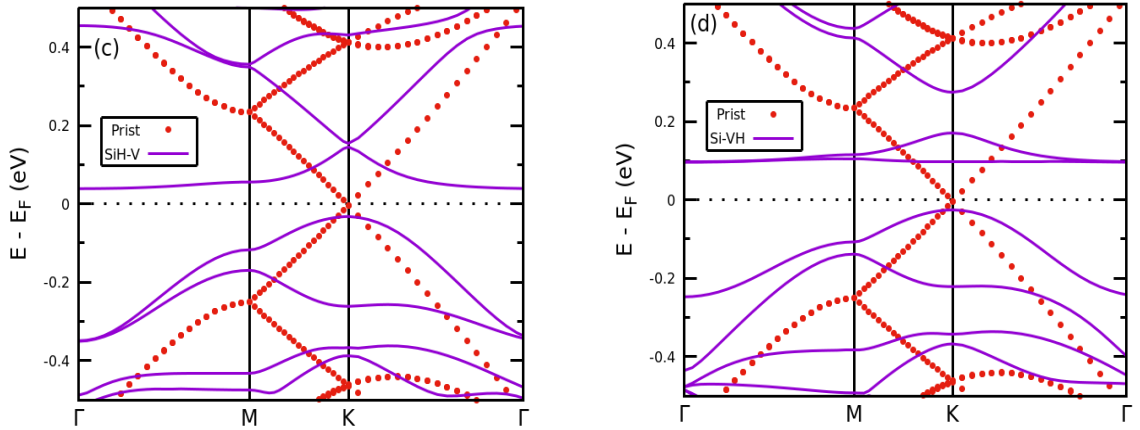Figure 7.13: Band structures of V-doped silicene with H adsorbates (c) *SiH-V* and (d) *Si-VH*. The red dot line is the band for pristine silicene, while the purple line represents the bands for *SiH-V* and *Si-VH*, respectively. The Fermi level is set at zero as shown by the black dashed line.

Figures 7.10–7.11 and 7.12–7.13 shows the band structures of V-doped monolayer silicene with dopants of O_2 and O as well as H_2 and H, respectively. As explained in table 7.1, the relevant structures have been denoted as *Si-VO₂*, *SiO₂-V*, *SiO-V*, and *Si-VO*, the band structures of which are shown in figures 7.10–7.11, and *Si-VH₂*, *SiH₂-V*, *SiH-V* and *Si-VH* (figures 7.12–7.13). If figure 7.9 for adsorbate-free V-doped silicene is compared with V-doped silicene with hydrogen and oxygen adsorbates, one notices the lifting of degeneracy of the bands at the Γ-point and this applies to all the adsorbate-doped systems. Another observation is the complete annihilation of the Dirac point K in all the adsorbate systems. The lifting of bands degeneracy results in the creation of a band gap in the systems *SiO-V* (figure 7.11(c)), *SiH-V* (figure 7.13(c)) and *Si-VH* (figure 7.13(d)), which turn these systems

into a non-metallic material, whereas for the other systems such as *Si-VO₂* (figure 7.10(a)), *Si-VH₂* (figure 7.12(a)), *SiH₂-V* (figure 7.12(b)) and *Si-VO* (figure 7.11(d)), the crossing of the Fermi level by the bands results in these systems to retain metallicity. In the case of *SiO₂-V* (figure 7.10(b)), one of the split bands slightly touches the Fermi level, thus making it a metallic material. Where the band gap appears due to the V and adsorbate inclusion, its creation is due to the splitting of the *p* bands, in particular around the Dirac point. The identical p bands crossing the Fermi energy level results in metallic silicene. We can thus summarize as follows: Substitutional vanadium atom inclusion in monolayer silicene makes it metallic with a finite magnetization. However, the adsorption of environmental gases such as H_2, H, O_2, and O may make the material non-metallic.

Table 7.4: Summary of the magnetization and material type for V-doped silicene containing hydrogen and oxygen gases.

Serial	Samples	Magnetization (μ_B)	Final conductivity of the material	
1	*SiH₂-V*	1.36	metallic	
2	*Si-VH*	0.00	non-metallic/semiconducting	
3	*SiH-V*	2.03	non-metallic/semiconducting	🟢
4	*Si-VH₂*	0.00	metallic	
5	*SiO₂-V*	0.82	metallic	
6	*SiO-V*	-1.07	non-metallic/semiconducting	🟢
7	*Si-VO*	0.64	metallic	
8	*Si-VO₂*	-0.02	metallic	
1	V-doped silicene	1.00	metallic	
2	Pristine monolayer silicene	0.00	non-metallic/semiconducting	

In table 7.4, we seek to combine two important properties of modified silicene samples: Magnetization and band gap. The green dot structures, that is, *SiH-V* and *SiO-V*, have near finite magnetization and semiconducting property. Thus, they may be likened to ferromagnetic semiconductors. It should be noted that in both cases, the H and O atoms are on the nearest-neighbour silicene atom next to substitutional vanadium atom. However, molecular H and O on silicene atom nearest to the V atom, that is *SiH₂-V* and *SiO₂-V*, does not result in ferromagnetic semiconductor. They are metallic instead, with finite

magnetization. Other metallic structures with finite magnetization are as indicated in table 7.4.

CHAPTER 8

Conclusion and Recommendation

8.1 Summary and conclusions

Our model systems consist of vanadium atoms embedded in a monolayer silicene, where the latter may or may not contain a pre-existing structural defects such as self-vacancies. The structures are then relaxed to obtain the ground-state or minimum energy configurations. We have considered intrinsic defects such as a single and double vacancies and defect complexes consisting of vacancies complexes, vacancy-vanadium complexes, vanadium clusters, in a monolayer silicene. We also considered the interactions of these defects with hydrogen and oxygen atoms. To determine the stability of the defect structures, we calculated the formation energy and the binding energy. To acquire knowledge about the electronic interactions underpinning a stable defect configuration, we calculated the electronic structures such as the band structure and the projected DOS (PDOS). We also obtained the magnetic properties of the defects such as the spin moments and the exchange energy. The major results of the thesis are summarized in the following.

We obtained a vacancy formation energy of 3.52 eV for silicene, which is consistent with values of between 2.47 eV and 4.30 eV as obtained in other theoretical studies. We have found no experimental value in literature for the vacancy formation energy in silicene. In our convention, the positive value of formation energy means that vacancy is not easily produced in silicene and may need external perturbation such as electron bombardment to be produced. Also, the total magnetic moment obtained for silicene with a single vacancy is 2.02 μB per unit cell, which is comparable to 2.33 μB obtained in other studies. Thus, silicene vacancy induces magnetization in its structure, thus making it a low-dimensional magnetic material. Also, from the band structure, we found that the introduction of a single vacancy on silicene sheet annihilates the Dirac point, thus rendering this material system to acquire semiconductor characteristics. Regarding a double vacancy or divacancy which in this case means empty lattice sites created by missing two nearest-neighbour silicene atoms, we obtained a formation energy of 2.13 eV which is surprisingly similar to that of a single vacancy. In addition, we calculated the binding energy of this double vacancy as -2.79 eV.

A negative value in our convention means that the defect complex is more stable relative to the individual defects forming the complex. Thus, this negative value suggests that a missing two nearest-neighbour silicene atoms, that is, divacancy, is more stable than a single vacancy. Furthermore, the total magnetic moment obtained for a double vacancy silicene is 0.00 μB per unit cell which makes it non-magnetic. Similar to the case of a single vacancy, a double vacancy annihilates the silicene's Dirac point. It should be mentioned that two vacancies at different separation, that is, double vacancies in the silicene lattice have a similar formation energy irrespective of their separation.

A single vanadium atom occupying a substitutional or interstitial site in silicene is the simplest external impurity defect. We found the vanadium atom to bind to silicene substitutional site with a large binding energy of -6.08 eV and a formation energy of 1.37 eV. The positive value of formation energy suggest that the inclusion of vanadium is an endothermic process requiring external energy. Also, when inserted in the silicene atomic site, it induces a total magnetic moment of 2.61 μ_B per unit cell. The spin moment on the vanadium atom however is 1.30 μ_B. Since the experimental protocol of vanadium injection into silicene lattice involves energetic process which is able to create vacancy defects, it is intuitive to consider defects complexes consisting of substitutional vanadium and vacancy. Therefore, we studied a simple vacancy-vanadium defect complex. The vacancy-vanadium configuration is such that a vanadium atom is placed at a varying atom distance from a single vacancy. A total of eight interactions were investigated. We find a very strong binding when vanadium has a vacancy as its nearest-neighbour (NN). This defect configuration is equivalent to a vanadium atom in a divacancy. The configuration has a binding energy of ~ -2.8 eV. This is to be compared with the binding energy of ~-6.1eV obtained for a single substitutional vanadium, suggesting that vanadium atom is more stable in single vacancy. This may be due to more or stronger bonding between the three NN Si atoms and vanadium atom in the case of vanadium in a single substitutional site in silicene. Furthermore, the binding of vanadium decreases rapidly when the vacancy is more than one atomic distance away from it, that is, the binding decreases to between ~-0.5 eV and -0.1 eV for all vacancy-vanadium separations. Most importantly, at all of the vacancy-vanadium separations, the corresponding configurations are stable which indicates that vacancy-substitutional vanadium complexes are stable in silicene. Focusing on the most stable vanadium in a divacancy, the total magnetic moment per unit cell of 2.69 μ_B is similar to that of a single substitutional vanadium, that is 2.61 μ_B. However, the induced magnetism on the vanadium

is enhanced to 2.32 μ_B, which is about 1.0 μ_B larger than magnetic moment of a single substitutional vanadium.

We also considered vanadium defect complexes consisting of vanadium atoms only and vacancy-vanadium combinations such that the vanadium atoms are either at the substitutional or interstitial hole sites. The main idea is to investigate the possibility of clustering of vanadium atoms as inclusions in silicene, and whether vacancy defect enhances the clustering. In general, we have investigated three different types of vanadium dimer while exploiting the symmetric points of the silicene lattice. In the first case involving vanadium pairs at varying separation along the zig-zag path in the silicene lattice, we have found that when the V-V dimer are on a similar sublattice type, they prefer to couple together antiferromagnetically. However, when they are on a different sublattice type, the V-V pair prefer to be in ferromagnetic configuration. Therefore, the relative stability of the V-V pair is sublattice dependent which oscillates between FM and AFM configuration as the substitutional lattice sites of the V-V pair changes. Also, where the V-V pair are at the nearest-neighbour substitutional sites, they have the highest binding energy of -6.43 eV, which is the highest stability obtained for all the pair considered, whereas all the other V-V pairs have a binding energy that is $\leq \sim\pm0.1$ eV. The binding energy of -6.43 eV is higher than -2.80 eV obtained for the nearest-neighbour vacancy-vanadium defect complex. This may suggest that vanadium clustering is more probable without the vacancy than with vacancy. Furthermore, the magnetic moments for the FM configurations vary between ~3 μ_B and 4 μ_B as the separation of the V-V pair increases.

Aside from the substitutional V-V pair, we also considered interstitial hole V-V pair wherein the vanadium atoms are coupled in FM or AFM configurations, and are located at the centre of silicene hexagons while their separating distances vary. We determined that the interstitial hole V-V pair are most strongly binded when both are nearest-neighbours with a $E_b = \sim$-0.5 eV. When the V atoms were separated farther apart, the E_b reduced drastically, to less than 0.01 eV. Therefore, similar to the case of substitutional V-V pair and vacancy-vanadium pair, the nearest-neighbour V-V defect pairs are most stable. We have also considered various interstitial V-V pairs wherein we exploited high-symmetry points in silicene structure. We have found that interstitial V-V pairs are stable in cases with significantly high binding energy of about -3.0 eV, which is still less than -6.43 eV. Based on the aforementioned, we are able to make the following deductions: Firstly, V-V pair at

the nearest substitutional sites has the highest binding energy compared to V-V pair at any other sites in silicene lattice. Secondly, in general, V-V atom pair are stable when at the nearest-neighbour sites and the stability decrease as their separation decreases. This suggests that V atom clustering is feasible in a silicene monolayer. Thirdly, V atoms induces finite magnetic moment in the silicene lattice although their presence annihilates the Dirac point while opening a small band gap, often less than 0.1 eV in the silicene electronic band structures.

Since hydrogen and oxygen are ubiquitous atoms which are often introduced during the synthesis protocol, we have also considered their impacts on the properties of vanadium in silicene monolayer. We found that the V atom attracts the O and H either in atomic or molecular form. The adsorption may be to the V atom or to the nearest-neighbour silicene atom to the V atom inclusion. However, when adsorbed they impact on the magnetization of V-doped silicene. As an example, when the O_2 molecule is adsorbed on the V atom in a substitutional V-doped silicene, the magnetic moment per unit cell is annihilated compared to the oxygen-free V-doped silicene, which has a total magnetic moment of ~2.61 μ_B. In a case where the O_2 molecule is adsorbed on the nearest-neighbour silicene atom to the substitutional V atom, the magnetization in the system reduces to 0.82 μ_B. Thus, we may conclude that the presence of molecular H_2 and O_2 reduces or annihilates the magnetization in an otherwise magnetic V-doped monolayer silicene. Furthermore, it is observed that for a V-doped silicene wherein the adsorbed atomic H and O atoms is located on the nearest-neighbour silicene atom to substitutional V atom, the H- and O-containing V-doped silicene behaves like a ferromagnetic semiconductor. On the other hand, molecular H_2 and O_2 on the silicene atom nearest to the V atom, do not result in a ferromagnetic semiconductor, however, the resulting structures are metallic with finite magnetizations. Thus, one may conclude that the impact of H and O on the electronic and magnetic properties of V-doped silicene depends on their respective lattice locations, that is, whether on the V atom or on the silicene atom near to the V dopant. However, a comprehensive calculation of substitutional V and molecular H_2 and O_2 or atomic O and H which exploit the bipartite lattice structure of silicene would be needed to affirm this conclusion.

8.2 Recommendations for future work

Silicene's bipartite structure makes it an excellent atomic lattice where site-dependent interactions between point defects could be studied. This may open the possibilities for future research work involving multiple vacancies on silicene of different arrangement and their interactions with external impurities atoms, including metals and non-metals. We have shown in this work that such defects may induce magnetic properties in a hitherto non-magnetic silicene. But various defect configurations are also possible, which may involve interactions between silicene's intrinsic defects and dopant atoms. It is suggested that a more detailed defect configurations involving three-dimensional dopant atoms anchoring on silicene sheet and their interactions with environmental atoms such as hydrogen and oxygen, will serve to reveal a more interesting electronic and magnetic properties of silicene. Also, our work only focuses on a monolayer silicene whereas multilayer silicene, that is, 2 or 3 layers are also possibilities- the stability, structure, electronic and magnetic properties of which can be investigated in future studies. In general, monolayer and multilayer silicene can be further studied to explore the interactions of substitutional and interstitial atoms of various geometries. Finally, a further extension of the present study may involve charged defect configurations.

9. References

[1] K.S. Novoselov, A.K. Geim, S.V. Morozov, D. Jiang, Y. Zhang, S.V. Dubonos, I.V. Grigorieva and A.A. Firsov, Nature **306** (2004) 666.

[2] J. Zhuang, X. Xu, H. Feng, Z. Li, X. Wang and Y. Du, Sci. Bull. **60** (2015) 1551.

[3] H.H. Gürel, V.O. Özçelik and S. Ciraci, J. Phys. Chem. C **118** (2014) 27574.

[4] R. John and B. Merlin, Cryst. Struct. Theory Appl. **5** (2016) 43.

[5] A. Kara, H. Enriquez, A.P. Seitsonen, L.C. Lew Yan Voon, S. Vizzini, B. Aufray, Surf. Sci. Rep. **67** (2012) 1.

[6] J. Zhao, H. Liu, Z. Yu, R. Quhe, S. Zhou, Y. Wang, C.C. Liu, H. Zhong, N. Han, J. Lu, Y. Yao and K. Wu, Prog. Mater. Sci. **83** (2016) 24.

[7] J.W. Morris, *Defects in Crystals in Materials Science and Engineering: An Introduction* (John Wiley & Sons Inc., 2013) 76.

[8] Z. Wu and Z. Ni, Nanophotonics, **6** (2017) 1219.

[9] F. Banhart, J. Kotakoski and A.V. Krasheninnikov, ACS Nano **5** (2011) 26.

[10] C.E. Dreyer, A. Alkauskas, J.L. Lyons, A. Janotti and C.G. Van de Walle, Annu. Rev. Mater. Res. **48** (2018) 1.

[11] W. Kohn and L.J. Sham, Phys. Rev. A **140** (1965) 1133.

[12] X. Sun, L. Wang, H. Lin, T. Hou and Y. Li, Appl. Phys. Lett. **106** (2015) 222401.

[13] X. Zhang, H. Xie, M. Hu, H. Bao, S. Yue, G. Qin and G. Su, Phys. Rev. B **89** (2014) 054310.

[14] S. Cahangirov, M. Topsakal, E. Akturk, H. Sahin and S. Ciraci, Phys. Rev. Lett. **102** (2009) 236804.

[15] A. Geim, K. Novoselov, Nature Mater. **6** (2007) 183.

[16] L.C. Lew Yan Voon, J. Zhu and U. Schwingenschlögl, Appl. Phys. Rev. **3** (2016) 040802.

[17] S. Lebègue and O. Eriksson, Phys. Rev. B. **79** (2009) 115409.

[18] A. Feyzi and R. Chegel, Eur. Phys. J. B **89** (2016) 193.

[19] Q. Man, Y. An, H. Shen, C. Wei, S. Xiong and J. Feng, Mater. Today **67** (2023) 566.

[20] K. Takeda and K. Shiraishi, Phys. Rev. B. **50** (1994) 14916.

[21] L.C. Lew Yan Voon, E. Sandberg, R.S. Aga and A.A. Farajian, Appl. Phys. Lett. **97** (2010) 163114.

[22] G.G. Guzmán-Verri and L.C. Lew Yan Voon, Phys. Rev. B. **76** (2007) 075131.

[23] S. Cahangirov, M. Topsakal, E. Aktürk, H. Şahin and S. Ciraci, Phys. Rev. Lett. **102**

(2009) 23.

[24] C.C. Liu, W. Feng and Y. Yao, Phys. Rev. Lett. **107** (2011) 076802.

[25] C. Léandri, H. Oughaddou, B. Aufray, J.M. Gay, G. Le Lay, A Ranguis and Y. Garreau, Surf. Sci. **601** (2007) 262.

[26] B. Aufray, A. Kara, S. Vizzini, H. Oughaddou, C. Léandri, B. Ealet and G. Le Lay, Appl. Phys. Lett. **96** (2010) 183102.

[27] P. De Padova, C. Quaresima, B. Olivieri, P. Perfetti and G. Le Lay, Appl. Phys. Lett. **98** (2011) 081909.

[28] P. De Padova, C. Quaresima, C. Ottaviani, P.M. Sheverdyaeva, P. Moras, C. Carbone, D. Topwal, B. Olivieri, A. Kara, H. Oughaddau, B. Aufray and G. Le Lay, Appl. Phys. Lett. **96** (2010) 261905.

[29] M.R. Tchalala, H. Enriquez, A.J. Mayne, A. Kara, S. Roth, M.G. Silly, A. Bendounan, F. Sirotti, T. Greber, B. Aufray, G. Dujardin, M.A. Ali and H. Oughaddou, Appl. Phys. Lett. **102** (2013) 083107.

[30] P. Vogt, P. De Padova, C. Quaresima, J. Avila, E. Frantzeskakis, M.C. Asensio, A. Resta, B. Ealet and G. Le Lay, Phys. Rev. Lett. **108** (2012) 155501.

[31] B. Feng, Z. Ding, S. Meng, Y. Yao, X. He, P. Cheng, L. Chen and K. Wu, Nano Lett. **12** (2012) 3507.

[32] C.L. Lin, R. Arafune, K. Kawahara, N. Tsukahara, E. Minamitani, Y. Kim, N. Takagi and M. Kawai, Appl. Phys. Exp. **5** (2012) 045802.

[33] H. Jamgotchian, Y. Colignon, N. Hamzaoui, B. Ealet, J.Y. Hoarau, B. Aufray and J.P. Bibérian, J. Phys. Condens. Matter. **24** (2012) 172001.

[34] D. Chiappe, C. Grazianetti, G. Tallarida, M. Fanciulli and A. Molle, Adv. Mater. **24** (2012) 5088.

[35] A.F.R. Fleurence, T. Ozaki, H. Kawai, Y. Wang and Y.T. Yukiko, Phys. Rev. Lett. **108** (2012) 245501.

[36] T. Aizawa, S. Suehara and S. Otani, J. Phys. Chem. C **118** (2014) 23049.

[37] L. Meng, Y. Wang, L. Zhang, S. Du, R. Wu, L. Li, Y. Zhang, G. Li, H. Zhou, W.A. Hofer and H.J. Gao, *Nano Lett.* **13** (2013) 685.

[38] D. Chiappe, E. Scalise, E. Cinquanta, C. Grazianetti, B. van den Broek, M. Fanciulli, M. Houssa and A. Molle, Adv. Mater. **26** (2014) 2096.

[39] H. Oughaddou, H. Enriquez, M. R. Tchalala, H. Yildirim, A. J. Mayne, A. Bendounan, G. Dujardin, M. A. Ali and A. Kara, Progress in Surface Science **90**

(2015) 46.

[40] H. Sahin, J. Sivek, S. Li, B. Partoens and F. M. Peeters, Phys. Rev. B **88** (2013) 045434.

[41] N.R. Abdullah, M.T. Kareem, H.O. Rashid, A. Manolescu and V. Gudmundsson, Physica E **129** (2021) 114644.

[42] P. Aghdasi, S. Yousefi, R. Ansari and M.B. Tagani, Applied Physics A **128** (2022) 716.

[43] R. Pablo-Pedro, M.A. Magaña-Fuentes, M. Videa, J. Kong, M. Li, J.L. Mendoza -Cortes and T.V. Voorhis, Nano Lett. **20** (2020) 6336.

[44] X. Chen, P. Wang, J. Jin, B. Song and P. He, J. Phys. Chem. C **126** (2022) 5682.

[45] T. Hussain, T. Kaewmaraya, S. Chakraborty and R. Ahuja, J. Phys. Chem. C **120** (2016) 25256.

[46] X. Si, Z. Li, S. Wang, Q. Xu, J. Lin and G. Yang, Applied Surface Science **605** (2022) 154673.

[47] D.S. Sholl and J.A. Steckel, *Density Functional Theory: A Practical Introduction* (John Wiley & Sons Inc., New Jersey, 2009).

[48] M.C. Payne, M.P. Teter, D.C. Allan, T.A. Arias and J.D. Joannopoulos, Rev. Mod. Phys. **64** (1992) 1045.

[49] C.D. Sherill, http://vergil.chemistry.gatech.edu/notes/quantrev/quantrev.html (2001) (Accessed December 2019).

[50] C.D. Sherill, http://vergil.chemistry.gatech.edu/notes/hf-intro.pdf (2000) (Accessed December 2019).

[51] R.M. Martin, *Electronic Structure: Basic Theory and Practical Methods* (Cambridge University Press, Cambridge, 2004).

[52] J. Toulouse, *Review of Approximations for the Exchange-Correlation Energy in Density-Functional Theory. In: E. Cancès and G. Friesecke (eds) Density Functional Theory. Mathematics and Molecular Modeling* (Springer, Cham, 2023).

[53] C.D. Sherill, http://vergil.chemistry.gatech.edu/notes/DFT-intro.pdf. (2000) (Accessed December 2019).

[54] K. Burke and L. O. Wagner, Int. J. Quantum Chem. **113** (2013) 96.

[55] A. Phusittrakool, https://www.yumpu.com/en/document/read/28531524/dft-basic idea-and-practical-calculations (2007) (Accessed December 2019).

[56] K. Berland, V.R. Cooper, K. Lee, E. Schröder, T. Thonhauser, P. Hyldgaard and B.I. Lundqvist, Rep. Prog. Phys. **78** (2015) 066501.

[57] A. Pribram-Jones, D.A. Gross and K. Burke, Annu. Rev. Phys. Chem. **66** (2015) 283.

[58] J. Klimeš and A. Michaelides, J. Chem. Phys. **137** (2012) 120901.

[59] Bloch's Theorem, http://zimp.zju.edu.cn/~yizhou/2014-Spring/Lecture-introduction BandTheory2.pdf (2014) (Accessed December 2019).

[60] E.J. Bylaska, Annu. Rep. Comput. Chem. **13** (2017) 185.

[61] J. Grotendorst, S. Blügel and D. Marx, Comput. Nanosci: Do It Yourself! **31** (2006) 71.

[62] A.E Mattsson, P.A. Schultz, M.P. Desjarlais, T.R. Mattsson and K. Leung, Modelling Simul. Mater. Sci. Eng. **13** (2005) R1.

[63] P.R. Tulip, *Dielectric and Lattice Dynamical Properties of Molecular Crystals via Density Functional Perturbation Theory: Implementation within a First Principles Code*: University of Durham, (2004).

[64] M.A. Råsander, *A Theoretical Perspective on the Chemical Bonding and Structure of Transition Metal Carbides and Multilayers*: Uppsala Universitet, (2010).

[65] R. Pollet, C. Clavaguéra and J.P. Dognon, J. Chem. Phys. **124** (2006) 164103.

[66] J. Neugebauer and T. Hickel, WIREs Comput. Mol. Sci. 3 (2013) 438.

[67] R.M. Nieminen, Theory of Defects in Semiconductors, D.A. Drabold and S.K. Estreicher (Eds), *Topics in Applied Physics*, 104 (2007) 29.

[68] C. Freysoldt, B. Grabowski, T. Hickel, J. Neugebauer, G. Kresse, A. Janotti and C.G. van de Walle, Rev. Mod. Phys. **86** (2014) 253.

[69] S.B. Zhang and J.E. Northrup, Phys. Rev. Lett. **67** (1991) 2339.

[70] C.G. Van de Walle, D.B. Laks, G.F. Neumark and S.T. Pantelides, Phys. Rev. B **47** (1993) 9425.

[71] A.Chroneos, B.P. Uberuaga and R.W. Grimes, J. Appl. Phys. **102** (2007) 083707.

[72] W.Z. Li, M.Y. Liu, L. Gong, Q.Y. Chen, C.Cao and Y. He, Superlattices Microstruct. **148** (2020) 106712.

[73] E.M. Benecha and E.B. Lombardi, Phys. Rev. B **84** (2011) 235201.

[74] E.R. Jones and R.L. Childers, *Contemporary College Physics* (Addison-Wesley Publishing Company, Reading, 1993).

[75] P.Giannozzi, QUANTUM ESPRESSO: a modular and open-source software project for quantum simulations of materials, J. Phys. Condens. Matter. **21** (2009) 395502

[76] Quantum Espresso, https://www.quantum-espresso.org (Accessed December 2019).

[77] A. Kokalj, J. Mol. Graph. Model. **17** (1999) 176.

[78] C. Kittel, *Introduction to Solid State Physics* (John Wiley & Sons Inc., Hoboken,

2005).

[79] McGraw-Hill, *Concise Encyclopedia of Physics* (McGraw-Hill Professional Publishing, New York, 2002).

[80] T. Ayalew, *SiC Semiconductor Devices Technology, Modelling and Simulation*: Technischen Universität Wien, (2004).

[81] P.B. Benasutti, *Electronic and Structural Properties of Silicene and Graphene Layered Structures*: Wright State University, (2012).

[82] W. Gös, *Hole Trapping and the Negative Bias Temperature Instability*: Technischen Universität Wien, (2011).

[83] A.J. Cohen, P. Mori-Sánchez and W. Yang, Chem. Rev. **112** (2012) 289.

[84] D. Vanderbilt, Phys. Rev. B **41** (1990) 7892(R).

[85] J.P. Perdew, K. Burke and M. Ernzerhof, Phys. Rev. Lett. **77** (1996) 3865.

[86] M. Råsander and M.A. Moram, J. Chem. Phys. **143** (2015) 144104.

[87] C.G. Broyden, J. Inst. Maths. Applics. **6** (1970) 222.

[88] R. Fletcher, Comput. J. **13** (1970) 317.

[89] D. Goldfarb, Math. Comput. **24** (1970) 23.

[90] D.F. Shanno, Math. Comput. **24** (1970) 647.

[91] N. Marzari, D. Vanderbilt, A. De Vita and M.C. Payne, Phys. Rev. Lett. **82** (1999) 3296.

[92] P.E. Blöchl, O. Jepsen and O.K. Andersen, Phys. Rev. B **49** (1994) 16223.

[93] D.R. Hamann, M. Schluter and C. Chiang, Phys. Rev. Lett. **43** (1979) 1494.

[94] G.B. Bachelet, D.R. Hamann and M.Schluter, Phys. Rev. B **26** (1982) 4199.

[95] D.M. Ceperley and B.J. Alder, Phys. Rev. Lett. **45** (1980) 566.

[96] J.P. Perdew and A. Zunger, Phys. Rev. B **23** (1981) 5048.

[97] M. Houssa, A. Dimoulas and A. Molle, J. Phys. Condens. Matter **27** (2015) 253002.

[98] C. Kamal, A. Chakrabarti, A. Banerjee and S.K. Deb, J. Phys. Condens. Matter **25** (2013) 085508.

[99] S. Cahangirov, M. Audiffred, P. Tang, A. Iacomino, W. Duan, G. Merino and A. Rubio, Phys. Rev. B **88** (2013) 035432.

[100] S. Cahangirov, H. Sahin, G. Le Lay and A. Rubio, *A Brief History of Silicene: An Introduction to the Physics of Silicene and other 2D Materials: Lecture Notes in Physics* (Springer, Cham, 2017).

[101] A.T. Raji and E.B. Lombardi, Physica B **464** (2015) 28.

[102] M. Ali, X. Pi and Y. Liu, AIP Adv. **7** (2017) 045308.

[103] X.Q. Dai, J.H. Zhao, M.H. Xie, Y.N. Tang, Y.H. Li and B. Zhao, Eur. Phys. J. B **80** (2011) 343.

[104] J. Gao, J. Zhang, H. Liu, Q. Zhang and J. Zhao, Nanoscale **5** (2013) 9785.

[105] S. Li, Y. Wu, Y. Tu, Y. Wang, T. Jiang, W. Liu and Y. Zhao, Sci. Rep. **5** (2015) 7881.

[106] V.O. Özçelik, H.H. Gurel and S. Ciraci, Phys. Rev. B **88** (2013) 045440.

[107] X. Sun, Y. Liu, Z. Song, Y. Li, W. Wang, H. Lin, L. Wang and Y. Li, J. Mater. Chem. C **5** (2017) 4159.

[108] P.D. Townsend, Rep. Prog. Phys. **50** (1987) 501.

[109] H.S. Liu, N.N. Han and J.J. Zhao, Chin. Phys. B **24** (2015) 087303.

[110] F. Liu, S.N. Khanna and P. Jena, Phys. Rev. B **43** (1991) 8179.

[111] E.M. Sosa-Hernandez, P.G. Alvarado-Leyva, J.M. Montejano-Carrizales and F. Aguilera-Granja, Rev. Mex. de Fis. **50** (2004) 30.

[112] H. Sun, Y. Luo, J. Zhao and G. Wang, Phys. Stat. Sol. B **215** (1999) 1127.